

JOINT CONFERENCES ON ADVANCED MATERIALS

6th Workshop on Functional
and Nanostructured Materials

10th Conference on Intermolecular
and Magnetic Interactions in Matter

27–30 September 2009, Sulmona–L’Aquila, Italy



ABSTRACT BOOK

TITLE

*Abstract Book: Joint Conferences on Advanced Materials,
6th Workshop on Functional and Nanostructured Materials,
10th Conference on Intermolecular and Magnetic Interactions in Matter*

EDITOR

Jarosław Rybicki

TYPESETTING using TeX
BOP s.c., www.bop.com.pl

TASK PUBLISHING 2009

GDANSK, POLAND

ISBN 978-83-908112-7-7

JOINT CONFERENCES ON ADVANCED MATERIALS

6th WORKSHOP ON FUNCTIONAL
AND NANOSTRUCTURED MATERIALS

10th CONFERENCE ON INTERMOLECULAR
AND MAGNETIC INTERACTIONS IN MATTER

27–30 SEPTEMBER 2009, SULMONA–L’AQUILA, ITALY

O R G A N I Z E D B Y

University of L’Aquila, Italy

Istituto Nazionale di Fisica della Materia, Italy

Gdansk University of Technology, Poland

Institute of Molecular Physics, Poznan, Poland

PWSZ im. St. Wojciechowskiego, Kalisz, Poland

University of Athens, Greece

University of Zielona Góra, Poland

Technical University of Lublin, Poland

Koszalin University of Technology, Poland

I N C O O P E R A T I O N W I T H

Istituto Nazionale di Fisica Nucleare, Italy

Comune dell’Aquila, Italy

Comune di Sulmona, Italy

Provincia dell’Aquila, Italy

Regione Abruzzo, Italy

Polish Society for Crystal Growth, Poland

Polish Physical Society, Poland

COMMITTEES

HONORARY CHAIRMEN

Sir Sam Edwards (Cambridge, England)
J. T. Devreese (Antwerp, Belgium)
G. J. Papadopoulos (Athens, Greece)

SCIENTIFIC COMMITTEE

I. Berbezier (Marseille, France)
L. Casalis (Trieste, Italy)
N. Guskos (Athens, Greece) – Co-Chairman
J. Hanuza (Wroclaw, Poland)
W. G. Hoover (Livermore & UCD, CA, USA)
Y. Ishibashi (Kyushu, Japan)
T. Kanaya (Kyoto, Japan)
T. Klimczuk (Los Alamos NL, USA)
O. Kazakova (London, UK)
S. Kruchinin (Kiev, Ukraine)
R. Lakes, (Wisconsin, USA)
A. V. Meletchko (North Carolina, USA)
U. Narkiewicz (Szczecin, Poland)
M. Passacantando (L'Aquila, Italy)
P. Razis (Nicosia, Cyprus)
R. Reisfeld (Jerusalem, Israel)
J. Rybicki (Gdansk, Poland) – Chairman
S. Santucci (L'Aquila, Italy) – Co-Chairman
T. Tsuboi (Kyoto, Japan)
K. W. Wojciechowski (Poznan, Poland) – Co-Chairman

PROGRAMME COMMITTEE

S. M. Kaczmarek (Szczecin, Poland)
L. Lozzi (L'Aquila, Italy)
S. Mudry (Lviv, Ukraine)
J. Olchowik (Lublin, Poland) – Co-Chairman
L. Ottaviano (L'Aquila, Italy) – Chairman
S. Picozzi (L'Aquila, Italy)
W. Sadowski (Gdansk, Poland) – Co-Chairman
J. Typek (Szczecin, Poland)

INDUSTRIAL ADVISORY BOARD

A. Banaszkiewicz (ALSTOM Poland)
F. Famà (Micron Technology Italia)
P. Gepner (INTEL Technology Poland)
A. Gołyga (Jabil Circuit Poland)
A. Synowiecki (Radmor Poland)

ORGANIZING COMMITTEE

M. Bobrowski (Gdansk, Poland)
P. De Marco (L'Aquila, Italy)
M. Dudek (Zielona Góra, Poland) – Co-Chairman
M. Kowalik (Kalisz, Poland)
M. Nakonieczny (Gdansk, Poland)
L. Ottaviano (L'Aquila, Italy) – Chairman
S. Prezioso (L'Aquila, Italy)
J. Rybicki (Gdansk, Poland) – Co-Chairman
M. Stroiński (Poznan, Poland)
A. Witkowska (Gdansk, Poland)

CONTENTS

Lectures

<u>M. Aziz</u>	
<i>Novel Semiconductors and Nanoscale Patterning Using Energetic Beams</i>	24
<u>P. Barbara</u>	
<i>Carbon-nanotubes as 1D Probes for Superconductivity</i>	25
<u>P. Trocha, J. Barnaś</u>	
<i>Resonances in Electronic Transport Through Systems of Coupled Quantum Dots</i>	26
<u>I. Berbezier, G. Amiard, A. Ronda, A. El Hdyi, K. Gacem, D. Lockwood, N. Rowell, M. Scarselli, P. Castrucci, M. De Crescenzi</u>	
<i>Self Assembled Germanium Nanocrystals: Electrical and Optical Properties</i>	27
<u>L. Casalis</u>	
<i>DNA-based Functional Materials for Nano-Proteomics</i>	29
<u>R. Cingolani</u>	
<i>Nanotechnology for Human and Humanoid Systems</i>	30
<u>M. R. Dudek, M. Kośmider</u>	
<i>Absorption Properties of Carbon-Protected Magnetic Nanoparticles in a Pore</i>	31
<u>C. Falessi</u>	
<i>Finmeccanica Nanotechnology Studies and Developments</i>	32
<u>M. Fanciulli</u>	
<i>Oxides for Ultra-Scaled CMOS and Innovative Non-volatile Memory Devices</i>	34
<u>J. N. Grima</u>	
<i>Recent Advances in Non-conventional Systems</i>	35

<u>M. Grinberg</u>	
<i>Influence of Excited $4f^{n-1}5d^1$ State on Impurity Trapped Exciton States in Ln-Doped Materials.....</i>	36
<u>N. Guskos</u> , J. Typek, B. Padlyak, Yu. Gorelenko, P. Podsiadły, U. Narkiewicz, E. Senderek, A. Guskos, Z. Rosłaniec	
<i>Magnetic Properties of a PBT-Block-PTMO Polymer with a Small Amount of Nickel Magnetic Nanoparticles</i>	37
<u>S. M. Kaczmarek</u> , E. Tomaszewicz, H. Fuks	
<i>Spectroscopic Investigations of New Class of Rare-Earth and Zinc/Cadmium Tungstates and Molybdato-Tungstates</i>	39
<u>T. Kanaya</u>	
<i>Glassy Dynamics and Glass Transition of Polymer Nanometer Thin Films.....</i>	41
<u>O. Kazakova</u>	
<i>Nanowire-based Spintronics</i>	42
<u>S. P. Kruchinin</u> , A. Zolotovsky	
<i>Magnetic Properties of $NiFe_2O_4$ Nanoparticles</i>	43
<u>K. Ławniczak-Jabłońska</u> , M. S. Walczak, A. Wolska, M. Sikora, A. Sienkiewicz, L. Suarez, A. Kosar, M. J. Bellemare, D. S. Bohle	
<i>XAFS in Biotechnology: Studies of Malaria Pigment Substitute in Reaction with Chloroquine.....</i>	44
<u>M. Mączka</u> , L. Macalik, P. E. Tomaszewski, L. Kępiński, J. Hanuza	
<i>Phonon Properties of Nanocrystalline Bismuth Layered Ferroelectrics.....</i>	46
<u>A. V. Melechko</u> , T. E. McKnight	
<i>Vertically Aligned Carbon Nanofibers as Nanotools for Cellular Interfacing</i>	47
A. Locatelli, K. R. Knox, D. Cvetko, T. O. Mentes, M. A. Niño, S. Wang, M. B. Yilmaz, P. Kim, R. M. Osgood Jr., <u>A. Morgante</u>	
<i>Surface Corrugation, Morphology and Electronic Structure of Exfoliated Graphene: a LEEM, Micro-LEED and Micro-ARPES Study.....</i>	48
<u>S. Mudry</u>	
<i>Phase Diagrams and Cluster Structure Before Solidification</i>	50
<u>M. Mukherjee</u> , A. K. M. Maidul Islam	
<i>Systematic Study of Synthesis and Self-assembled Morphology of Silver Triblock Copolymer Nanocomposite.....</i>	51
<u>U. Narkiewicz</u> , A. Pietrasz	
<i>Removal of SO_2 from Gases on Carbon Materials</i>	52

<u>G. J. Papadopoulos</u>	
<i>Scattering of Electrons by a Two-dimensional Parabolic Repeller in a Magnetic Field.....</i>	54
<u>R. Reisfeld, T. Saraidarov, V. Levchenko</u>	
<i>Luminescent Solar Concentrators Cased on Hybrid Materials</i>	55
<u>P. Romiszowski</u>	
<i>Confinement Effects in Polymer Systems: Monte Carlo Simulations.....</i>	56
<u>C. W. Smith</u>	
<i>Tailoring Thermal Expansivity in Cellular Solids</i>	57
<u>T. Tsuboi</u>	
<i>White Organic Light Emitting Diodes for Super-thin Flat Panel Lighting</i>	58
<u>A. Verna, B. A. Davidson, A. Yu. Petrov, A. Mirone, N. Mahne, A. Giglia, S. Nannarone</u>	
<i>Interface Magnetization in Half-metallic Manganites: a Synchrotron Radiation Approach.....</i>	60
<u>H. Weitering</u>	
<i>Electronic Instabilities, Fluctuations and Charge Transport in Quantum Chains</i>	61
<u>K. W. Wojciechowski</u>	
<i>Anomalous Mechanical Properties of Various Models in Two Dimensions.....</i>	62
<u>G. P. Yablonskii, E. V. Lutsenko, S. V. Ivanov, I. V. Sedova, S. V. Sorokin, P. S. Kop'ev</u>	
<i>ZnMgSSe/ZnSe/CdSe Quantum Dot Heterostructures for Green Laser Applications</i>	63
<u>F. Krzyżewski, M. Załuska-Kotur, S. Krukowski</u>	
<i>Surface Patterns Due to Step Flow Anisotropy Formed in Crystal Growth Process.....</i>	66

Oral communications

<u>A. Ambrosio, V. Grossi, P. Maddalena</u>	
<i>Optical Trapping of Carbon Nano-Tubes of Specific Spectral Characteristics.....</i>	68
<u>R. D. Boyd, A. Cuenat</u>	
<i>Nanoparticle Measurement: From Size Distribution and Shape to Advanced Characterisation.....</i>	70

<u>A. Carbone</u> , C. Pennetta, L. Reggiani	
<i>Trapping-Detrapping Fluctuations in Organic Space-Charge Layers.....</i>	72
<u>P. Carelli</u> , A. Di Gaspare, L. Di Gaspare, M. Giammatteo, A. Notargiacomo, E. Palange, S. Piersanti	
<i>Size Control and Localised Growth of Si Nanowires on Silicon Oxide Substrates</i>	73
<u>P. Castrucci</u> , S. Del Gobbo, C. Scilletta, E. Speiser, M. Scarselli, M. De Crescenzi, G. Amiard, A. Ronda, I. Berbezier	
<i>Enhanced Quantum Efficiency of Silicon with Ge Quantum Dots.....</i>	75
<u>M. Cavallini</u> , A. Calò, P. Stoliar, J. C. Kengne, S. F. C. Matacotta, F. Quist, Y. H. Geerts, F. Biscarini	
<i>Patterning of Discotic Liquid Crystals: a New Time Temperature Integrating Framework</i>	77
<u>S. Ciuchi</u> , S. Fratini	
<i>Reconciling Coherent Band Motion and Incoherent Diffusion in Organic Molecular Semiconductors</i>	78
<u>F. De Angelis</u> , G. Das, M. Lazzarino, A. Bek, P. Candeloro, C. Liberale, F. Mecarini, A. Pujia, E. Di Fabrizio	
<i>3D Adiabatic Compression of Plasmon Polariton for Nanomapping at 10 nm Resolution.....</i>	79
<u>J. Dziedzic</u> , J. Rybicki	
<i>Divide-and-Conquer Learn-on-the-Fly: A Hybrid Quantum-Classical Approach for Simulation of Nanoscale Metallic Systems</i>	82
<u>S. Gardonio</u> , T. O. Wehling, L. Petaccia, S. Lizzit, A. Goldoni, P. Vilmercati, S. Lebeque, O. Eriksson, M. I. Katsnelson, A. I. Lichtenstein, P. Gambardella, M. Veronese, P. Moras, C. Carbone	
<i>Photoemission from Diluted Magnetic Atoms on Metal Surfaces</i>	84
<u>M. Gazda</u> , T. Klimczuk	
<i>Influence of Magnetic Field on the Electronic Conduction of (Bi,Pb)-Sr-Ca-Cu-O Granular Superconductors</i>	86
<u>S. Gibilisco</u> , G. Faraci, A. R. Pennisi	
<i>Role of Adsorbates in Photoluminescence Emission of Si Nanocrystals.....</i>	87
<u>S. Gulkowski</u> , J. M. Olchowik, P. Moskvin	
<i>Modelling of Interface During Si Layer Growth on Partially Masked Substrate.....</i>	88

<u>R. Gunnella</u> , M. Ali, F. D'Amico, M. Abbas <i>Control of Polymers Assembling in Thin P3HT Films Grown by Electrospray</i>	90
<u>J. Kaiser</u> , M. Galiová, R. Malina, K. Novotný, L. Ottaviano, A. Poma, S. Prezioso, L. Reale, A. Ritucci, P. Zuppella <i>Laser-induced Breakdown Spectroscopy Using Table-top Short-wavelength (46.9 nm) Radiation Laser</i>	91
<u>S. Kondej</u> <i>Nanostructure Modelled by δ Type Potential: Estimates for the Number of Bound States</i>	93
<u>R. Larciprete</u> , S. Gardonio, L. Petaccia, S. Lizzit <i>Atomic Oxygen Functionalization of Double-walled C Nanotubes</i>	94
<u>A. E. Maccallini</u> , B. G. Kalantzopoulos, B. A. Policicchio, B. M. G. Buonomenna, B. G. Golemme, C. R. G. Agostino <i>Gas Solubility and Mobility in Modified and Unmodified Zeolites at Low and High Pressures by PCT Kinetic and Equilibrium Sorption</i>	95
<u>L. Ortolani</u> , A. Migliori, <u>V. Morandi</u> , F. Houdellier, M. Monthioux <i>3D Reconstruction of Graphene Waviness</i>	98
<u>L. Ortolani</u> , V. Morandi, M. Monthioux <i>Graphene as Nanoscale Tangential Sieve for Selecting Achiral SWCNTs</i>	101
<u>A. Capobianchi</u> , D. Fiorani, P. Imperatori, S. Laureti, S. Foglia, <u>E. Palange</u> <i>General Strategy for Direct Synthesis of $L1_0$ FePt Nanoparticle Alloys from Layered Precursor</i>	104
<u>P. Parisse</u> , A. Lucesoli, S. Radovic, M. Castronovo, L. Casalis, M. Morgante, G. Scoles <i>Enzymatic Reactions on Surface-bound DNA Nanostructures</i>	105
<u>M. Pedio</u> , A. Resta, M. Kumar, R. Felici <i>Photoemission of Metalloporphyrins Self-assembling Monolayer on Noble Metal $\{111\}$ Substrates</i>	108
<u>M. Solzi</u> , C. Pernechele, M. Ghidini, M. Natali, M. Bolzan <i>Magnetocaloric Behaviour of Epitaxial MnAs Thin Films Grown on Different GaAs Substrates by MOVPE</i>	109
<u>L. Petaccia</u> , P. Vilmercati, S. Lizzit, S. Gorovikov, A. C. Wade, C. Cepek, M. Fanetti, E. Gayone, J. Wells, Ph. Hofmann, A. Goldoni <i>Fulleride Films: Band Dispersion and Bulk vs Surface Contribution by Low-energy Angle-Resolved Photoemission Spectroscopy</i>	111

<u>A. Ponzoni</u> , A. Vomiero, E. Comini, M. Ferroni, G. Faglia, G. Sberveglieri <i>Gas Sensors Based on Metal Oxide Nanowire Bundles: Preparation and I-V Characterization</i>	113
<u>L. Pranevicius</u> , D. Milcius, C. Templier, L. L. Pranevicius, A. Bacianskas <i>Hydrogenation of Thin Mg Films in CH₄ + Ar Plasmas</i>	115
<u>E. Principi</u> , A. Witkowska, S. Dsoke, R. Marassi, A. Di Cicco <i>A X-ray Absorption Spectroscopy Study of a Low-Pt Content Nano-catalyst Operating in a PEM Fuel Cell</i>	116
L. Vesce, R. Riccitelli, <u>A. Reale</u> , T. M. Brown, A. Di Carlo <i>Nanostructured Titania Photoanodes for Dye-sensitized Solar Cells: Optimization of Deposition Techniques</i>	118
P. Adamczyk, P. Polanowski, <u>A. Sikorski</u> <i>Percolation in Polymer-Solvent Systems. A Computer Simulation Study</i>	120
<u>A. Stroppa</u> , S. Picozzi <i>Hybrid Functional Study of Prototypical Multiferroic Systems</i>	121
<u>C. Visani</u> , N. Nemes, M. Rocci, Z. Sefrioui, C. Leon, J. Santamaria, M. G. Hernandez, S. G. E. te Velthuis, A. Hoffmann, J. W. Freeland, M. R. Fitzsimmons, F. Simon, T. Feher <i>Effect of Magnetic Anisotropy on the Inverse Superconducting Spin-switch in LCMO-YBCO-LCMO Hybrids</i>	122
<u>S. Żurek</u> , M. Kośmider, Z. Dendzik, K. Górný <i>Relaxation Characteristics of Low-molecular-weight Systems in Porous Host Matrix: Computer Simulation Study</i>	123

Posters

<u>O. I. Aksimentyeva</u> , L. S. Monastyrskyy, B. R. Tsizh, V. P. Savchyn, L. I. Yaryc'ka <i>Hybrid Organic-Inorganic Nanosystems Based on Polypnenylacetylene and Fullerene Integrated with Porous Silicon Matrix</i>	126
<u>O. I. Aksimentyeva</u> , V. P. Dyakonov, S. Piechota, A. Shapovalov, H. Szymczak, B. R. Tsizh <i>Structure and Magnetic Properties of Metal Organic Magnet Based on Iron Complex with 2-hydroxy-1-nitrozonaphthalene</i>	128
<u>G. Amiard</u> , I. Berbezier, M. Aouassa, L. Favre, A. Ronda, C. Marcus, I. Alonso <i>FIB Nanopatterning for SiGe Nanostructures Self-assembly on Si Substrate</i>	130

<u>A. Amirabadizadeh, H. Farsi, H. Arabi, M. Dehghani</u>	
<i>Effect of Substitutions of Zn for Mn on Size and Magnetic Properties of Mn–Zn Ferrite Nanoparticles.....</i>	131
<u>E. A. Anagnostakis</u>	
<i>Wavefunction-Engineering of Intersubband THz-Laser Nanoheterointerfaces</i>	132
<u>M. Aouassa, I. Berbezier, L. Favre, G. Amiard, A. Ronda, H. Maaref, A. Miranda, P. D. Vedova, F. Traversi, R. Sordan</u>	
<i>Formation and Ordering of Si and Ge Dots by Dewetting</i>	133
<u>D. Bagnis, L. Valentini, A. Facchetti, T. J. Marks, J. M. Kenny</u>	
<i>Role of Processing in Structure–Function Relationship of Polymeric Bulk Heterojunction Solar Cells.....</i>	135
<u>R. J. Barczyński</u>	
<i>Nonlinear Impedance as an Indication of Ionpolaron Interraction in Cu₂O–Al₂O₃–SiO₂ Glass</i>	137
<u>R. J. Barczyński, P. Król, L. Murawski</u>	
<i>AC and DC Conductivity in V₂O₅P₂O₅ Glasses Containing Alkaline Ions.....</i>	138
<u>L. Bednarska, M. Kovbuz, A. Budniok, J. Kubisztal, J. Panek, M. Popczyk</u>	
<i>Influence of Iron Additives on Semiconduction Properties of Al-based Amorphous Metallic Alloys.....</i>	139
<u>S. Bellucci</u>	
<i>Carbon Nanotube Cuckypaper: Low Toxicity and Decreased Proliferation of Human Cancer Cell Lines.....</i>	140
<u>L. Benea, P. Ponthiaux, F. S. Sorcaru, F. Wenger</u>	
<i>Dispersed CeO₂ in Cobalt: a Way to Improve the Coating Properties</i>	141
<u>L. Benea, A. Ciubotariu, B. Tribollet, W. Sand</u>	
<i>Influence of Nano SiC Co-deposition with Nickel to Biofilm Formation on Nanocomposite Coatings.....</i>	143
<u>S. Bertho, W. D. Oosterbaan, V. Vrindts, J. D’Haen, T. J. Cleij, L. Lutsen, J. Manca, D. Vanderzande</u>	
<i>Nanofiber Organic Solar Cells: Device Performance and Active Layer Morphology</i>	145
<u>M. Białykórski, J. Rybicki</u>	
<i>Tensile Strength of Carbon Nanotubes.....</i>	147

N. Guskos, E. A. Anagnostakis, G. Źołnierkiewicz, J. Typek, <u>A. Biedunkiewicz, A. Guskos</u>	
<i>Annealing Effect on EPR Spectra of Ti–Si–C–N System Samples</i>	148
<u>I. Bobowska, P. Wojciechowski</u>	
<i>Hybridization of Basic Copper Salt Using (2-hydroxypropyl)Cellulose/Titania Nanosheet Composite</i>	149
<u>M. Bobrowski</u>	
<i>Energetics of the Reactions of Reduction of Metal Salts by Biradical Di-para-xylylens</i>	151
<u>T. Bodziony, S. M. Kaczmarek</u>	
<i>Magnetic Properties of $LiNbO_3$: Er, Tm Single Crystal</i>	152
<u>F. Bonfigli, S. Almaviva, F. Flora, R. M. Montereali, A. Reale, A. Ritucci, P. Zuppella</u>	
<i>Color-center Photoluminescent Nano-patterns Induced in Lithium Fluoride by Soft X-ray Laser Beam</i>	153
<u>A. Capasso, E. R. Waclawik, J. M. Bell, S. Ruffel, M. Scarselli, A. Sgarlata, N. Motta</u>	
<i>Carbon Nanotubes Synthesis from Germanium Nano-particles</i>	154
<u>L. Ponta, A. Carbone, M. Gilli, P. Mazzetti</u>	
<i>Avalanche Noise in Granular Disordered High-T_c Superconductors</i>	156
<u>A. Ambrosio, M. Ambrosio, G. Cerulo, C. de Lisio, S. Lettieri, P. Maddalena, P. Castrucci, M. Scarselli, M. De Crescenzi</u>	
<i>Study of Dynamical Relaxation in MWCNs Films by Optical Pump-probe Technique</i>	158
<u>K. Cieślak, S. Gułkowski, J. M. Olchowik</u>	
<i>Influence of Dielectric Coverage on Epitaxial Thin Films and Photovoltaic Conversion in Solar Cells Obtained by Epitaxial Lateral Overgrowth</i>	160
<u>G. Ambrosone, D. K. Basa, U. Coscia</u>	
<i>Study on Structural and Optical Properties of Nanostructured Silicon Carbon Films</i>	161
<u>P. De Marco, F. Fioriti, P. Parisse, D. Luciani, S. Santucci, P. Zuppella, P. Tucceri, A. Reale, L. Ottaviano</u>	
<i>Structural and Optical Characterizations of 6,13 Pentacenequinone Thin Film on Different Substrates</i>	162
<u>P. De Marco, M. Nardone, S. Santucci, A. Del Vitto, M. Alessandri, L. Ottaviano</u>	
<i>Rapid Identification of Graphene Sheets: Alumina Does It Better</i>	165

<u>S. Di Buccianico</u> , M. F. Giardi, P. De Marco, L. Ottaviano, D. Botti <i>Cytogenetic Stability of Chicken T-cell Line Transformed with Marek's Disease Virus: Atomic Force Microscope, a New Tool for Investigation.....</i>	168
<u>F. Di Pompeo</u> , R. M. Montereali, E. Nichelatti, M. A. Vincenti <i>Optical Spectrophotometric Characterization of Organic TPB Films for Dark Matter Particle Detectors.....</i>	169
<u>A. Duda</u> , K. W. Wojciechowski <i>Effective Elastic Properties of Polycrystalline Samples of Anisotropic Auxetic Materials</i>	170
<u>J. Dziedzic</u> , J. Rybicki <i>Structure of Liquid Cu by a Novel Quantum-Classical Approach.....</i>	171
<u>W. Arabczyk</u> , <u>E. Ekiert</u> , M. Bałanda <i>Preparation and Magnetic Properties of Magnetite Dispersed in a Carbon Matrix.....</i>	172
<u>G. Fioravanti</u> <i>Artificial Molecular Machines: Stimuli Induced Motion from Solution to Surface.....</i>	173
<u>F. Flora</u> , S. Bollanti, F. Bonfigli, A. Gerardino, P. Di Lazzaro, L. Mezi, R. M. Montereali, D. Murra, A. Reale, A. Torre, P. A. Vincenti <i>The First Italian Micro-exposure Tool for EUV Nanolithography</i>	176
<u>F. Galanello</u> , S. Guerrieri, A. D'Anna <i>Metal Voids in 110 nm Lines Due to Thermal Diffusion of Aluminum in Large Metal Plate</i>	177
<u>F. Galanello</u> , G. De Amicis, M. Cichocki, A. D'Anna <i>Polymer Material Integration in Light Pipes Module of CMOS Imager Devices.....</i>	178
<u>P. Gargiani</u> , S. Achilli, M. I. Trioni, F. Bussolotti, M. G. Betti <i>Domain Wall Formation and Electron-Phonon Interaction of Bi Reconstructed Phases on Cu(100)</i>	179
<u>P. Gargiani</u> , C. Mariani, M. G. Betti <i>3d-metal Phthalocyanines Chains on Au(110): Electronic Structure Dependence on 3d Metal Occupancy</i>	180
<u>A. Mielewczyk</u> , K. Gdula, S. Molin, P. Jasiński, B. Kusz, <u>M. Gazda</u> <i>Structure and Electrical Properties of Ceramic Proton Conductors Obtained with Solid-state and Molten-salt Synthesis Methods.....</i>	181

<u>M. Julianini</u> , E. R. Waclawik, J. M. Bell, M. Scarselli, P. Castrucci, M. De Crescenzi, N. Motta	
<i>Microscopic and Spectroscopic Study of Poly(3-hexylthiophene)/Carbon Nanotube Composites for Solar Cells Applications</i>	182
<u>B. Brzostowski</u> , V. Cao Long, <u>B. Grabiec</u> <i>Four-Level Model for EIT of Cold ^{85}Rb</i>	184
<u>G. Greco</u> , A. Witkowska, S. Dsoke, A. Di Cicco, A. Cognigni, N. Menguy, J-M. Guigner	
<i>Atomic Structure Stability of PtCo Electrocatalysts in Proton Exchange Membrane Fuel Cell Subjected to Ageing Process</i>	185
<u>V. Grossi</u> , L. Ottaviano, S. Santucci, M. Passacantando <i>XPS and SEM Studies of Oxide Reduction of Germanium Nanowires</i>	186
<u>V. Grossi</u> , A. Urbani, M. Ambrosio, A. Ambrosio, P. Maddalena, S. Santucci, M. Passacantando	
<i>Novel Photosensor Made of MWCNTs Grown on Silicon Substrate</i>	187
<u>S. Guerrieri</u> , G. Testa, G. Mattioli, S. Sellitto, A. Stilo, A. D'Anna <i>Aluminum Process Integration in Copper Metallization Multi Stack for 90 nm Technology Node CMOS Image Sensor Applications</i>	189
<u>S. Guerrieri</u> , G. Testa, A. D'Anna <i>Characterization of PVD Ta and Ti Copper Diffusion Barriers</i>	190
<u>R. Marinelli</u> , <u>S. Guerrieri</u> , G. De Amicis, A. Del Monte, M. Faccio, E. Palange, A. D'Anna	
<i>Polymer Material Characterization with High Refractive Index for 90 nm Technology Node CMOS Imager Sensor Applications</i>	191
<u>N. Guskos</u> , G. Źołnierkiewicz, J. Typek, <u>A. Guskos</u> , D. Petridis <i>Influence of Magnetic Agglomerates on EPR Spectrum of Free Radicals in Organic Matrix</i>	192
<u>N. Guskos</u> , J. Majszczyk, J. Typek, J. Rybicki, I. Kruk, <u>A. Guskos</u> , G. Źołnierkiewicz, C. Adinis	
<i>Photoacoustic Response of Common Starfish Tissue</i>	193
<u>G. Il'chuk</u> , V. Kusnezh, P. Shapowal, R. Petrus' <i>Chemical Surface Deposition of CdS Thin Films from Aqueous Solutions</i>	194
<u>M. Mazurek</u> , <u>E. Jartych</u> , A. Lisińska-Czekaj, D. Czekaj, D. Oleszak <i>Structure and Hyperfine Interactions of Big $\text{Ti}_3\text{Fe}_5\text{O}_{27}$ Multiferroic Ceramic Prepared by Sintering and Mechanical Alloying Methods</i>	196

S. M. Kaczmarek, E. Tomaszewicz, <u>A. Jasik</u> <i>EPR and IR Studies of Some Praseodymium(III) Tungstates</i>	198
V. Kondrat, O. Hrytsyna <i>Formation of Near-surface Inhomogeneity of Electromechanical Fields and Size Effect in Thin Dielectric Films</i>	200
B. Kościelska, A. Winiarski, W. Jurga <i>Structure and Superconductivity of VN-SiO₂ Films Obtained by Thermal Nitridation of Sol-gel Derived Coatings</i>	201
M. Kośmider, S. Żurek, Z. Dendzik, K. Górný <i>Dynamics of Ethylene Glycol and Propylene Glycol Molecular Clusters Embedded in Carbon Nanotubes: Computer Simulation Study</i>	202
S. A. Kostyrya, V. I. Tkatch, S. G. Rassolov, K. W. Wojciechowski, B. Idzikowski <i>Numerical Approach to Cooling and Crystallization in Melt-spinning Process of Fe₄₀Ni₄₀P₁₄B₆ Alloy</i>	203
M. Kowalik, K. W. Wojciechowski <i>Free Energy of Hard Multisphere Crystals</i>	204
S. P. Kruchinin, A. Zolotovsky, J. Dow <i>Band Structure for Fe-based and Ruthenate Superconductors</i>	205
D. B. Chesnokova, V. A. Moshnikov, A. E. Gamarts, O. A. Aleksandrova, V. V. Kuznetsov <i>Photoluminescence of Nanostructured Pb_{1-x}Cd_xSe (x = 0–0.20) Layers</i>	206
J. Hassinen, J. Hölsä, T. Laamanen, M. Lastusaari, P. Novák <i>Electronic Structure of Defects in Sr₂MgSi₂O₇:Eu²⁺,R³⁺ Persistent Luminescence Materials</i>	208
Z. Lendzion-Bieluń, W. Arabczyk, U. Narkiewicz <i>Effect of Promotors on Structure and Thermostability of Nanocrystalline Cobalt Catalyst for Ammonia Synthesis</i>	210
E. Tomaszewicz, S. M. Kaczmarek, <u>G. Leniec</u> <i>Re-investigations of Thermal Decomposition of Gadolinium Sulfate Octahydrate</i>	212
D. A. Kudryashov, <u>R. V. Levin</u> , V. I. Ratushnyi, L. S. Lunin, V. V. Kuznetsov, B. V. Pushnyi, V. M. Andreev <i>Epitaxial Growth of GaSb-based Nanoheterostructures by MOCVD</i>	213
N. Guskos, <u>V. Likodimos</u> , S. Glenis, K. Karkas, G. Żołnierkiewicz, M. Bosacka <i>Transport Properties of M₂InV₃O₁₁ (M(II) = Zn(II) and Co(II)) Compounds</i>	214

M. Malvestuto

<i>XAFS Study of Ru 4d Orbital Occupation in Ruddlesden-Popper Strontium Ruthenates $Sr_{n+1}Ru_nO_{3n+1}$ ($n = 1, 2, 3$): Influence of Lattice Distortions on Electronic Structure</i>	216
V. A. Moshnikov, I. E. Gracheva, V. V. Kuznetsov, <u>A. I. Maximov</u> , S. S. Karpova, A. A. Ponamoreva	
<i>Hierarchical Nanostructured Porous Semiconductors for Gas Sensors</i>	217
Y. M. Spivak, <u>V. A. Moshnikov</u> , V. V. Kuznetsov, A. Yu. Savenko, N. E. Preobrajensky, P. G. Travkin	
<i>Self-Organized Porous Structure with Several Levels of Pores in Electrochemical Anodized Silicon</i>	219
P. Moskvin, E. Avramchuk, L. Rashkovetskyi, G. Olchowik, J. M. Olchowik, A. Zdyb, W. Sadowski	
<i>Low Temperature Liquid Phase Epitaxy of Zn-Cd-Te System</i>	221
S. Mudry, I. Shtablavyi	
<i>Liquid-Solid Interaction at Formation of Nanocomposite Systems</i>	223
S. Mudry, Yu. Plevachuk, V. Sklyarchuk, A. Yakymovych, V. Sidorov	
<i>Influence of Antimony on Structure and Physical Properties of Tin</i>	224
L. Murawski, R. J. Barczyński, K. Trzebiatowski, L. Wicikowski	
<i>Effects of Heating Atmospheres on Surface Conductivity in $Cu_2O-Al_2O_3-SiO_2$ Glass</i>	225
N. Guskos, G. Żołnierkiewicz, J. Typek, D. Sibera, <u>U. Narkiewicz</u>	
<i>FMR Study of Temperature Dependence of Magnetic Anisotropy of Nanocrystalline Fe_2O_3 Doped with ZnO</i>	226
U. Narkiewicz, J. Kaszewski, M. Godlewski, S. Yatsunenko, W. Łojkowski	
<i>Influence of Annealing Temperature on Light Emission Efficiency of ZrO_2 Doped with Tb^{3+} Ions</i>	228
J. Narojczyk, K. W. Wojciechowski	
<i>Elastic Properties of Three-dimensional System of Soft Dimmers at Zero Temperature</i>	229
G. Olchowik, M. Tomaszewska, M. Tomaszewski	
<i>Modification of Bone Structure After Corticotherapy by Microwave Irradiation</i>	230
B. Padlyak, W. Ryba-Romanowski, R. Lisiecki, Ya. Burak, V. Adamiv, I. Teslyuk	
<i>Synthesis and Spectroscopy of Lithium and Potassium-Lithium Tetraborate Glasses Doped with Copper</i>	232

A. Capobianchi, D. Fiorani, C. Veroli, M. V. Mansilla, S. Foglia, <u>E. Palange</u> <i>Direct Synthesis of L1₀ FePt Nanoparticles within Carbon Nanotubes</i> by Wet Chemical Procedure.....	234
C. Rizza, P. Carelli, <u>E. Palange</u> , S. Lupi, O. Limaj, A. Nucara, M. Ortolani <i>Frequency Filters in Terahertz Region Based on Induced Dipolar Response</i> of 2-dimensional Array of Functional Metamaterials	235
<u>M. Passacantando</u> , F. Bussolotti, S. Santucci <i>Tuning the Electromechanical Response of an Individual CNT by Selective</i> <i>Electron Beam Induced Deposition</i>	236
<u>I. Pelech</u> <i>Removal of Amorphous Carbon and Metal Particles from MWNTs Using</i> <i>Hydrogen and Acid Treatment</i>	237
<u>U. del Pennino</u> , F. Moro, V. Corradini, M. Evangelisti, R. Biagi, V. De Renzi, U . del Pennino, J. C. Cezar, R. Inglis, C. J. Miliros, E. K. Brechin <i>Magnetic Properties of Mn₆ Sub-monolayers on Au(111) Investigated by</i> <i>X-ray Magnetic Circular Dichroism</i>	238
<u>L. Peponi</u> , A. Tercjak, J. Gutierrez, M. Cardinali, I. Mondragon, L. Valentini, J. M. Kenny <i>EFM Imaging of Carbon Nanotubes Sequestered into Polystyrene Domains</i> of Poly(styrene- <i>b</i> -isoprene- <i>b</i> -styrene) Block Copolymer Matrix.....	239
<u>S. Picozzi</u> , G. Giovannetti, A. Stroppa, T. Fukushima, K. Yamauchi <i>The BISMUTH Project</i>	240
<u>F. Piersimoni</u> , K. Vandewal, S. Chambon, S. Filippone, N. Martin, J. Zhao, G. Van Assche, B. Van Mele, L. Lutsen, P. Adriaansens, D. Vanderzande, J. Manca <i>Influence of Fullerene Side Chain Functionalization on Open-Circuit-Voltage</i> of Polymer: Fullerene Bulk Heterojunction Solar Cells.....	241
<u>A. Poma</u> , S. Di Bucchianico, A. Galano, S. Santucci <i>Interactions and Potential Cytotoxicity of TiO₂ Nanoparticles and Thin</i> <i>Films on Murine Macrophages RAW 264.7 Cell Line</i>	243
<u>M. Dispenza</u> , P. Farinelli, <u>I. Pomona</u> <i>Development of Compact Ka-Band MEMS Phase Shifter for Electronic Beam</i> <i>Scanning Antennas</i>	244
<u>D. Joskowska</u> , <u>K. Pomoni</u> , A. Vomvas, B. Kościelska, D. Anastassopoulos <i>On Electrical and Photoconductive Properties of Nb-doped TiO₂ Sol-gel Thin</i> <i>Films</i>	247

A. A. Poźniak, P. Kędziora, H. Kamiński, B. Maruszewski, T. Stręk, K. W. Wojciechowski	
<i>Anomalous Deformation of Constrained Auxetic Square Under Pressure</i>	248
S. Prezioso, D. Luciani, P. Tucceri, P. De Marco, A. Gaudieri, J. Kaiser, S. Santucci, L. Ottaviano, P. Zuppella	
<i>Morphology Investigation of Periodic Nano-patterns Produced by Large Area X-ray Interference Lithography</i>	249
S. Prezioso, L. Ottaviano, A. Ritucci, P. Tucceri, F. Flora, L. Mezi, P. Dunne, P. Zuppella	
<i>A Xe Based Plasma Source for EUV Nano-lithography Applications</i>	250
S. Prezioso, S. M. Hossain, A. Anopchenko, L. Ferraioli, Zhizhong Yuan, M. Wang, G. Pucker, P. Bellutti, S. Binettir, M. Acciarri, L. Pavesi	
<i>Silicon Quantum-dots Based Solar Cells for Third Generation Photovoltaics</i>	251
A. A. Donskov, L. I. D'yakonov, A. V. Govorkov, Y. P. Kozlova, V. V. Kuznetsov, S. S. Malakhov, A. V. Markov, M. V. Mezhennyi, V. F. Pavlov, A. Y. Polyakov, V. I. Ratushnyi, N. B. Smirnov, T. G. Yugova	
<i>Non-Polar GaN Films Prepared on Si Substrates Using Porous Al_2O_3 Anodic Oxide Masks</i>	252
E. Leonardi, S. Penna, A. Reale, T. M. Brown, A. Di Carlo	
<i>Stability of Dye-sensitized Solar Cells: Comparison of Sealing Strategies</i>	254
M. Rinaldi, F. Ruggieri, L. Lozzi, S. Santucci	
<i>Well-Aligned Nanofibers Grown by Near-Field Electrospinning</i>	256
O. S. Roik, O. V. Samsonnikov, V. P. Kazimirov, S. M. Galushko, V. E. Sokol'skii	
<i>Local Order in Liquid Al-Cu, Al-Co and Al-Cu-Co Alloys</i>	258
E. Rysiakiewicz-Pasek, A. Naberezhnov, A. Fokin, P. Jagus, E. Koroleva, Yu. Kumzerov, L. Korotkov, M. Tovar, S. Vakhrushev	
<i>Phase Transformations in Nanocomposites with Ferroelectrics in Restricted Geometry: Phase Transitions and Macroscopic Properties</i>	260
W. Sadowski, P. Fiertek, J. M. Olchowik	
<i>Doping Effect at Grain Boundary of $YBa_2Cu_3O_{7-y}$: Fe Ceramic System</i>	262
W. Sadowski, T. Klimczuk, J. M. Olchowik	
<i>The Influence of the Annealing Temperature on the $NdCeCuO-214$ Crystals Surface</i>	263
O. V. Samsonnikov, O. S. Muratov, O. S. Roik, V. P. Kazimirov	
<i>Modeling Structure of Liquid Al</i>	264

<u>B. Sanavio, C. Grunwald, G. Legname, L. Casalis, G. Scoles</u>	
<i>Selective Confinement of Proteins by AFM for Characterization Studies</i>	265
<u>A. Shalimov, K. Potzger, D. Geiger, G. Talut, A. Misiuk, S. Zhou, C. Baehtz, J. Fassbender</u>	
<i>Structural and Magnetic Properties of Fe and FePt Nanoparticles in MgO Synthesized by Ion Implantation</i>	266
<u>R. Signerski, G. Jarosz, B. Kościelska</u>	
<i>Photovoltaic Effect in Hybrid Heterojunction Formed from Cadmium Telluride and Zinc Perfluorophthalocyanine Layers</i>	267
<u>A. A. Solodovnik, V. V. Danchuk</u>	
<i>Structure of Condensed Films of Molecular Cryocrystals</i>	268
<u>M. Villani, G. Calestani, M. Solzi, C. Pernechele</u>	
<i>Direct Synthesis of Tetragonal L1₀ Ferromagnetic FePt Nanoparticles</i>	271
<u>P. Konsin, B. Sorkin</u>	
<i>Surface Superconductivity in Transverse Electric Field in Two-component Model</i>	273
<u>A. Makal, K. Woźniak, A. Szady-Chełmieniecka, E. Tomaszewicz, G. Leniec, S. M. Kaczmarek, E. Grech</u>	
<i>Synthesis, Crystal Structure and Characterization of a New Monohydrate NCS⁻ and a Schiff Base Copper(II) Complex</i>	274
<u>E. Tomaszewicz, G. Dąbrowska, S. M. Kaczmarek, H. Fuks</u>	
<i>Solid-State Synthesis and Characterization of New Cadmium and Rare-earth Metal Molybdato-tungstates Cd_{0.25} RE_{0.50} (MoO₄)_{0.25} (WO₄)_{0.75}</i>	275
<u>V. M. Rubish, B. R. Tsizh, S. M. Gasynets, O. G. Guranich, P. P. Guranich</u>	
<i>Obtaining and Dielectric Properties of Ferroelectric Glassceramics on the Basis of Sn₂P₂S₆</i>	277
<u>T. Tsuboi, Y. Torii</u>	
<i>Photoluminescence Characteristics of Green and Blue Emitting Alq₃ Organic Molecules in Crystals and Thin Films</i>	278
<u>N. Guskos, G. Żołnierkiewicz, J. Typek, A. Guskos, D. Petridis</u>	
<i>EPR/FMR Study of Nanocrystalline Hematite–Ilmenite Solid Solutions</i>	279
<u>J. Typek, N. Guskos, G. Żołnierkiewicz, E. Filipiak</u>	
<i>Magnetic Resonance Study of Sb₃ V₂Mo₃ O₂₁</i>	280
<u>J. Typek, N. Guskos, G. Żołnierkiewicz, A. Szymczyk</u>	
<i>Magnetic Resonance Study of Poly(ether-block-ester) Copolymers with Ferrocene Units</i>	281

<u>B. Ya. Venhryny, I. I. Grygorchak, S. Mudry, Yu. O. Kulyk</u>	
<i>Influence of Ni-intercalative Modification of Nanoporous Carbon on Structure and Properties of Electric Double-layer at Boundary with Electrolyte</i>	282
<u>A. Witkowska, G. Greco, A. Moretti, G. Giuli, R. Marassi</u>	
<i>Structure vs Catalytic Activity in Carbon Supported Pt-based Catalysts.....</i>	283
<u>K. Yamauchi, S. Picozzi</u>	
<i>Ab initio Study on Ferroelectric Stability in Charge-ordered Multiferroic Iron Oxides.....</i>	285
<u>F. M. Zanzotto, D. Croce, S. Prezioso</u>	
<i>Reading what Machines “Think”: a Challenge for Nanotechnology</i>	287
<u>N. Guskos, G. Żołnierkiewicz, J. Typek, D. Sibera, U. Narkiewicz</u>	
<i>Magnetic Resonance Study of ZnO–MnO System</i>	288
<u>P. K. Sharma, A. C. Pandey, C. Rudowicz, N. Guskos, G. Żołnierkiewicz</u>	
<i>Copper Doping Concentration Dependence of Structural and Electron Paramagnetic Resonance Properties of ZnO Nanorods.....</i>	289
<u>N. Guskos, G. Żołnierkiewicz, J. Typek, R. Szymczak, C. Rudowicz,</u>	
<u>A. Błońska-Tabero, H. Ohta, S. Okubo</u>	
<i>Study of Magnetic Properties of $Co_3Fe_4V_6O_{24}$.....</i>	290
<i>Index of authors</i>	292

LECTURES

Novel Semiconductors and Nanoscale Patterning Using Energetic Beams

M. Aziz

*Harvard School of Engineering and Applied Sciences
29 Oxford Street, 02138 Cambridge MA, U.S.A.*

maziz@harvard.edu

The recent discovery of semiconductor materials whose properties depend dramatically on the introduction of an alloying species at levels below a few atomic percent has opened opportunities for the synthesis of quantum structures and hitherto unexplored device structures. Examples of these dilute alloys are $\text{GaN}_x\text{As}_{1-x}$, which is characterized by a giant bandgap bowing that makes it ideal for quantum confinement; $\text{Ga}_{1-x}\text{Mn}_x\text{As}$, which displays ferromagnetic behavior that makes it a prime candidate for spintronics applications; and $\text{Si}_{1-x}\text{S}_x$, which displays sub-bandgap optoelectronic absorption that makes it an intriguing candidate for IR photodetection and photovoltaic applications. In all of these alloys, the very low value of x opens new routes to their synthesis and integration. Additionally, the discovery of electroluminescence from silicon controllably injected with native point defects creates the opportunity for the development of an electrically pumped silicon laser operating at important communications wavelengths.

I will report on the explorations of my collaborators and my group on the synthesis and patterning of these materials using ion implantation and Pulsed Laser Melting (PLM) induced rapid solidification. PLM has unique advantages for point defect manipulation. PLM also enables an entirely new approach to the realization of novel 1D and 0D quantum structures from compound semiconductor materials in an arbitrarily programmable direct writing process creating concentration changes with lateral resolution that could approach 10 nm. Structurally, these materials appear single crystalline with small variations in alloy composition; however, from an electronic point of view they should exhibit an arbitrarily patterned band structure.

Carbon-nanotubes as 1D Probes for Superconductivity

P. Barbara

*Department of Physics, Georgetown University
Washington, DC 20057, USA*

Single-walled carbon nanotubes are seamless cylinders made of a monolayer of carbon atoms. They can be either metallic or semiconducting and the conductance of a semiconducting nanotube can be tuned by applying a voltage to a nearby gate electrode, providing a one-dimensional field-effect transistor at the nanometer scale. These systems can be used to explore physics in reduced dimensions as well as for technological applications.

Here I will describe experiments on carbon nanotube field effect transistors with superconducting and normal electrodes, to probe superconducting proximity effect in one dimension. When the electrodes are made of normal/superconductor bilayers, carbon nanotubes can be used as point contacts for Andreev reflection spectroscopy, to study proximity effect at the normal/superconductor interface [1]. When the electrodes are normal metals, anomalous transport features indicate that the nanotube may become superconducting when the gate voltage shifts the Fermi energy into van Hove singularities of the electronic density of states. In this scenario, proximity effect occurs at the interface between the superconducting nanotube and the normal electrode [2].

Acknowledgements

Work supported by the NSF (DMR 0239721 and DMR 0907220).

References

- [1] Tselev A, Yang Y, Zhang J, Barbara P, and Shafranjuk S E, Carbon nanotubes as nanoscale probes of the superconducting proximity effect in Pd–Nb junctions, submitted to *Phys Rev. B*
- [2] Zhang J, Tselev A, Yang Y, Hatton K, Barbara P, and Shafraniuk S, Zero-bias anomaly and superconductivity in single-walled carbon nanotubes, 2006 *Phys. Rev. B* **74** 155414

Resonances in Electronic Transport Through Systems of Coupled Quantum Dots

P. Trocha¹, J. Barnas^{1,2}

¹*Faculty of Physics, Adam Mickiewicz University
Umultowska 85, 61-614 Poznań, Poland*

²*Institute of Molecular Physics, Polish Academy of Sciences
Smoluchowskiego 17, 60-179 Poznań, Poland*

Charge and spin transport through quantum dots is of current interest. We investigated theoretically the electronic transport through systems of coupled quantum dots which are generally attached to magnetic and/or nonmagnetic electron reservoirs (electrodes). In particular, we focused our considerations mainly on systems consisting of two and three quantum dots coupled to the electrodes. The transport properties of such dot arrays were analyzed in both weak and strong coupling regimes, and the main attention was paid to various interference effects, including also the Kondo phenomenon. Some of these effects resemble similar effects which are well known in atomic physics, like for instance Dicke and Fano resonances. The transport characteristics, including current, linear and nonlinear conductance, shot noise, and tunnel magnetoresistance, were calculated using several theoretical techniques. To describe transport properties in various regimes, we made use of the nonequilibrium Green function (NEGF) formalism, slave-boson mean field (SBMF) theory, and the real-time diagrammatic technique. The Kondo temperature (in the case of the orbital Kondo phenomenon) was evaluated from the scaling approach and slave boson techniques.

Acknowledgements

This work, as part of the European Science Foundation EUROCORES Program SPIN-TRA, was supported by funds from the Ministry of Science and Higher Education as a research project in the years 2006–2009 and the EC Sixth Framework Program, under Contract N.ERAS-CT-2003-980409.

References

- [1] R. H. Dicke, Phys. Rev. 93, 99 (1954)
- [2] U. Fano, Phys. Rev. 124, 1866 (1961)
- [3] P. Trocha, J. Barnaś, Phys. Rev. B 76, 165432 (2007)
- [4] P. Trocha, J. Barnaś, phys. stat. sol. (b) 244, 2553 (2007)
- [5] P. Trocha, J. Barnaś, J. Phys.: Condens. Matter 20 (2008) 125220
- [6] P. Trocha, J. Barnaś, Phys. Rev. B 78, 075424 (2008)

Self Assembled Germanium Nanocrystals: Electrical and Optical Properties

I. Berbezier¹, G. Amiard¹, A. Ronda¹, A. El Hdyi²,
K. Gacem², D. Lockwood³, N. Rowell³,
M. Scarselli⁴, P. Castrucci⁴, M. De Crescenzi⁴

¹IM2NP, CNRS – Université d’Aix Marseille
Campus St Jérôme, Case 142, 13397 Marseille CEDEX 20

²LMEN, Case 15, UFR Sciences, Université de Reims
Champagne-Ardenne, 51687 Reims Cedex 2, France

³National Research Council of Canada
1200 Montreal Road, Ottawa, ON K1A 0R6, Canada

⁴Università di Roma 2 Tor Vergata
Via della Ricerca Scientifica, Roma, Italy

In the last decade, a significant progress has been made towards development of new processes for integrating nanostructured materials into novel micro-and opto-electronic devices. The nanostructures of interest include arrays of clusters, nanoparticles, quantum dots and wires. For most of the potential applications the nanostructures must be ordered and highly homogeneous in size in order to exploit the quantum effects for device applications.

In the first part of the presentation, a review of the recent advances in self-assembly mechanisms and processes will be given [1]. The talk will particularly address the mechanisms of formation of highly ordered arrays of Ge quantum dots during the growth on nano-patterned Si(001) substrates [2,3].

The second part of the talk will be devoted to a new fabrication process of Ge nanocrystals (NC) embedded in an SiO₂ amorphous matrix. The two step fabrication process is based on the Ge QD self-assembly on an SiO₂/Si(001) substrate nanopatterned by Focused Ion Beam (FIB). During the first step, FIB direct writing is used to create an array of ultra-small holes with high density ($> 10^{11} \text{ cm}^{-2}$) in a thin thermal SiO₂ layer on a Si(001) substrate. New results obtained with the Orsay Physics FIB apparatus implemented with an in situ mass filter and permitting high resolution nanopatterning with Si (or gold) ion beams will be presented. During the second step, Ge quantum dots are obtained by the conjunction of crystallization and dewetting of an amorphous Ge layer during MBE in situ annealing [4].

The third part of the talk is focused on the structural, electrical and optical properties of Ge dots. We show by the transmission electron microscopy that both Si and Ge NC exhibit a pseudo-equilibrium shape independent of the annealing conditions. The bandgap of individual NC determined by scanning tunneling spectroscopy is directly correlated to their size as predicted by quantum confinement predictions [5].

Optical and electronic properties of Ge NC embedded in an oxide matrix were studied [6,7]. In particular, hysteresis loops observed in the capacitance-voltage curves were attributed to electron injection/emission process in Ge NC, which is representative of the memory effect. New optical and electronic properties are evidenced for ultra-small Ge NCs (3 nm mean diameter).

References

- [1] I. Berbezier, A. Ronda, *Surf. Sci. Rep.* (2009)
- [2] A. Pascale, I. Berbezier, A. Ronda, P. Keliros, *Phys. Rev. B* 075311 (2008)
- [3] I. Berbezier, A. Ronda, *Phys. Rev. B* 195407 (2007)
- [4] A. Karmous, I. Berbezier, A. Ronda, *Phys. Rev. B* 075323 (2006)
- [5] I. Berbezier, A. Karmous, A. Ronda, A. Sgarlata, A. Balzarotti, P. Castrucci, M. Scarselli, M. De Crescenzi, *Appl. Phys. Lett.* 063122 (2006)
- [6] M. Scarselli, S. Masala, P. Castrucci, M. De Crescenzi, E. Gatto, M. Venanzi, A. Karmous, PD Szkutnik, A. Ronda, I. Berbezier, *Appl. Phys. Lett.* 141117 (2007)
- [7] A. El Hdiy, K. Gacem, M. Troyon, A. Ronda, F. Bassani, I. Berbezier, *J. A.P.* 104, 063716 (2008)

DNA-based Functional Materials for Nano-Proteomics

L. Casalis

*Sincrotrone Trieste, ss14, km 163.5, Basovizza
34014 Trieste, Italy*

loredana.casalis@elettra.trieste.it

The development of protein arrays with feature sizes at the micrometer length scale is currently of great interest for biomedical diagnostics and life sciences because these devices promise to evolve into a powerful technological platform for a high-throughput analysis of biomolecular interactions with low requirements for the amount of samples and hands-on processing time. An important area in the development of protein and small molecule arrays concerns their further miniaturization to the nanometer regime. Although various methods have been developed based on the scanning-probe lithography or micro contact printing, it is currently still very difficult to fabricate nanoarrays containing multiple features, such as a range of different proteins or small-molecule ligands.

We report here a novel approach to the fabrication of protein nanoarrays which takes advantage of Atomic Force Microscopy (AFM)-based Nanografting, previously developed and applied in our group for hybridization studies of DNA and other nucleic acids, and DNA-directed Immobilization (DDI) of semisynthetic protein-DNA conjugates. The latter method, which takes advantage of the specific Watson-Crick hybridization of oligonucleotide-modified proteins to surface-bound complementary oligomers, has previously been developed and extensively applied for the generation of self-assembled protein arrays at the micrometer length scale.

It will be shown that a combination of these two methods can be used to synergistically enable fabrication of protein nanoarrays with high control over the spot size and the molecular orientation, as well as options for reliable read-out, based on topographic AFM measurements. Moreover, it will be shown that by using such device it is possible to study the affinity and kinetics parameters of bio-recognition events.

Nanotechnology for Human
and Humanoid Systems

R. Cingolani

*Istituto Italiano di Tecnologia (IIT)
Via Morego, 30 16163 Genova, Italy*

Absorption Properties of Carbon-Protected Magnetic Nanoparticles in a Pore

M. R. Dudek, M. Kośmider

*Institute of Physics, University of Zielona Góra
ul. Szafrana 4a, 65-069 Zielona Góra, Poland*

A computer simulation study of the absorption properties of the magnetic nanoparticles inside pores is discussed. The analysis is restricted to the case when the dynamics of a single nanoparticle in a pore is controlled by two factors: a DC magnetic field and an AC radiofrequency electromagnetic field which is used for heating the magnetic nanoparticle. The theoretical model includes magnetization dynamics in the Landau–Lifshitz formulation and a molecular dynamics method for describing the mechanical properties of magnetic nanoparticles.

References

- [1] J. H. Van Vleck, *Physical Review* 78, 266–274 (1950)
- [2] L. Landau, E. Lifshitz, *Phys. Z. Sovjetunion* 8 (1953) 153

Finmeccanica Nanotechnology Studies and Developments

C. Falessi

*SELEX Sistemi Integrati, a Finmeccanica Company
Strategic and Planning Directorate, Technology Strategy
Via Tiburtina Km. 12.4, 00131 Rome, Italy*

*cfalessi@selex-si.com
www.selex-si.com*

Finmeccanica is a financial and industrial holding company whose production activities are concentrated in aeronautics, helicopters, space and defense, with additional well-established skills and production assets in the transport, energy, homeland protection and security sectors providing applications, sensors, systems and systems of systems.

The main companies of the Group are Alenia Aeronautica, Thales Alcatel Space Italia, Agusta, SELEX Sensors and Avionic Systems, SELEX Communications, SELEX Sistemi Integrati, MBDA Italia, STMicroelectronics, ELSAG-Datamat and Ansaldo.

The Finmeccanica Group is present in the world with more than seventy thousand employees on about 500 operating sites; the turnover exceeds 16 000 M euros and over 14% of the revenues is invested in R&D.

To compete in the world open market a continuous innovation is mandatory. In order to build emerging technologies Finmeccanica has sponsored a project, named MindSh@re, among more than 25 companies. The project aims at creating value in the FNM Group through the practice of team building and co-operation within the Companies, capitalization of activities, knowledge, processes and best practices within the Group, sharing of common technology platforms.

More precisely, fourteen main companies and four research centers are working together in a Finmeccanica Focus Group on Nanomaterials and Nanotechnologies, since it is necessary to find out new approaches to become a future “technology differentiator” to maintain and strengthen the position of a world leader in the state-of-the-art applications.

The Finmeccanica Nanotechnology Focus Group is investigating:

- Nanostructured RF Absorbent Materials and Frequency Selective Surfaces.
- Vacuum Tube NanoAmplifier (Tx NanoValves): transmitters based on Carbon Nanotubes that could generate an emission field with a very high efficiency and at a low temperature.

The efficient realization of elementary nanovalves could be based on nanotube arrays which could supply more than 25 db of current gain up to 37 THz.

- Carbon NanoTubes adoption for dense electronic devices
- Thermal Management and Interconnection (Flip Chip & Face Up configuration).

Nanostructured high strength alloys adopting severe plastic deformation techniques such as Accumulative Roll-Bonding (ARB) techniques for aeronautics and ballistic protection applications.

- Nanosensors for Bio-Chemical Agents Detection and Control (Future Soldier) making use of a vapor phase deposition technology type - Pulsed Microplasma Cluster Source (PMCS).

In addition the Finmeccanica Focus Group Nano is coordinating a Multiscale NanoScience – Engineering Integration Initiative. The “NanoTechnology Multiscale Project – NMP” is partially funded by the Italian MoD and is a complete realization of the Vertical and Horizontal Integration recognized as a condition for the NanoTechnology application to Industry and Society. NMP includes the development of 9 nano-demonstrators and aims at the definition & development of integrated methodologies and environments to study, design, develop and test nanotechnology based metamaterials, devices, sensors and systems.

Oxides for Ultra-Scaled CMOS and Innovative Non-volatile Memory Devices

M. Fanciulli

*INFM - MDM Lab. C/o ST Microelectronics
via C. Olivetti, 2 20041 Agrate B.za (Mi) Italy*

The availability of the next generations of silicon-based devices depends on the solution of the challenging problems related to the capability of growing advanced materials, controlling their interface structure and stability on Si or other high-mobility semiconductors, understanding the dopant interaction and charge transport in sub-micron regions, and realizing new functionalities. The astonishing advances in nanoelectronics will continue until the sizes of device approach atomic dimensions, a realm where a wide variety of novel device concepts will play a relevant role. High- k dielectric materials in combination with high mobility substrates represent a promising way for the further development of CMOS based nanoelectronics. The dielectrics have also the potential to play an important role in novel and emerging devices. I shall focus on some concepts related to nanoelectronics, for both logic and memory functionalities, pointing out the experimental challenges related to material science aspects, such as the quality of the layers and the interfaces, to metrology issues, such as the availability of very sensitive characterization tools, and to fundamental solid-state physics such as switching mechanisms in resistive RAM. The application of advanced dielectrics in other novel nanoelectronic devices will be also briefly discussed.

Recent Advances in Non-conventional Systems

J. N. Grima

*Department of Chemistry, Faculty of Science, University of Malta
Msida, Malta*

Most materials we encounter are such that they get thinner when stretched (i.e. exhibit a positive Poisson’s ratio) and expand when heated (i.e. exhibit a positive thermal expansion coefficient). Nevertheless, not all materials behave like this and it is possible for materials and structures to get fatter stretched (i.e. exhibit a negative Poisson’s ratio, NPR, commonly referred to as auxetic) and contract when heated (i.e. exhibit a negative thermal expansion coefficient, commonly referred to as NTE materials). It is also possible for materials and structures to neither get thinner nor fatter when stretched (i.e. exhibit a zero Poisson’s ratio, ZPR) or neither expand nor contract when heated (i.e. exhibit a zero thermal expansion coefficient, may be referred to ZTE materials).

In this paper we present some recent advances we made in this field. In particular we discuss a new manufacturing process for the production of NPR foams from conventional foams, together with ways which can be used to re-convert the auxetic foam back to conventional foam. We also present a novel system exhibiting ZTE and some other very interesting properties.

Finally, we show how NTE and ZTE multi-layered systems can be manufactured using conventional materials having different mechanical and thermal properties. In particular we show that to optimise (NTE) characteristics, the systems must be constructed by combining thin layers of stiff materials having high positive coefficient of thermal expansion (CTE) characteristics bonded together through thicker layers of soft material having low CTE values and, more importantly, having Poisson’s ratio as high as possible.

Acknowledgments

This work is financed by the Malta Council for Science and Technology.

Influence of Excited $4f^{n-1}5d^1$ State on Impurity Trapped Exciton States in Ln-Doped Materials

M. Grinberg

*Institute of Experimental Physics, University of Gdańsk
Wita Stwosza 57, 80-952 Gdańsk, Poland*

fizmgr@univ.gda.pl

In rare earth ion doped solids the emission takes place usually due to $4f^n \rightarrow 4f^n$ and $4f^{n-1}5d^1 \rightarrow 4f^n$ internal transitions of lanthanide ions. In the case of band to band excitation the effective energy transfer from the host to the impurity requires the existence of localized impurity trapped exciton states that cause the localization of the electron and the hole at the dopant site. Such states appear since the location of a single charge (electron or hole) at the electrically insensible impurity creates the long range Coulomb potential. In several cases, however the impurity trapped exciton state becomes stable and it produces anomalous luminescence instead of the Ln emission.

In this contribution the pressure effect on energies of the $4f^{n-1}5d^1 \rightarrow 5f^n$ transitions in Ln doped oxides and fluorides as well as the influence of pressure on the energy of impurity trapped exciton states is discussed. The latest results on high pressure investigations of luminescence related to Pr^{3+} and Eu^{2+} in different lattices are presented. The influence of pressure on anomalous luminescence in $\text{BaSrF}_2:\text{Eu}^{2+}$ and $\text{LiBaF}_3:\text{Eu}^{2+}$ systems is presented and discussed. A theoretical model describing the impurity trapped exciton as a system where a hole is localized at the impurity and an electron is captured by the Coulomb potential at Rydberg-like states is developed. The model is used to analyze the anomalous luminescence in Eu^{2+} doped fluorides and pressure quenching of Pr^{3+} luminescence in some oxides. The contribution presents the effect of mixing between the Rydberg-like electrons and the localized electrons, which is significantly different for the $4f^n$ and $4f^{n-1}5d$ electronic manifolds. The results show the importance of the local lattice relaxation for the creation of stable impurity trapped exciton states. Additionally, the influence of macroscopic quantities such as bulk modulus and dielectric constant on the possibility of creating an impurity trapped exciton is discussed.

Magnetic Properties of a PBT-Block-PTMO Polymer with a Small Amount of Nickel Magnetic Nanoparticles

N. Guskos^{1,2}, J. Typek², B. Padlyak^{3,4},
Yu. Gorelenko⁵, P. Podsiadły⁶, U. Narkiewicz⁶,
E. Senderek⁷, A. Guskos², Z. Rosłaniec⁷

¹*Solid State Section, Department of Physics, University of Athens
Panepistimiopolis, 15 784, Greece*

²*Institute of Physics, West Pomeranian University of Technology
Al. Piastów 48, 70-311 Szczecin, Poland*

³*Institute of Physical Optics
Dragomanov Str. 23, 79-005 L’viv, Ukraine*

⁴*Institute of Physics, University of Zielona Góra
Prof. Szafrana Str. 4a, 65-516 Zielona Góra, Poland*

⁵*Department of Chemistry, Ivan Franko National University of L’viv
Kyryla & Mefodiya Str. 6, 79-005 L’viv, Ukraine*

⁶*Institute of Chemical and Environmental Engineering
West Pomeranian University of Technology
Al. Piastów 17, 70-310 Szczecin, Poland*

⁷*Institute of Materials Science and Engineering
West Pomeranian University of Technology
Al. Piastów 17, 70-310 Szczecin, Poland*

Samples containing fine particles of a face-centred cubic (fcc) phase of Ni embedded in a PBT-block-PTMO polymer at concentrations of 0.1 and 0.25 wt.% were synthesized. The mean size of Ni crystalline particles varied from 8 to 30 nm. A ferromagnetic resonance (FMR) study was carried out in the 4–300 K temperature range. A symmetrical and very intense magnetic resonance line was recorded in the investigated samples for all temperatures while an additional line connected with an anisotropic magnetic interaction appeared below 100 K. At low temperature, an electron paramagnetic resonance (EPR) spectrum from isolated Ni ions was registered. At room temperature, a resonance line was registered at $g = 2.240(2)$ ($H_r = 2989(1)$ kOe) with linewidth $\Delta H_{pp} = 644(2)$ kOe. The resonance field ($\Delta H_r/\Delta T$) gradient for the PBT-block-PTMO polymer containing 0.25 wt. % of Ni strongly depended on temperature with the following values in different temperature ranges: from 44 to 295 K – $\Delta H_r/\Delta T = 2.4$ kOe/K, (1.1 kOe/K for 0.1 wt. % of Ni [1]) and from 19 to 35 K – $\Delta H_r/\Delta T = 84.7$ kOe/K (70.7 kOe/K for 0.1 wt. % of Ni [1]). The internal magnetic

field strongly increased with the decreasing temperature and concentration of magnetic nanoparticles. A strong temperature dependence of the linewidth as well as some other anomalies in the FMR line intensity were registered.

The static magnetic susceptibility of Ni–C ferromagnetic nanopowders and the PBT-block-PTMO polymer samples with Ni nanoparticles was investigated by the Faraday balance technique in the 100–400 K temperature and 1 – 10 kOe magnetic field range. The PBT-block-PTMO polymer samples containing 0.1 and 0.25 wt. % of Ni showed approximately a linear dependence of the magnetic susceptibility *vs* a reciprocal magnetic field what could be taken as evidence of their superparamagnetic properties. The magnetic susceptibility for both samples showed a temperature dependence similar to bulk Ni. Nevertheless, the temperature dependence in a high temperature range suggested that the process of reorientation of magnetic nanoparticles strongly depended on the matrix (polymer – glass transition). The following $\Delta\chi/\Delta T$ gradient values were obtained: $\Delta\chi/\Delta T$ (at $T > 265$ K) = $2.2 \cdot 10^{-9}$ emu/g·K, $\Delta\chi/\Delta T$ (at $T < 265$ K) = $0.5 \cdot 10^{-9}$ emu/g·K for the polymer sample containing 0.25 wt. % of nickel and $\Delta\chi/\Delta T$ (at $T > 265$ K) = $2.1 \cdot 10^{-9}$ emu/g·K, $\Delta\chi/\Delta T$ (at $T < 265$ K) = $1.6 \cdot 10^{-9}$ emu/g·K for the polymer sample containing 0.1 wt. % of nickel.

The peculiarities of the FMR spectra and the static magnetic properties of the PBT-block-PTMO polymer samples containing 0.1 and 0.25 wt. % of Ni are considered and discussed.

References

[1] N. Guskos, M. Maryniak, J. Typek, P. Podsiadły, U. Narkiewicz, E. Senderek, and Z. Rosłaniec, to be published.

Spectroscopic Investigations of New Class of Rare-Earth and Zinc/Cadmium Tungstates and Molybdate-Tungstates

S. M. Kaczmarek¹, E. Tomaszewicz², H. Fuks¹

¹ *West Pomeranian University of Technology
Institute of Physics
Al. Piastów 17, 70-310 Szczecin, Poland*

² *West Pomeranian University of Technology
Department of Inorganic and Analytical Chemistry
Al. Piastów 42, 71-065 Szczecin, Poland*

In the last decades, a large number of tungstates and molybdates of rare-earth metals have been extensively investigated. In most cases, the emission of rare earth ions is due to optical transitions within the $4f$ orbitals and their $f-f$ emission spectra consist of sharp lines. The $f-f$ transitions in RE^{3+} ions have found practical applications in laser host materials in quantum electronics, phosphor materials used in fluorescent lamps and scintillators in medical devices.

Our earlier studies concerning a reactivity zinc tungstate (wolframite type structure) with rare-earth metal tungstates RE_2WO_6 ($RE = Y, Nd, Sm-Ho$) showed the existence of a new series of zinc and rare-earth metal tungstates with the formula $ZnRE_4W_3O_{16}$ [1]. These compounds were synthesized by high-temperature solid-state reaction according to the following equation:



The obtained compounds crystallized in the orthorombic system and melted incongruently or decomposed in the solid state in temperatures above 1250°C [1].

In turn, new zinc and rare-earth metal molybdate-tungstates $ZnRE_2MoWO_{10}$ ($RE = Sm, Eu, Gd, Dy$) were prepared by a conventional solid-state reaction between $ZnWO_4$ and RE_2MoO_6 mixed at the molar ratio of 1:1 [2]. The obtained compounds crystallized in the monoclinic system and melted incongruently within the temperature range of 1016–1033°C [2].

Very interesting magnetic and luminescent properties were shown by new cadmium and rare-earth metal tungstates [3–5]. The $Cd_{0.25}RE_{0.50}\square_{0.25}WO_4$ compounds ($RE = Nd, Sm, Eu, Gd$; \square – randomly distributed vacancies in the cation sublattice) crystallized in a scheelite type structure and were obtained by heating equimolar $RE_2W_2O_9/CdWO_4$ mixtures in air [3]. The double tungstates with the general formula $CdRE_2W_2O_{10}$ ($RE = Y, Pr, Nd, Sm-Er$) were obtained from $CdWO_4$ and an adequate RE_2WO_6 through a solid-state reaction [4,5]. $CdPr_2W_2O_{10}$ crystallized

in the orthorhombic system [5], while the other cadmium and rare-earth tungstates $\text{CdRE}_2\text{W}_2\text{O}_{10}$ crystallized in the monoclinic system [4].

In this work EPR and luminescent properties of the some above-mentioned compounds were studied and analyzed.

References

- [1] E. Tomaszewicz, *Solid State Sci.*, 8 (2006) 508
- [2] E. Tomaszewicz, G. Dąbrowska, *J. Therm. Anal. Cal.*, 94 (2008) 189
- [3] E. Tomaszewicz, S. M. Kaczmarek, H. Fuks, accepted for publication in *J. Rare Earth*
- [4] E. Tomaszewicz, S. M. Kaczmarek, accepted for publication in *J. Opt. Adv. Mat.*
- [5] E. Tomaszewicz, *J. Therm. Anal. Cal.*, 93 (2008) 711

Glassy Dynamics and Glass Transition of Polymer Nanometer Thin Films

T. Kanaya

*Institute for Chemical Research, Kyoto University
Uji, Kyoto-fu 611-0011, Japan*

Confined glass-forming materials in nanometer thin films show very different properties from bulk such as thermal and mechanical ones. Their properties are very interesting and important from not only scientific but also industrial points of view because they are related to important phenomena such as surface friction, adhesion, surface coating. Hence, confined systems are one of the current topics in condensed matter physics as well as polymer physics.

We studied polystyrene (PS) thin films by X-ray and neutron reflectivity [1–3] and found that glass transition temperature T_g decreased with film thickness below about 40 nm, there existed ultra-slow relaxation process in thin films, and thermal expansivity in glassy states decreased with film thickness.

In order to understand the glassy dynamics and the glass transition mechanism in thin films, we also studied dynamics of PS thin films (20–100 nm) by inelastic neutron scattering (INS) [4–7]. In the meV region we found that mean square displacement $\langle u^2 \rangle$ as well as the density of phonon states $G(\omega)$ decreased with the film thickness below about 100 nm. We also studied dynamic heterogeneity of the glassy thin films in terms of non-Gaussian parameter and found that it increased with decreasing the film thickness below about 40 nm. This has been assigned to the dynamic heterogeneity of the thin films. In the μ eV region, we evaluated the glass transition temperature from the mean square displacement $\langle u^2 \rangle$. As the film thickness decreased, the glass transition temperature thus evaluated increased. This observation completely contradicts the results revealed by X-ray and neutron reflectivity, where T_g decreased with film thickness [1–3].

In the conference we will discuss the molecular origin of these anomalous properties of PS thin films in terms of dynamic heterogeneity of polymer thin films.

References

- [1] T. Kanaya, T. Miyazaki, H. Watanabe, K. Nishida, H. Yamano, S. Tasaki, D. Bucknall, *Polymer*, **38**, 3769 (2003)
- [2] T. Miyazaki, K. Nishida, T. Kanaya, *PRE*, **69**, 022802 (2004)
- [3] T. Miyazaki, K. Nishida, T. Kanaya, *PRE*, **69**, 061803 (2004)
- [4] R. Inoue, T. Kanaya, K. Nishida, I. Tsukushi, K. Shibata, *PRL*, **95**, 56102 (2005)
- [5] R. Inoue, T. Kanaya, K. Nishida, I. Tsukushi, K. Shibata, *PRE*, **74**, 021801 (2006)
- [6] R. Inoue, T. Kanaya, K. Nishida, I. Tsukushi I, J. Taylor, S. Levett, B. Gabrys, *EPJE*, **24**, 55 (2007)
- [7] R. Inoue, T. Kanaya, K. Nishida, I. Tsukushi, K. Shibata, *PRE*, **77**, 032801 (2008)

Nanowire-based Spintronics

O. Kazakova

*National Physical Laboratory
Hampton Road Teddington, Middlesex TW11 0LW, United Kingdom*

Modern electronics in its rapid development towards even higher-speed digital circuits and ever diminishing transistor size still vastly relies on semiconductor heterostructures. Nevertheless novel materials become increasingly important in the view of sustaining the Moore’s law. One of these emerging approaches is to use diluted magnetic semiconductors (DMS). The search for an ideal DMS material with tunable ferromagnetic behavior is being actively pursued for realization of spintronics devices. In such materials a Curie temperature, T_c , far in excess of 300 K is essential for practical applications. Besides they should be compatible with conventional silicon technology to have a chance of rapid rollout. From this point of view, magnetically doped group-IV semiconductors (Ge and Si) would be ideal candidates. Room-temperature ferromagnetism in $\text{Ge}_{1-x}\text{Mn}_x$ [1] and $\text{Si}_{1-x}\text{Mn}_x$ [2] nanowires and nanocolumns [3] was recently demonstrated and a perfect dilution of Mn ions in the host was proven [1]. Germanium is an especially attractive material with high carrier mobility and hence ideally suitable for ultra-high-speed electronics.

In this talk we summarise our recent experimental results on magnetic properties of $\text{Ge}_{1-x}\text{Mn}_x$ nanowires and emphasise the important role of dimensionality in spin-dependent scattering and dynamic magnetic properties of DMS materials. We also present our results on realization of a first field effect transistor based on a $\text{Ge}_{1-x}\text{Mn}_x$ nanowire [4]. Integration of such nanowires may eventually provide a route towards smaller, lighter but still more powerful and faster computers, mobile phones and music players.

References

- [1] O. Kazakova, *et al.*, *Phys. Rev. B*, 72, (2005) 094415
- [2] M. Jamet, *et al.*, *Nature Materials*, 5, (2006) 653
- [3] H. W. Wu, *et al.*, *Appl. Phys. Lett.*, 90, (2007) 043121
- [4] M. I. van der Meulen, *et al.*, *Nano Lett.*, 9, 50 (2009)

Magnetic Properties of NiFe_2O_4 Nanoparticles

S. P. Kruchinin¹, A. Zolotovsky²

¹ *Bogolyubov Institute for Theoretical Physics, NASU
Kiev, 03143, Ukraine*

² *Lashkaryov Institute of Semiconductor Physics
Kiev, Ukraine*

The magnetic properties of nanoparticles of nickel ferrite, NiFe_2O_4 , have been recently investigated experimentally. In the present lecture we consider the theory of the physical properties of such nanoparticles. In particular, we investigated the band structure and density of states of the NiFe_2O_4 nanoparticles. We also studied their magnetic properties and size effects using the renormalization group approach.

XAFS in Biotechnology: Studies of Malaria Pigment Substitute in Reaction with Chloroquine

K. Ławniczak-Jabłońska¹, M. S. Walczak¹, A. Wolska¹,
M. Sikora^{2,3}, A. Sienkiewicz⁴, L. Suarez⁵,
A. Kosar⁵, M. J. Bellemare⁵, D. S. Bohle⁵

¹*Institute of Physics, Polish Academy of Sciences
Al. Lotników 32/46, 02-668 Warsaw, Poland*

²*Faculty of Physics and Applied Computer Science
AGH University of Science and Technology
Al. Mickiewicza 30, 30-059 Cracow, Poland*

³*European Synchrotron Radiation Facility
BP 220, 38043 Grenoble, France*

⁴*Institute of Physics of Complex Matter
Ecole Polytechnique Fédérale de Lausanne
Lausanne, CH-1015, Switzerland*

⁵*Department of Chemistry, McGill University
801 Sherbrooke Street West, Montreal, Canada*

The X-ray absorption fine structure (XAFS) analysis is a powerful technique to determine the local atomic structure around a given atom. This information can be very useful for conclusions about the position of a particular atom in a crystal net in case of dopants in a crystalline matrix or its chemical bonding. Moreover, it helps in resolving the phase contents in complex composites or minerals. In case of materials with a high level of disorder like e.g. natural chitosan polymers used as heavy metal sorbents it can be used to determine the metal bonding inside the polymer. In the present lecture the application of XAFS for the study of liquids will be presented. It will be shown how to determine the influence of a given solvent on the compound in a solution, and next, the influence of this compound on specific chemicals used in medical treatment will be found out.

Knowing that malaria remains the world’s most prevalent disease which causes severe health problems particularly in African and Asian countries, an example of using the XAFS technique for a problem related to this disease will be demonstrated. The most severe form of malaria is caused by the *Plasmodium falciparum* (Pf) parasite. The intraerythrocytic stage of Pf involves hemoglobin proteolysis and detoxify heme into an inert crystalline material, called malarial pigment or hemozoin. The crystal structure of hemozoin has been solved by X-ray powder diffraction in recent years and its synthetic analogue, beta-hematin, has been synthesized. The ferriprotoporfiryn IX is believed to be a target for commonly used antimalarial drugs but its interactions

are still not understood on the molecular level. In the presented work we are especially interested in drug-induced perturbations of structures of a soluble beta-hematin-like compound, iron(III) (meso-porphyrin-IX anhydride) called mesohematin. Similarly to its insoluble parent compound, beta-hematin, this compound is also built of dimers which was confirmed by the EXAFS analysis. The XAS measurements on a frozen sample of mesohematin in a solution were performed at ESRF (station ID26). Two kinds of solvents were tested: dimethylsulfoxide and acetic acid. In the case of the latter pure acetic acid and acetic acid with water with a volume ratio of 30:1 and 15:1, respectively were used as solvents. The high resolution XANES and EXAFS spectra on the iron K-edge enabled us to reveal the differences in the local environment of Fe atoms inside a mesohematin structure in investigated solutions before and after the chloroquine drug addition.

Acknowledgements

This work was supported by research grant N20205332/1197 and special project ESRF/73/2006 from the Ministry of Science and Higher Education.

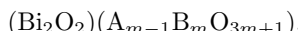
Phonon Properties of Nanocrystalline Bismuth Layered Ferroelectrics

M. Mączka¹, L. Macalik¹, P. E. Tomaszewski¹,
L. Kępiński¹, J. Hanuza^{1,2}

¹*Institute of Low Temperature and Structure Research
Polish Academy of Sciences, P. O. Box 1410, 50-950 Wrocław 2, Poland*

²*Department of Bioorganic Chemistry, Faculty of Industry and Economics
University of Economics, ul. Komandorska 118/120, 53-345, Wrocław, Poland*

Bismuth layered compounds (Aurivillius family) of general formula



where A = Na, K, Ca, Sr, Ba, Pb etc. and B = W, Ta, Nb, Ti etc. [1], have received much attention for device applications. For instance, these compounds are important candidates for the development of ferroelectric random access memories [2]. They constitute also an important class of oxide anion conductors [1]. Recently, Bi₂WO₆ and Bi₂MoO₆ have been found to be excellent photocatalytic materials and solar-energy conversion materials [3,4].

The change in crystallite size may lead to significant structural changes, for instance to stabilization of the high-temperature phase or even the appearance of new phases not observed for the bulk material [5,6]. Although a number of papers have been published reporting synthesis of nanocrystalline bismuth layered ferroelectrics, no attempts have been made to investigate the dependence between the crystallite size and the structure and phonon properties for $m = 1$ members of this family of compounds. Therefore, we decided to perform such studies for Bi₂WO₆ and Bi₂MoO₆. In particular, we used Raman and IR spectroscopies as tools for structural investigations since these techniques were shown to be very useful in studies of nanocrystalline materials. We will show that the phonon and structural properties of these compounds exhibit very significant changes with a decrease in the crystallite size which must have a significant impact on their photocatalytic, ionic conductivity and ferroelectric properties.

References

- [1] M. S. Islam, S. Lazure, R. N. Vannier, G. Nowogrocki and G. Mairesse, *J. Mat. Chem.*, 1998, **8**, 655
- [2] Y. Noguchi, K. Murata and M. Miyayama, *Appl. Phys. Lett.*, 2006, **89**, 242916
- [3] L. Zhang, W. Wang, L. Zhou and H. Xu, *Small*, 2007, **3**, 1618
- [4] H. Li, C. Liu, K. Li, H. Wang, J. Mater. Sci. 2007, **43**, 7026
- [5] Y. Shiratori, A. Magrez, J. Dornseiffer, F.-H. Haegel, C. Pithan and R. Waser, *J. Phys. Chem.*, 2005, **109**, 20122
- [6] K. Hermanowicz, M. Mączka, P. E. Tomaszewski, L. Krajczyk, J. Hanuza and J. Baran, *J. Nanosci. Nanotechnol.*, 2008, **8**, 1

Vertically Aligned Carbon Nanofibers as Nanotools for Cellular Interfacing

A. V. Melechko¹, T. E. McKnight²

¹ *Materials Science and Engineering Department
North Carolina State University, Raleigh, NC 27695, USA*

² *The Measurement Science and Systems Engineering Division
Oak Ridge National Laboratory, Oak Ridge, TN 37831, USA*

The advances in synthesis of vertically aligned carbon nanofibers and development of methods to integrate them into functional multiscale structures opened new possibilities to exploit the properties of carbon nanofibers in interfacing with live cells and tissues. Most significantly, the geometry and dimensions of VACNFs make them suitable for nondestructively penetrating cell membranes and probing or modifying cell function; the side wall chemistry makes them amenable to a wide variety of functionalization strategies, turning them from simple graphitic sticks into “smart carbons”. The efficient electron transport across the sidewalls and acceptable electrical conductivity makes them suitable for interfacing electrogenic cells and nanoscale probes for electroanalyticals on a level of a single cell. Two implementations of a nanostructured interface to live systems will be presented. Impalefection, or transfection by impalement, is VACNF-based gene delivery method that relies on both mechanical ability of nanofibers to penetrate nuclear domain and their chemical functionality to allow DNA attachment (Figure 1). Neuronal interface is based on combining VACNF geometry with their electrical properties and holds a promise to significantly impact the fields of electrophysiology and neuroscience by enabling multimode recordings (electrical and neurotransmitter) at high spatial resolution.

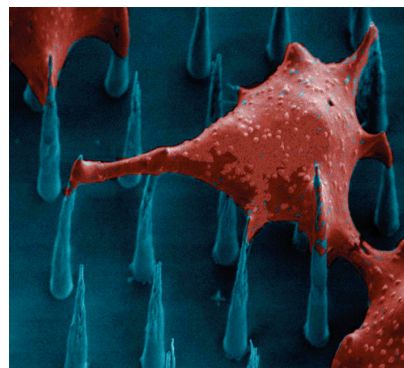


Figure 1: SEM image of Chinese hamster ovary cells impalefected with VACNFs

Surface Corrugation, Morphology and Electronic Structure of Exfoliated Graphene: a LEEM, Micro-LEED and Micro-ARPES Study

A. Locatelli¹, K. R. Knox^{2,3}, D. Cvetko^{4,5},
T. O. Mentes¹, M. A. Niño¹, S. Wang⁶,
M. B. Yilmaz³, P. Kim², R. M. Osgood Jr.², A. Morgante^{4,7}

¹*Elettra – Sincrotrone Trieste S.C.p.A., 34012 Basovizza, Trieste, Italy*

²*Department of Physics, Columbia University
New York, New York 10027, USA*

³*3Department of Applied Physics, Columbia University
New York, New York 10027, USA*

⁴*Laboratorio TASC-INFN-CNR, 34012 Basovizza, Trieste, Italy*

⁵*Faculty for Mathematics and Physics, University of Ljubljana
Ljubljana, Slovenia*

⁶*Department of Physics, Renmin University of China, Beijing, P. R. China*

⁷*Department of Physics, Trieste University, Trieste, Italy*

The recent availability of exfoliated graphene sheets has opened unprecedented opportunities for the study of this intriguing material and its unique physical properties. Although transport measurements are typically conducted on exfoliated graphene, the microscopic size of the flakes impedes access to its electronic structure using laterally averaging photoelectron spectroscopy. Synchrotron-based spectromicroscopy offers a powerful means to overcome this problem and enable their experimental investigation.

Our study reveals the morphology and electronic structure of suspended and SiO₂ supported exfoliated single and multi-layer graphene. Graphene samples were probed up to mesoscopic length scales using an array of complementary photon and electron probes operated in a microscopy mode, namely low energy electron microscopy (LEEM) micro-spot low energy electron diffraction (μ -LEED), and micro-spot angle resolved photoelectron spectroscopy (μ -ARPES). Our observations support the picture that ultra-thin SiO₂ supported graphene layers partially conform to the underlying substrate. They reveal that the interaction energy at the SiO₂ interface can effectively induce a significant deformation in the graphene stack up to thicknesses of several layers. An inverse dependence proportionality between thickness (number layers) and degree of corrugation has been found. Surface corrugation gives rise to characteristic diffraction patterns of low energy electrons, and also strongly influences the ARPES spectra [1]. Compared to supported flakes, suspended graphene displays a much improved planarity. In particular, the smoothness of suspended bilayers is comparable to that of thick graphite films, producing very sharp diffraction patterns.

Such morphology could correlate with the significantly improved transport properties of suspended graphene devices [2].

References

- [1] K. R. Knox, S. Wang, A. Morgante, D. Cvetko, A. Locatelli, T. O. Mentes, M. A. Niño, P. Kim, and R. M. Osgood Jr. *Phys. Rev. B* **78** (08) 201408
- [2] K. I. Bolotin, K. J. Sikes, Z. Jiang, G. Fudenberg, J. Hone, P. Kim, H. L. Stormer *Solid State Communications* **146** (08) 351

Phase Diagrams and Cluster Structure Before Solidification

S. Mudry

*Ivan Franko National University of L’viv, Physics of Metal Department
Kyrylo and Mephodiy str., 8, Ua-79005 Lviv, Ukraine
mudry@physics.wups.lviv.ua*

It is known that the liquid-solid phase transition is accompanied by disorder- order changes in the atomic arrangement. Numerous studies of such transition by means of theoretical and experimental methods have yielded a lot information about the thermodynamic and kinetic conditions of this transformation, but the understanding of these processes, occurring just before solidification is scarce. Moreover, the assumption about the existence of clusters as main structural units in a liquid state needs more motivation and detail studying.

Most information about the behaviour of liquid alloys just before solidification is commonly taken from equilibrium phase diagrams which are established for most binary systems. Unfortunately, to date there has been no information on the interrelation between the kind of phase diagram and the cluster structure in a liquid state before solidification. Studying of such interrelation is also important from the viewpoint of many technologies dealing with the nanoscale structure formation.

In this work, the results of features concerning a cluster structure in molten binary alloys with a different kind of a phase diagram are presented. Four groups of phase diagrams were studied: eutectic, monotectic, systems with chemical compounds and systems with unlimited solubility in liquid and solid states. The cluster structure parameters were obtained by means of X-ray diffraction and viscosity measurements. It is shown that the chemical ordering in clusters, their size and temperature dependence are correlated with the “liquidus” curve profile in an equilibrium phase diagram.

Systematic Study of Synthesis and Self-assembled Morphology of Silver Triblock Copolymer Nanocomposite

M. Mukherjee, A. K. M. Maidul Islam

*Surface Physics Division, Saha Institute of Nuclear Physics
1/AF, Bidhannagar, Saltlake, Kolkata-64, India*

Preparation of silver nanoparticles can be achieved from a silver ammonia complex, $[\text{Ag}(\text{NH}_3)_2]^+$ in aqueous solution of a hydroxyl terminated amphiphilic tri-block copolymer of poly(ethylene oxide)-poly(propylene oxide)-poly(ethylene oxide). The conventional chemical reducing and stabilizing agents are not necessary in this method. The tri-block copolymers with a long hydrophilic chain are amphiphilic in nature and can act as reductants as well as colloidal stabilizers and are very efficient in both functions.

It is known that PEO-PPO-PEO in aqueous solution is strongly thermo-responsive. In the preset study the effect of temperature on formation and stabilization of silver nanoparticles was investigated systematically. Real time UV-Vis and Dynamic Light Scattering spectroscopy was used to monitor the particle growth at different temperatures in the solution stage. The size and the distribution of nanoparticles were investigated using TEM. A bimodal distribution of particles was observed at lower temperatures. At intermediate temperatures particles of a very small size with a narrow distribution were achieved. At higher temperatures the particle size increased and the monodispersity was lost.

Self-assembly thin films from a silver polymer composite were prepared by dip coating on silicon substrates. The morphology of the films prepared at different temperatures on hydrophilic and hydrophobic substrates was studied using SEM and angle resolved XPS. From the XPS analysis we find that the reduction of silver ions to silver nanoparticles follows different oxidation steps of poly (ethylene oxide) at different temperatures. We will discuss the mechanisms of the nanoparticle growth and structural aspects of the thin films formed by the self-assembly of the polymer silver nanocomposite.

Removal of SO₂ from Gases on Carbon Materials

U. Narkiewicz, A. Pietrasz

*Institute of Chemical and Environmental Engineering
 West Pomeranian University of Technology
 ul. Pułaskiego 10, 70-322 Szczecin, Poland*

The aim of the work is to describe a capability of active carbon CARBON L-2-4 (AC) and nanocarbon (NC) materials containing iron nanoparticles to continuously remove SO₂ from inert atmosphere.

A vertical glass tubular reactor packed with AC or NC was used to study the conversion of SO₂ (0,25% and 0,8%) into H₂SO₄ in the presence of O₂, N₂ and H₂O, in the temperature range of 30–80°C. The process of SO₂ removal was carried out on a dry catalyst and on a catalyst wetted with H₂O carbon.

Carbon nanomaterials containing iron nanoparticles (NC) were synthesised using a CVD method – through catalytic decomposition of ethylene on nanocrystalline iron.

The obtained results (changes of the outlet SO₂ concentration with time) for both kind of catalysts are shown in the figures below.

The level of a steady-state SO₂ concentration at the reactor outlet increases with the increasing inlet SO₂ concentration and decreases with the increasing concentration of O₂, N₂ as well as H₂O. The effectiveness of SO₂ removal using dry active carbon (two-phase system, Figure 1) at lower temperatures is better than in the case of wetted carbon (three-phase system, Figure 2). In the temperature 60°C and above the effectiveness of SO₂ removal is better on wetted activated carbon (Figure 2) than on the dry one (Figure 1). The best effectiveness of SO₂ removal for dry carbon is reached in the temperature of 30°C, however the best results for wetted carbon are

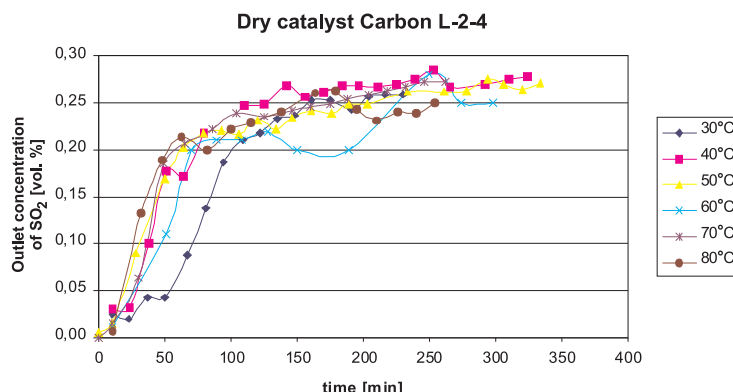


Figure 1: Changes of outlet SO₂ concentration in the temperature range 30–80°C for dry catalyst Carbon L-2-4

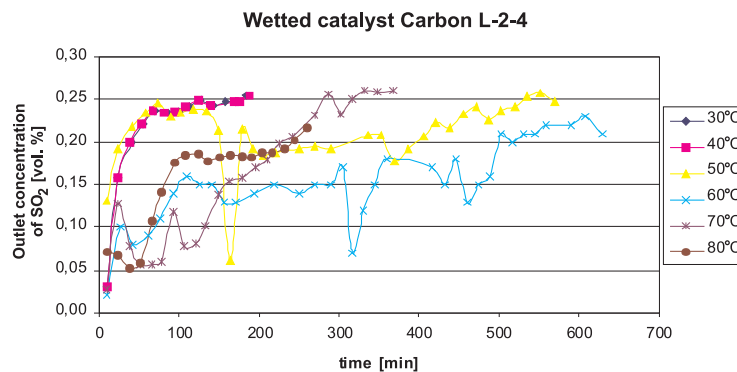


Figure 2: Changes of outlet SO₂ concentration in the temperature range 30–80°C for wetted catalyst Carbon L-2-4

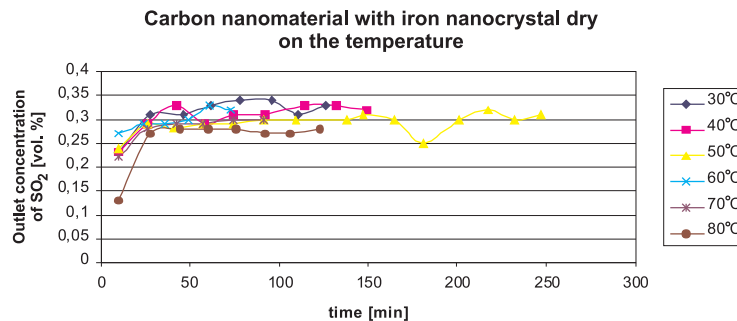


Figure 3: Changes of outlet SO₂ concentration in the temperature range 30–80°C for dry NC catalyst

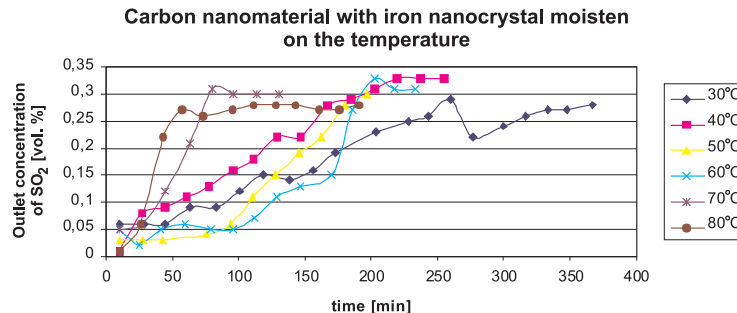


Figure 4: Changes of outlet SO₂ concentration in the temperature range 30–80°C for wetted NC catalyst

obtained at 70°C. In the case of a nanocarbon material, the removal of SO₂ is more effective in the three-phase system (wetted catalyst, Figure 4) than in case of the two-phase system (Figure 3) and it is more effective at lower temperatures. In the case of this catalyst the initial reduction with hydrogen is planned, to increase the free area of iron nanoparticles. Further experiments at higher temperatures (100–300°C) are planned as well.

Scattering of Electrons by a Two-dimensional Parabolic Repeller in a Magnetic Field

G. J. Papadopoulos

*Department of Physics, Solid State Physics Section, University of Athens
Panepistimiopolis, Athens 157 84, Zografos Athens, Greece*

The distributions for the charge and current density of an electron incident on a 2D symmetric parabolic repeller under the influence of a perpendicular magnetic field are obtained, utilizing the evolving wave function stemming from a wave packet locating the particle at a certain distance from the barrier center and carrying the initial electron momentum targeting the center. The corresponding charge and current densities are, then, derived as functions of space and time. There follow numerical calculations with initial expected energies below the barrier height, seen by the particle at its initial position, as well as for various values of the magnetic field and the barrier strength. For small magnetic fields the charge and current density spatial and temporal distributions are mildly affected by the field. However, for large magnetic fields capable of superseding the repelling effect of the barrier through the cyclotronic motion there appear interesting effects. E.g. the charge and density distributions at a given location rise from and fall asymptotically with time to zero for small magnetic fields, while for large enough, higher than a critical value, there appears repetition in rise and fall with a gap of almost zero charge density followed by reversal in the current density components. The frequency of the above repetitions increases with increase in the magnetic field. Finally, the results, obtained, may be of some use in relation to experiments involving tunneling arrangements with extended antidots in a perpendicular magnetic field.

Luminescent Solar Concentrators Cased on Hybrid Materials

R. Reisfeld^{*}, T. Saraidarov, V. Levchenko

*Department of Inorganic Chemistry, The Hebrew University
Jerusalem, 91904, Israel*

**Enrique Berman Professor of Solar Energy
The Hebrew University of Jerusalem*

In recent years because of the rapid increase of the cost of fuel there is renewed great interest in solar energy and specifically in Luminescent Solar Concentrators. Luminescent Solar Concentrator (LSC) in which the solar light falling on a large area of luminescent plate concentrates on a small area of a plate edge allows to decrease the cost of the photovoltaic electricity by permitting to use smaller amounts of costly photovoltaic cells. Limitations to produce effective stable LSC still exist and these have to be improved. We present here a model by which the plate efficiency will be increased by incorporate of stable fluorescent dye in conjunction with plasmons.

Confinement Effects in Polymer Systems: Monte Carlo Simulations

P. Romiszowski

*Department of Chemistry, University of Warsaw
Pasteura 1, 02-093 Warszawa, Poland*

The properties of a polymer chain confined to a slit, a tube or a spherical pore are quite different from those of a chain in a bulk. The changes of polymer properties in confinement are important because such systems have such practical applications as chromatography, colloidal stabilization, lubrication etc. A study of the influence of a confinement on polymer chains is a theoretical challenge because the presence of confining surfaces changes significantly the properties of the system. The presented study was an investigation of polymer molecules located between two parallel and impenetrable surfaces. The properties of the chains depend strongly on the width of the slit. Also the case of confinement between the adsorbing surfaces is shown and discussed. The chains were constructed of identical segments and were restricted to knots of a simple cubic lattice. The properties of the model chains were determined by means of Monte Carlo simulations with a sampling algorithm based on local changes of chain conformation. The differences and similarities in the structure for different adsorption regimes and the slit size were shown and discussed. It was observed that at certain conditions the polymer chain was adsorbed at one of the confining surfaces, and then, after a certain period of time, it detached from this surface and approached the opposite wall; this switch was repeated many times during the simulation run – a fragment of the trajectory is presented in Figure 1. The influence of the adsorption strength, the slit size and the chain length on the frequency of those jumps was determined. The mechanism of the chains motion during the switch was also shown. An analysis of the structures (trains, loops, tails and bridges) which can be found in a confined polymer system will be presented.

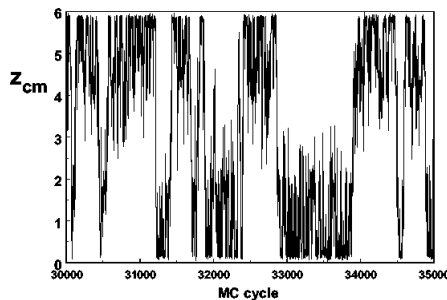


Figure 1: Plot of z-position of the center of mass of the polymer molecule located in the slit

Tailoring Thermal Expansivity in Cellular Solids

C. W. Smith

*NMA Palumbo, W Miller School of Engineering
Mathematics and Physical Sciences, University of Exeter
Exeter, EX4 4QF, UK*

c.w.smith@ex.ac.uk

The coefficient of thermal expansivity (CTE) is insensitive to structural disorder in monolithic materials and structures. Monolithic cellular solids such as honeycombs and foams are no different in this respect. The CTE of a multi-phase or composite materials, such as particulate filled polymers, is usually satisfactorily predicted by simple rule of mixtures type relationships, except however where there is significant internal ordering. In these cases CTE is not bounded by rule of mixtures type relations. Since cellular solids are not usually structured at atomistic size scales the differences between a material and a structure are ignored here. Examples of cellular solids which have been postulated include those formed from bi-material strips and wireframe constructs. None of these however have much potential as structural elements since they sacrifice much of their stiffness for extreme CTE values. A system of using internal constraints to force swapping of thermally driven distortion for thermally driven stress has been developed for scale independent truss-type structures, e.g. extruded 2D honeycombs or truss cores for sandwich panels. This system offers the possibility for tailored CTE (within some limits) but with near zero penalties in stiffness and weight. Such systems can be realised via standard current manufacturing techniques, at appropriate size scales. An overview of these systems, how they work, and their limitations will be presented.

White Organic Light Emitting Diodes for Super-thin Flat Panel Lighting

T. Tsuboi

*Faculty of Engineering, Kyoto Sangyo University
Kamigamo, Kyoto 603-8555, Japan*

Organic light emitting diode (OLED) generates electroluminescence (EL). This diode is currently used for flat panel displays including television monitor. The EL panels are manufactured by aligning three red, green, and blue OLED devices. Each of these mono-color OLEDs consists of thin films of cathode, electron injection layer, electron transporting layer, emitting layer, hole transporting layer, hole injection layer, and transparent anode. When voltage is applied to the OLED, electrons and holes are injected from cathode and anode, respectively, then molecular exciton is formed by recombination of electron and hole at the same single molecule in the emitting layer, giving rise to light emission (monomer exciton emission). Its color depends of the organic material in the emission layer.

Unlike such a mono-color OLEDs, white OLED generates blue to red multi-color emissions from a single device. The white OLED is one of the candidates for the next generation solid state lighting alternative to conventional incandescent bulbs and fluorescent lamps. White OLED makes possible lighting of low-cost power consumption, very light-weight, and flexibility. We review current science and technology of white OLEDs, and discuss their EL processes.

The white emission from a single OLED device is generated from (1) blue B-, green G-, and red R-emitting layers, (2) B- and R-emitting layers, or (3) single emitting layer which emits RGB or RB lights. Three or two emitting layers are stacked in the first two cases, while three or two different emitter dopants are doped in the same host material in the last case. In addition to the white emission by two or three monomer emissions, there is another white emission using exciplex. Exciplex is formed from two distinct molecules with one in the excited state and the other in the ground state, an electron donor (D) with low ionization potential and an electron acceptor (A) with high electron affinity, when D-located hole (D^+) approaches A-located electron (A^-). In this case white emission is generated by simultaneous emission from monomer and exciplex since the exciplex emission locates at lower energy of the monomer emission.

Fabrication of white OLEDs is made by mixing blue, green, and red emitting dopants in host material. This method gives rise to different degradation rates and phase segregation among the different dopants, resulting in instability of OLED device operation. Emission from excimer is used to avoid such a segregation. Excimer is formed from two same molecules with one in the excited state and the other in the ground state. When the dopant concentration is low, only monomer is formed, while both the monomer and excimer are formed with increasing concentration of the dopant. The excimer emission locates at the low energy of the monomer emission,

leading to white emission by adjusting the relative intensity ratio between the red excimer emission and the blue monomer emission. Besides the excimer method, dual or triple emission has been observed from single molecule with mixed ligand molecules in not only polymer but also small molecules.

We present the various techniques to obtain white emission suitable for lighting and discuss the advantage and disadvantage among them.

Interface Magnetization in Half-metallic Manganites: a Synchrotron Radiation Approach

A. Verna¹, B. A. Davidson¹, A. Yu. Petrov¹, A. Mirone²,
N. Mahne¹, A. Giglia¹, S. Nannarone^{1,3}

¹*Laboratorio Nazionale CNR-INFN TASC
Area Science Park, Basovizza S.S. 14 Km 163.5, 34012 Trieste, Italy*

²*European Synchrotron Radiation Facility
6 rue Jules Horowitz, 38043 Grenoble Cedex, France*

³*Dipartimento di Ingegneria dei Materiali e dell’Ambiente
Università di Modena e Reggio Emilia
Via Vignolese 905, 41100 Modena, Italy*

Transition metal manganites are from a theoretical point of view ideal materials for production of spintronic devices due to their intrinsic half-metallic behavior. Nevertheless, their performance as sources and collectors of spin-polarized currents is strongly weakened by the reduced magnetization shown by them at the interface with a non-magnetic material, the so called magnetic “dead layer” effect [1]. A detailed understanding of this detrimental mechanism, and of the strategies to exclude it, requires an accurate measurement of magnetization gradients with a spatial (vertical) resolution of a single monolayer. X-ray resonant magnetic scattering (XRMS) is the most innovative and promising technique to this aim [2]. First, the principles of this technique, based on the interference effects that occur when circularly polarized light is scattered by differently magnetized regions of the same sample are illustrated. Then, the application of XRMS in specular geometry to determine the magnetization profiles in titanate/manganite heterostructure is discussed. The presence of a sharp magnetic profile, and then of a completely nonmagnetic manganite region at a titanate/manganite interface, is easily identified by the presence of oscillations and a sign reversal in the XRMS signal as a function of an exchanged momentum: the oscillation period is inversely proportional to the dead layer thickness that can be measured with a unit cell (~ 4 Å) resolution. The presence of a smoothed magnetic profile and residual interfacial magnetization, instead, produces a decrease in the oscillation amplitude and alters the periodicity at a higher grazing angle. The application of this technique to the experimental determination of magnetic dead layers in an atomically engineered $\text{La}_{1-x}\text{Sr}_x\text{MnO}_3/\text{SrTiO}_3$ ultrathin heterostructure grown by oxygen-assisted molecular beam epitaxy is presented.

References

- [1] Yamada H, Ogawa Y, Ishii Y, Sato H, Kawasaki M, and Akoh H 2004 *Science* **305** 646
- [2] Freeland J W, Gray K E, Ozyuzer L, Berghuis P, Badica E, Kavich J, Zhengh H, and Mitchell J F 2005 *Nature Materials* **4** 62

Electronic Instabilities, Fluctuations and Charge Transport in Quantum Chains

H. Weitering^{1,2}

¹ *Department of Physics and Astronomy, The University of Tennessee Knoxville
Knoxville, TN 37931, U.S.A.*

² *Materials Science and Technology Division, Oak Ridge National Laboratory
Oak Ridge, TN 37831, U.S.A.*

One-dimensional quantum conductors have always captured the imagination of physicists. While a strictly one-dimensional material mostly remains a theoretical construct, a vast number of materials can be viewed as macroscopic ensembles of weakly-coupled quantum chains, making them interesting test cases for theoretical models and even some practical applications in nanotechnology. I will discuss the electronic properties of some quasi one-dimensional electronic materials grown on Si surfaces. Highlights include the self-assembly of indium atoms on Si(111) into a weakly-coupled two-dimensional array of parallel atom wires [1], and the formation of highly uniform YSi_2 nanowires on Si(100) [2]. The silicide nanowires exhibit electronic properties reminiscent of a multichannel one-dimensional conductor. These include the stepwise increase of the tunnel current as a function of tip bias in scanning tunneling microscopy and the appearance of a fluctuating charge-density-wave instability at low temperature, opening up a small band gap. The indium wires also undergo an insulator-metal transition. Here, we show that although these electronic instabilities arise from the low dimensional nature of these materials, they should not be attributed to Fermi surface nesting. Instead, the insulator-metal transition arises from dynamical fluctuations that are driven by lattice entropy, which is more consistent with an order-disorder transition. I will finally describe recent efforts in my group to utilize some of these nanowires in a nanoscale Coulter counter for the electrical read out of base pair sequences in DNA molecules.

References

- [1] C. Gonzalez, J. D. Guo, J. Ortega, F. Flores, and H. H. Weitering, *Phys. Rev. Lett.* **102**, 115501 (2009)
- [2] C. Zeng, P. R. C. Kent, T.-H. Kim, A. P. Li, and H. H. Weitering, *Nat. Mater.* **7**, 539 (2008)

Anomalous Mechanical Properties of Various Models in Two Dimensions

K. W. Wojciechowski

*Institute of Molecular Physics, Polish Academy of Sciences
M. Smoluchowskiego 17, 60-179 Poznań, Poland*

kww@man.poznan.pl

Mechanical properties of materials are crucial for various applications. Studies of relations between the interactions, structure and phenomena occurring in materials are required to design materials of desirable properties. Studies of simple models are of help in establishing and understanding such relations. Two-dimensional models are both simpler for solving and easier to visualize than their three-dimensional counterparts.

In this lecture a few two-dimensional models will be presented which were solved analytically, numerically, or by computer simulations. The models illustrate the mechanisms underlying various anomalous behaviour observed in certain real systems, like a negative Poisson’s ratio, negative thermal expansion, negative compressibility and other surprising effects.

ZnMgSSe/ZnSe/CdSe Quantum Dot Heterostructures for Green Laser Applications

G. P. Yablonskii¹, E. V. Lutsenko¹, S. V. Ivanov², I. V. Sedova²,
S. V. Sorokin², P. S. Kop’ev²

¹ Stepanov Institute of Physics of NASB
Independence Ave. 68, 220072 Minsk, Belarus

² Ioffe Physical Technical Institute
Polytekhnicheskaya 26, St. Petersburg 194021, Russia

Compact green semiconductor lasers with a long operation time can be used for numerous applications such as local networks, space-underwater communication, navigation, projection TV, etc. An overview of the main problems related to the development of such lasers based on different material systems will be given in the paper. Laser diodes (LDs) based on ZnSe heterostructures have up to now exhibited not a sufficient operation time of about 400 hours, although the reason for the slow degradation has been established to be due to the non-stable nitrogen acceptor in selenides. Another possibility to cover the green spectral region is an improvement of the growth technology of InGaN/InGaN quantum well (QW) heterostructures with a high In content, using mainly the advantages of homoepitaxy and a proper design of the laser structures. However, undoped ZnSe/ZnCdSe laser heterostructures with QWs or quantum dots (QDs) pumped by an electron beam or optically, using the radiation of a blue-violet III-N LD (laser converter), may compete successfully with the above approaches. It can be expected that the lifetime of such lasers will be much longer than that of II-VI LDs.

Our work is devoted to an elaboration of the growth technology and optical properties of the ZnMgSSe/ZnSSe/ZnSe/CdSe QD heterostructures with a low laser threshold. The structures were grown by molecular beam epitaxy on GaAs(100). In order to reach a low laser threshold, separate confinement double heterostructures (SC DH) of a special design and quality were optimized by using calculations of the optical confinement factor and determination of a feedback between the emission (laser) properties, structure and the growth technology of QD heterostructures. The active region of heterostructures comprises from one to nine (1–2)-nm-thick ZnSe QWs separated by thin ZnSSe barriers or ZnSe/ZnSSe superlattices (SL) for elastic stress compensation. A 2.5-monolayer-thick CdSe QD plane was incorporated into each QW. The 200-nm-thick ZnS_{0.15}Se_{0.85}/ZnSe SL waveguide was asymmetrical to place the active region in the maximum of the electromagnetic field of the fundamental mode. This waveguide was sandwiched between Zn_{0.88}Mg_{0.12}S_{0.16}Se_{0.84} bottom and cap cladding layers. Photoluminescence (PL) and laser parameters of optically pumped lasers cleaved from the heterostructures were investigated using excitation by a pulsed N₂ laser ($\lambda = 337.1$ nm, $\tau_p = 8$ ns, $P = 40$ kW), a CW HeCd laser

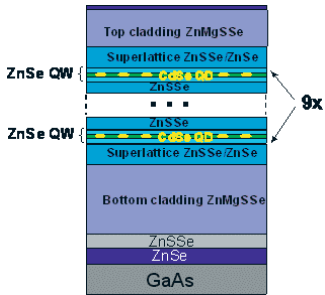


Figure 1: ZnMgSSe/ZnSSe/ZnSe/CdSe laser heterostructure design

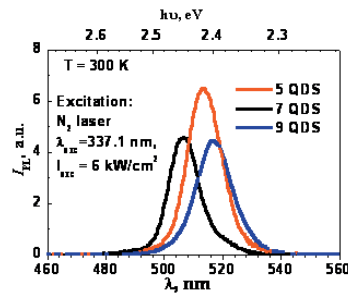


Figure 2: PL spectra of heterostructures with different QD plane numbers at high excitation intensity

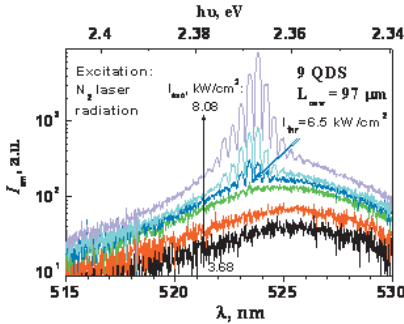


Figure 3: Emission spectra from the cavity edge as a function of I_{exc} of N_2 laser radiation

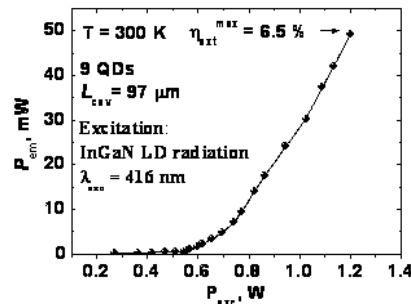


Figure 4: Laser converter pulse power as a function of the III-N LD excitation power

($\lambda = 325$ nm, $P = 15$ mW) and a commercial InGaN/GaN violet LD ($\lambda = 416$ nm, $\tau_p = 50$ ns, $P_{pulse\ max} = 2$ W).

The influence of the layer thickness, the number of the QD planes, the energy and intensity of the exciting light on the optical and laser properties of these heterostructure were studied. The PL spectra revealed the band maxima between 520 and 540 nm, while the laser spectra were positioned near 525 nm. The heterostructures with 5 electronically-coupled QD planes in the active region demonstrated higher PL efficiency and a lower laser threshold than those with 7 and 9 QD planes. A reduction of the ZnSe QW thickness and an increase in the thickness of the ZnSSe barrier led to a drop in the PL intensity. The laser emission exhibited TE polarization and lasing at a fundamental transversal mode. The laser threshold value for the cavity length of 680–630 μ m was 2.3 kW/cm², 2.8 kW/cm² and 3.5 kW/cm² for the structures with 5, 7 and 9 QD planes, respectively. The external laser quantum efficiency reached its maximum of 50% under the excitation by the N_2 laser for the laser structure with the active region comprising 5 QD planes. The first prototype of the laser converter

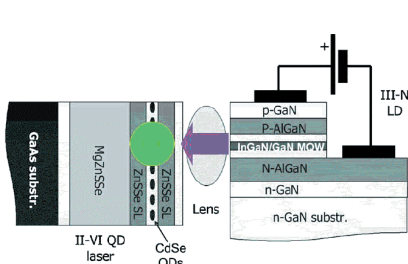


Figure 5: Sketch of the II-VI/III-N blue-green laser converter

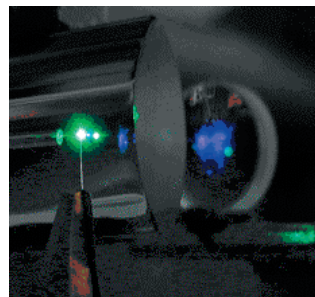


Figure 6: Photo of the ZnSe/CdSe green laser pumped by pulsed radiation of the violet InGaN LD

of the violet radiation of the InGaN/GaN QW pulsed LD into the green coherent emission of the optically pumped ZnSe/CdSe QD laser heterostructures was realized. The conversion quantum efficiency of violet (416 nm) into green emission was 8% for the active region with the 5 QD planes at room temperature.

The optical and laser properties of different ZnSe/CdSe QD heterostructures, as well as of the III-N/II-VI laser converter, are analyzed and possible directions of further investigations and development are discussed.

Surface Patterns Due to Step Flow Anisotropy Formed in Crystal Growth Process

F. Krzyżewski¹, M. Załuska-Kotur¹, S. Krukowski²

¹*Instytut of Physics, Polish Academy of Sciences*

²*Institute of High Pressure Physics (UNIPRESS), Polish Academy of Sciences*

The growth of a gallium nitride on a GaN(0001) surface is a process controlled by surface diffusion of Ga adatoms and occurs in an N-rich state for both MOVPE and HVPE growth conditions. In a supersaturated state two consecutive steps of a GaN(0001) surface have one or two broken bonds. As a result, their kinetics is different. The simplest model that describes a growing crystal of GaN has hexagonal symmetry, and one or two broken bonds for every second step orientation and for every second surface step, as well.

The results of crystal growth simulations for such a model show that depending on the terrace width the steps tend to group in a double step structure, or for thicker terraces, the steps form wave-like structures. The model behavior exactly reconstructs the effects that are observed experimentally.

ORAL COMMUNICATIONS

Optical Trapping of Carbon Nano-Tubes of Specific Spectral Characteristics

A. Ambrosio¹, V. Grossi², P. Maddalena¹

¹ *CNR-INFM CRS-COHERENTIA and Dipartimento di Scienze Fisiche
Complesso Universitario di Monte Sant’Angelo
Via Cintia, I-80126 Napoli, Italy*

² *Dipartimento di Fisica, Università degli Studi dell’Aquila
Via Vetoio 10, I-67010 Coppito (L’Aquila), Italy*

The two main challenges in carbon nanotube science are the synthesis of single-walled nanotubes (SWNTs) in high quantity and purity on the one hand and the availability of SWNTs with well defined properties, on the other hand [1]. The development of strategies for their property-controlled fabrication, sorting, and assembly has only been commenced. At present, e.g., there are no reliable methods reported which allow for sorting single SWNTs according to their chirality-dependent metallic or semiconducting (SC) character. Nevertheless, noticeable and enhanced photo-emissive [2], photoconductive [3] or nonlinear optical properties [4–6] promise to realize new added-value functions.

We plan to elaborate radically new optical functions fundamentally based on the properties of individual Single- (and Multi-) Walled Nano-Tubes (SWNTs/MWNTs) sorted in a sequential order versus their fundamental properties. This possibility is investigated by means of Holographic Optical Tweezers assisted by selective absorbing and photoluminescence properties of each nano-object. The nano-objects could be elaborated by optimised methods of homo and hetero atomic MWNT and SWNT. Furthermore, multiple and dynamic trapping is possible by introducing a Spatial Light Modulator into the Tweezers setup. This is a liquid crystal on silicon device that can turn a single laser beam into a multiple beam whose beams distribution can be turned with a rate of about 60 Hz. The setup is then equipped with a spectrograph in order to distinguish the spectroscopical fingerprints of the trapped object either by analysing the Raman spectrum or the photoluminescence.

Building-up optical functions linked to the fundamental character of a collection of sorted nano-objects will result from such a sort.

Acknowledgements

The authors are grateful to the European Collaborative Project “S-five” for financial support.

References

- [1] Dresselhaus M S et al. 2001 *CNT: Synthesis, structure, properties and applications* Springer
- [2] Lauret J et al. 2005 *Phys Rev. Lett.* 94 037405
- [3] Itkis M E et al. 2006 *Science* 312 413

- [4] Lecourt J B et al. 2005 *JNOPM* 14 427
- [5] Song Y W et al. 2005 *IEEE Photon. Techn. Lett.* 17 1623
- [6] Hagen A et al. 2005 *Phys Rev. Lett.* 95 197401

Nanoparticle Measurement: From Size Distribution and Shape to Advanced Characterisation

R. D. Boyd^a, A. Cuenat

*National Physical Laboratory
Teddington, Middlesex, TW11 0LW, United Kingdom*

^a *Robert.boyd@npl.co.uk*

To ensure the continuing development and safety of innovative nano materials and their related products, the core components (nanoparticles, tubes and fibres) need to be fully characterised in terms of their physical dimensions and chemical composition. This information will provide the size distribution, shape and structure of the consistent particles and of any agglomerates formed. It is important to have recognized sizing methods and reference materials in place; unfortunately no such procedures exist.

This presentation will form two parts. In the first we will present our results in determining the size and shape of standard spherical and non-spherical nanoparticles using several complementary techniques; electron and scanning probe microscopy (Figure 1) and dynamic light scattering. The strength and limitations of each technique will be highlighted.

In the second part, the application of advanced characterisation methods to determine the structure of individual particles and tubes will be described. In particular transmission electron microscopy (TEM), energy loss spectroscopy (EELS) and energy filtered TEM (EFTEM) will be demonstrated as providing unique information.

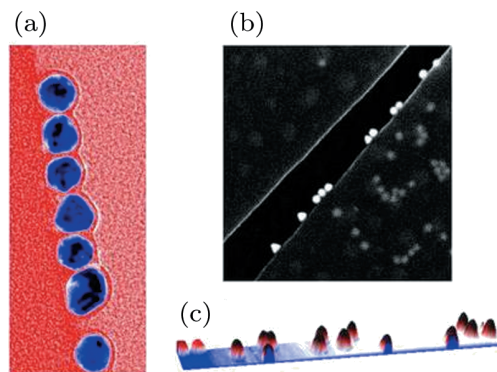


Figure 1: 30 nm gold nanoparticles imaged by (a) TEM, (b) SEM and (c) AFM

The aim is to demonstrate that selecting the correct technique to characterise a particular application is essential to obtain the relevant information and not to highlight the use of high performance instruments. Examples of which include core particle dimensions, extent of agglomeration and the structure and homogeneity of bespoke particles.

Trapping-Detrapping Fluctuations in Organic Space-Charge Layers

A. Carbone¹, C. Pennetta², L. Reggiani²

¹*Physics Department, Politecnico di Torino
Corso Duca degli Abruzzi 24, 10129 Torino, Italy*

²*Dipartimento di Ingegneria dell’Innovazione and CNISM
Università del Salento, 73100 Lecce, Italy*

Organic field-effect transistors (OFETs) and light-emitting diodes (OLEDs), organic solar cells and memories successfully compete with traditional electronic devices when the flexibility, large area, low cost and weight are the main requirements. The injection of charge carriers at molecule-metal interfaces plays a decisive role in the performance of organic semiconductor devices. Defect states drastically alter the injection mechanism, hence their origin and effect on the charge transfer across the interface are one of the main investigation issues. Charge carrier trapping-detrapping processes have been indeed recognized as a source of current instability and degradation of organic FETs.

Relative current spectral densities obtained on polyacenes have evidenced striking peaked behavior at voltages corresponding to the trap filling transition (TFT) between Ohmic (Ω) and Space Charge Limited Current (SCLC) regimes. These results have been interpreted as evidence for continuous percolation between the two regimes, considered as different electronic phases. Accordingly, at the TFT, the clustering of insulating regions should lead to a reduction in the ohmic paths.

The overall effect was expected to give a substantial increase in the noise in an analogy with the increasing of fluctuations near a structural phase transition. A complementary interpretation based on a trapping-detrapping fluctuation model can also explain such a sharp increase. The fraction of ionized traps obtained from the current-voltage characteristics is related to the relative current noise spectral density at the trap-filling transition. The agreement between theory and experiments validates the model and provides an estimate of the concentration and energy level of deep traps.

References

- [1] A. Carbone, B. K. Kotowska and D. Kotowski, Phys. Rev. Lett. **95**, 236601 (2005)
- [2] A. Carbone, B. K. Kotowska and D. Kotowski, Eur. Phys. J. B **50**, 77 (2006)
- [3] A. Carbone, B. K. Kotowska, D. Kotowski, AIP Conf. Proc. **922**, 267 (2007)
- [4] M. Tizzoni, A. Carbone, C. Pennetta, L. Reggiani, AIP Conf. Proc. **1129**, 109 (2009)

Size Control and Localised Growth of Si Nanowires on Silicon Oxide Substrates

P. Carelli¹, A. Di Gaspare¹, L. Di Gaspare², M. Giamatteo³,
A. Notargiacomo², E. Palange¹, S. Piersanti¹

¹ Dipartimento di Ingegneria Elettrica e dell’Informazione
Università dell’Aquila, 67040 Monteluco di Roio – L’Aquila, Italy

² Dipartimento di Fisica, Università Roma TRE
Via della Vasca Navale 84, 00146 Roma, Italy

³ Centro di Microscopia Elettronica
Università dell’Aquila, 67040 Monteluco di Roio – L’Aquila, Italy

The recent achievements in nanoscience regarding the understanding and tailoring of the physical properties of such nanostructures as semiconductor nanowires have had important implications in the implementation of novel devices. Thus, nanotechnology has grown exceptionally, especially in finding the best methods to fabricate electronic and optoelectronic devices at a nanometric scale. At present, nanotechnology has successfully demonstrated the feasibility of such individual nano-devices as nano-FET’s and nano-photodiodes that employ single nanostructures positioned on silicon oxide. As the best method to place and weld a large number of nanostructures on circuit locations, where they must operate, has not been found yet, a mixed top-down and bottom-up paradigm could be one of the most promising technique for

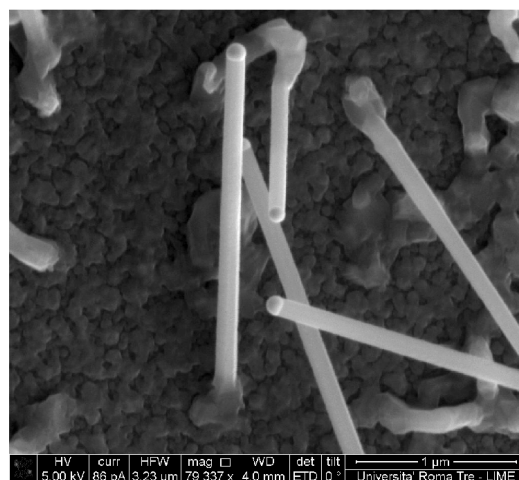


Figure 1: Example of nanowire of Si grown regularly on a matrix of gold dots

fabrication of arrays of nanodevices at the manufacturing level. In this communication the recent results on localized growths of high crystalline grade doped and undoped Si nanowires directly grown on SiO₂ films deposited on Si substrates are presented. The nanowires were grown by the Vapour-Liquid-Solid mechanism, assisted by a low pressure chemical vapour deposition and using gold nanodisks lithographically patterned on the SiO₂ film surface as the catalyst. The SEM and TEM analyses provided a detailed study on the crystalline properties, the size, growth rate and activation energy of nanowires as a function of the growth temperature and the dimension and mutual distances between the gold catalysts. To test the scalability of the technique, an appropriate sequence of sub-micrometric lithographic processes (spatial resolution less than 50 nm) was implemented to produce arrays of simple electrical nanodevices. The steps were: (a) growth of alignment Nb markers, (ii) partial etching of SiO₂ to obtain grooves capable of hosting a nanowire, (iii) growth of gold nanodisks close to the hosting grooves acting as the catalyst. Then, through a manipulation technique, each nanowire was arranged in the desired position. In the next lithographic step each nanowire was electrically contacted with four electrodes. This allowed accurate measurements of their electrical properties to be taken. This will be the first step to fabricate really usable devices based on nanowires.

Enhanced Quantum Efficiency of Silicon with Ge Quantum Dots

P. Castrucci¹, S. Del Gobbo¹, C. Scilletta¹, E. Speiser¹,
M. Scarselli¹, M. De Crescenzi¹, G. Amiard²,
A. Ronda², I. Berbezier²

¹*Dipartimento di Fisica, Unità CNISM, Università di Roma Tor Vergata
via della Ricerca Scientifica 1, 00133 Roma, Italy*

²*IM2NP CNRS 6137, Faculté des Sciences et Techniques
Campus de Saint Jerome, 13451 Marseille Cedex 20, France*

Nanomaterials offer exciting possibilities for photovoltaic applications because of the possibility of engineering their optical and electronic properties increasing the quantum confinement effects by tailoring the material size and the surface-to-volume ratio. In this research field, Ge nanodots have attracted much interest due to their possible applications as infrared photodetectors and waveguide systems [1] (and references therein).

Very few works have been dedicated to the use of the Ge nanostructures as devices for solar cells and have been focused on studying a possible enhancement of the quantum efficiency in the infrared part of the solar spectrum [2,3]. This is obtained by fabricating a stacking of several layers of Ge dots between p and n silicon films. In this way a p–i–n structure is built-up, where the intrinsic Ge dots form the heart of the whole system. An open problem is the actual influence of the Ge nanostructures on the alignment of the Ge Fermi level with those of the p and n silicon films, producing a cascade of electron-holes in two opposite directions. To shed some light on this point, we performed an experiment in which a single and homogeneous layer of Ge nanodots was grown on an ultrathin SiO₂ layer thermally grown on a Si(100) substrate n⁺ doped with As. Recently, in fact, we demonstrated that such a growth process produces a high density (2–3·10¹² of homogeneous Ge dots, quite spherical in shape [4,5]). We observed that while the bare substrate produced a low photocurrent upon illumination, the presence of the Ge dots induced a sizeable carrier generation that:

- a) involved both the electronic states of the Ge dots and the Si substrate,
- b) depended on the Ge dots size.

We interpret these experimental results as due to the ability of the Ge dots to induce a sizeable band bending at the silicon substrate interface thus producing a heterojunction behaving as an i–n solar cell.

Acknowledgements

P.C., M.S. and M.D.C thank the Italian Ministry of Foreign Affairs for financial support through Promotion and Cultural Cooperation Management.

References

- [1] Wang K L, Cha D, Liu J and Chen C 2007 *Proceedings of the IEEE* **95** 1866
- [2] Konle J, Presting H and Kibbel H 2003 *Physica E* **16** 596
- [3] Alguno A, Usami N, Ujihara T, Fujiwara K, Sasaki G, Nakajima K and Shiraki Y 2003 *Appl. Phys. Lett.* **83** 1258
- [4] Berbezier I, Karmous A, Ronda A, Sgarlata A, Balzarotti A, Castrucci P, Scarselli M, De Crescenzi M 2006 *Appl. Phys. Lett.* **89** 063122
- [5] Scarselli M, Masala S, Castrucci P, De Crescenzi M, Gatto E, Venanzi M, Ronda A, Karmous A, Szkutnik P D, Berbezier I 2007 *Appl. Phys. Lett.* **91** 141117

Patterning of Discotic Liquid Crystals: a New Time Temperature Integrating Framework

M. Cavallini¹, A. Calò¹, P. Stoliar¹, J. C. Kengne¹,
S. F. C. Matacotta², F. Quist², Y. H. Geerts³, F. Biscarini^{1,2}

¹*CNR-Institute for the Study of Nanostructured Materials
Via P. Gobetti 101, I-40129 Bologna, Italy*

²*SCRIBA Nanotecnologie srl
Via G. Fanin 48, I-40127 Bologna, Italy*

³*Université Libre de Bruxelles, Faculté des Sciences
Laboratoire de chimie des polymères, CP 206/1
Boulevard du Triomphe, 1050 Bruxelles, Belgium*

Liquid crystals (LCs) are a successful example of how the control of self-assembling and self-organization [1] via chemical design [2] leads to new applications. These are mostly based on such (quasi-) equilibrium properties as thermal stability, mesophase transition temperature, long-range molecular ordering and anisotropy. Here we present a new application of LCs based on non-equilibrium properties: a logic pattern which also records the thermal history of the system as a time temperature integrator. We control the multifunctionality of Discotic LCs (DLCs) by lithographic control to the self-assembling. DLCs are patterned into a “checker-board” of domains whose alignment differs from that of the surrounding dominant phase. Furthermore, these domains are distributed as a “logic pattern” containing information stored in binary code. When the temperature overcomes the phase transition temperature T_{r-h} between columnar rectangular and hexagonal mesophases, the domains progressively reorient into the dominant phase. The time spent above T_{r-h} is monitored by an optical microscope as the irreversible change of the local birefringence.

As T_{r-h} is tuned by the chemical design, a new application of non-equilibrium LC patterns as time-temperature integrators and as information storage media can be envisioned [3].

References

- [1] L. Schmidt-Mende, A. Fechtenkötter, K. Müllen, E. Moons, R. H. Friend, J. D. MacKenzie *Science* 2001, 293, 1119
- [2] T. Kato, *Science* 2002, 295, 2414
- [3] M. Cavallini et al. *Adv. Mater.* 2009

Reconciling Coherent Band Motion and Incoherent Diffusion in Organic Molecular Semiconductors

S. Ciuchi¹, S. Fratini^{2,3}

¹*SMC Research Center CNR-INFM and Dipartimento di Fisica
Università dell’Aquila, via Vetoio, I-67010 Coppito-L’Aquila, Italy*

²*Institut Néel – CNRS & Université Joseph Fourier
BP 166, F-38042 Grenoble Cedex 9, France*

³*Instituto de Ciencia de Materiales de Madrid, CSIC
Sor Juana Inés de la Cruz 3, E-28049 Madrid, Spain*

In the past decades the development of crystal growing techniques has led to the production of molecular organic semiconductors with an extremely low structural disorder, attaining an upper intrinsic limit of the carrier mobility, $\mu \sim 10^1$ – 10^2 cm²/Vs [1], whose explanation has challenged the scientific community for a long time [2]. In this class of materials, due to the inherently large thermal lattice fluctuations associated to the weak van der Waals inter-molecular bonds [3], a puzzling regime of transport shows up around room temperature where the electron mean-free-path becomes comparable with the inter-molecular spacing, yet exhibiting no sign of carrier localization. At the same time the particle (molecular, real-space) and wave (band-like, momentum-space) nature of the carriers becomes so entangled that different experiments may show results in agreement with either the molecular or the band identity. These concepts, that have been often discussed in the literature on a phenomenological basis, are now put on a rigorous basis by solving accurately a well-defined model relevant for the organic semiconductors.

Acknowledgements

S.C. gratefully acknowledges the hospitality of Instituto de Ciencia de Materiales de Madrid (CSIC) where a major part of this work was done.

References

- [1] M. E. Gershenson, V. Podzorov and A. F. Morpurgo. Colloquium: Electronic transport in single-crystal organic transistors. *Rev. Mod. Phys.* 78, 973 (2006)
- [2] Karl, N., 2001, in *Organic Electronic Materials*, edited by R. Farchioni and G. Grossi Springer-Verlag, Berlin, pp. 283–326.
- [3] Troisi, A., Orlandi, G. Charge-Transport Regime of Crystalline Organic Semiconductors: Diffusion Limited by Thermal Off-Diagonal Electronic Disorder. *Phys. Rev. Lett.* 96, 086601 (2006)

3D Adiabatic Compression of Plasmon Polariton for Nanomapping at 10 nm Resolution

F. De Angelis^{1a,2}, G. Das^{1,2}, M. Lazzarino³, A. Bek⁴, P. Candeloro¹,
C. Liberale^{1,2}, F. Mecarini^{1,2}, A. Pujia¹, E. Di Fabrizio^{1,2,3}

¹ BIONEM lab, University of Magna Graecia, Campus S. Venuta
Germaneto, viale Europa, 88100 Catanzaro, Italy

^a f.deangelis@unicz.it

² CalMED s.r.l., C. da Mula c/o Campus S. Venuta
Germaneto, viale Europa, 88100 Catanzaro, Italy

³ TASC National Laboratory, CNR-INFM, Area Science Park
Basovizza, 34012 Trieste, Italy

⁴ CBM (Centro Biomedicina Molecolare) Area Science Park
Strada Statale 14 – km 163,5 in 34012 Basovizza, Trieste, Italy

The interest in knowing the spectroscopic signature of a single molecule is wide and spans from physics, chemistry, material science to biology, where DNA or protein mutation due to a single gene or a single aminoacid can be evidenced. From an optical point of view, the detectability of a single molecule is related to the spatial confinement of the electromagnetic field. The interest here is not only in the detection of isolated molecules placed at specific “hot spots”, but also in employing dense samples where the molecules are in proximal contact. In the last five years, there has been a burst in the study and conceiving of new devices for the generation of surface plasmon polaritons (SPP) confined at the nanoscale, where radiation-matter interaction is strongly enhanced. Several fabrication methods are now available for material preparation and surface nanostructuring, but only few of them can ensure the stringent design control needed for an effective and reproducible generation and manipulation of SPP. Here, we report the design, fabrication, and characterization of a novel nanooptical device conceived for label-free detection and chemical mapping of few molecules by means of Raman Scattering combined with AFM. The device consists in a silver cone acting as a plasmonic nanoantenna, placed at the centre of a photonic crystal (PC) cavity (Figures 1 and 2, the device is fabricated on an AFM cantilever). The PC cavity produces an efficient coupling between the external optical source and the nanoantenna, in fact, direct coupling of the far field to the nanoantenna in the absence of a PC is inefficient, as we observed both theoretically and experimentally. The nanoantenna placed at the cavity centre supports SPP modes and acts as a nano-scale waveguide, able to propagate and focus the SPP towards the tip where strong enhancement of the e.m. field intensity occurs [1]. The geometry of the metallic nanoantenna plays an important role in defining the SPP mode profile details. When its shape is perfectly conical adiabatic behaviour is predicted [2,3]. This causes the SPP field being effective for scattering emission only at the tip where an enhancement factor of about 10^3

for the electrical field is theoretically reachable. Such stringent conditions force the choice toward top-down fabrication techniques that guarantee a strict dimensional and geometrical control. Our nanolithography technique of choice in this work relies on two powerful fabrication methods: focused ion beam (FIB) milling and chemical vapour deposition (CVD) induced by a focused electron beam.

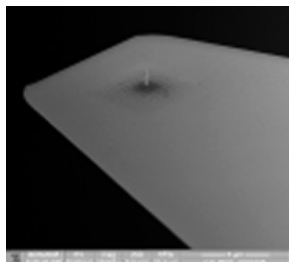


Figure 1: SEM image of the PC on silicon nitride cantilever with the silver cone acting as nanoantenna in the centre of the cavity

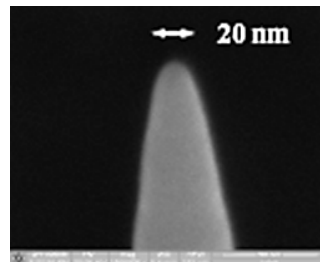


Figure 2: SEM image of the tip of the nanoantenna showing a radius of curvature down to 10 nm

Raman scattering and AFM measurements were performed with different substrate and experimental conditions; in particular the Raman spectrum of a silicon nanocrystal stripe on silica substrate is reported in Figure 3. When a scan is performed across a stripe of silicon a clear variation of the Raman signal (from silicon peak at 520 cm^{-1} to silica peak at 460 cm^{-1}) can be observed. The corresponding AFM topography is reported in Figure 4. In our best condition a chemical resolution of 7 nm is reached, also when Raman scattering and AFM topography are performed at the same time. The present results open up new perspectives on label-free single molecule detection in the subwavelength regime and in the far field configuration. We also aim at achieving unambiguous chemical information of molecular species localised in a region down to 5–10 nm and in label-free conditions. The major advantages of the present device are that the nano-waveguide provides a considerable SPP enhancement, and that the excitation source (focused on the PC cavity) is spa-

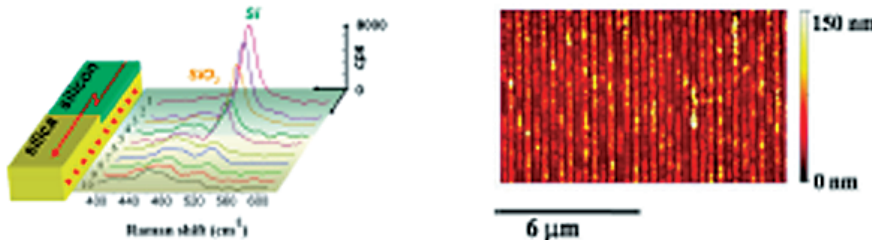


Figure 3: Raman spectrum measured across a strips of silicon nanocrystal (Figure 4). A clear variation of Raman signal can be observed when substrate changes from silicon (520 cm^{-1}) to silica (460 cm^{-1})

Figure 4: AFM topography of silicon nanocrystal strips growth on silicon substrate. The Raman spectrum performed across a single strip is reported in Figure 3

tially separated from the Raman active site. This decreases the perturbation effects of the source, the background signal, and provides increased sensitivity down to few-molecules detection. For the above reasons, the present experimental configuration is distinguished from the current research efforts in few/single-molecule detection, that are mainly based on tip enhanced near-field configurations (SERS, TERS, gap-mode TERS) where excitation and detection sites are spatially coincident.

References

- [1] F. De Angelis, M. Patrini, G. Das, I. Maksymov, M. Galli, L. Businaro, L. C. Andreani, and E. Di Fabrizio, *Nano Letts.* 8 (2008) 2321–2327
- [2] M. I. Stockman, *Phys. Rev. Letts.* 93 (2004) 137404(1)–137404(4)
- [3] C. Ropers, C. C. Neacsu, T. Elsaesser, M. Albrecht, M. B. Raschke, and C. Lienau, *Nano Letts.* 7 (2007) 2784–2788

Divide-and-Conquer Learn-on-the-Fly: A Hybrid Quantum-Classical Approach for Simulation of Nanoscale Metallic Systems

J. Dziedzic¹, J. Rybicki^{1,2}

¹*Faculty of Technical Physics and Applied Mathematics, Gdańsk University of Technology
Narutowicza 11/12, 80-233 Gdańsk, Poland*

²*TASK Computer Centre, Gdańsk University of Technology
Narutowicza 11/12, 80-233 Gdańsk, Poland*

The likely significance of nanoscale systems in the near future explains the recent interest in their study. High costs of an experimental analysis favour the use of computer simulation to investigate the properties and behaviour of such systems, where the motions of individual atoms are considered. Traditionally, the equation of motion is obtained either in the classical regime, by molecular-dynamics (MD), or quantum-mechanically, by *ab initio* methods. The simplicity of the MD approach allows for treatment of larger systems, but simple empirical interatomic potentials usually cannot capture all the relevant effects. *Ab initio* methods are of use only in the smallest systems, up to a thousand of atoms, because of their involvement. Multiscale approaches, which combine the two methodologies are a new addition to the toolbox of a computational material scientist [1].

We present a multiscale method targeted at non-equilibrium simulation of metals in which selected regions are modelled using a robust tight-binding (TB) scheme developed at the Naval Research Laboratory (NRL-TB) [2,3] and the rest of the system is treated with molecular-dynamics employing (in this case) the Sutton-Chen [4] many-body interaction potential. The parameters of the underlying MD potential are re-parametrized locally on-the-fly by the employment of an extension to the Learn-on-the-Fly [5] technique, in order to reproduce the forces obtained by local TB calculations. The technique is parallel-ready, with both the quantum-based calculation and the force-fitting procedure scalable to several tens of processors [6].

Apart from presentation of the method and implementation in a computer code, the results of a series of simulations of nanoindentation and nanoscratching of copper with an infinitely rigid tool, where the immediate region of contact between the tool and the workpiece is treated with the TB method, will be briefly discussed. With the system size of ca. 10000 atoms, ca. 1000 atoms were treated quantum-mechanically and ca. 3000 atoms took part in the force-fitting procedure.

References

- [1] Bernstein N, Kermode J R and Csànyi G 2009 *Rep. Prog. Phys.* **72** 026501
- [2] Cohen R, Mehl M and Papaconstantopoulos D 1994 *Phys. Rev. B* **50** 14694
- [3] Mehl M, Papaconstantopoulos D, Kioussis N and Herbranson M 2000 *Phys. Rev. B* **61** 4894

- [4] Sutton A P and Chen J 1990 *Phil. Mag. Lett.* **61** 139
- [5] Csányi G, Albaret T, Payne M C and De Vita A 2004 *Phys. Rev. Lett.* **93** 175503
- [6] Dziedzic J 2009 *Quantum-Classical Computations of the Nanomechanical Properties of Metals*, PhD thesis

Photoemission from Diluted Magnetic Atoms on Metal Surfaces

S. Gardonio¹, T. O. Wehling², L. Petaccia¹, S. Lizzit¹,
A. Goldoni¹, P. Vilmercati¹, S. Lebeque³, O. Eriksson³,
M. I. Katsnelson⁴, A. I. Lichtenstein², P. Gambardella⁵,
M. Veronese⁶, P. Moras⁶, C. Carbone⁶

¹*Sincrotrone Trieste S.C.p.A., Trieste, Italy*

²*Institute for Theoretical Physics, University of Hamburg, Hamburg, Germany*

³*Department of Physics and Materials Science, Uppsala University, Uppsala, Sweden*

⁴*Institute for Molecules and Materials, University of Nijmegen, Nijmegen, The Netherlands*

⁵*ICREA and Centre d’Investigacions en Nanociencia i Nanotecnologia, Barcelona, Spain*

⁶*Istituto di Struttura della Materia, CNR, Trieste, Italy*

Diluted magnetic atoms in a non-magnetic metallic host often display unconventional transport and magnetic phenomena.

In these systems, the interplay between the Coulomb interaction among *d* or *f* electrons and delocalization, mediated by the matrix electronic states, defines complex electronic and magnetic configurations which have not been fully understood, so far. When an isolated magnetic atom is in contact with a metal host its discrete atomic levels spread into resonances [1], whose energy, width and orbital character determine many properties of the system.

This situation can be realized and probed at the surface of metallic substrates on which dimensionality and distribution of magnetic impurities are under control. Scanning tunnelling spectroscopy reveals a characteristic feature in the local density of states at the Fermi level, i.e. the Kondo effect. However, direct spectroscopic investigations intended to shed light onto the electronic configuration of the impurities as a function of the hybridization strength with the metal host are still missing.

Here we report the results of photoemission studies on the electronic configuration of Fe impurities on alkali metal surfaces and Ce impurities on Ag(111), W(110) and Rh(111) crystals. In both cases, the evolution of the adatom electronic structure is followed from the localized to hybridized limit. The interaction of Fe with a free-electron environment is varied step-wise by changing the substrate species. The *d* multiplet structure evolves and gradually dissolves into a quasiparticle peak near the Fermi level with the host electron density increasing from Cs to Li [2], in agreement with a previous X-ray magnetic circular dichroism analysis [3].

Similar observations are reported for the *f* electron shell of diluted Ce impurities. In this case the resonant photoemission spectroscopy has been employed to extract the 4*f* signal of minute Ce amounts from the *d* electron bath of the metal hosts and to

follow the effect of increasing the hybridization strength along the sequence Ag–W–Rh. The good agreement between the photoemission spectra and the Dynamical Mean-Field Theory-like calculations highlights the importance of considering full electron correlation effects as well as the details of the hybridization function in the description of energy bands in diluted magnetic systems.

References

- [1] Anderson P W 1961 *Phys. Rev. B* **124** 41
- [2] Carbone C *et al.* 2009, submitted to *Phys. Rev. Lett.*
- [3] Gambardella P, Dhesi S S, Gardonio S, Grazioli C, Ohresser P and Carbone C 2002 *Phys. Rev. Lett.* **88** 047202

Influence of Magnetic Field on the Electronic Conduction of (Bi,Pb)-Sr-Ca-Cu-O Granular Superconductors

M. Gazda, T. Klimczuk

*Faculty of Applied Physics and Mathematics
Gdansk University of Technology
Narutowicza 11/12, 80-233 Gdansk, Poland*

Granular superconductors are composed of superconducting grains of a size between several and hundreds nanometers embedded in an insulating, semiconducting or metallic matrix. Their properties are very interesting due to the presence of Coulomb effects, electron tunneling, Josephson coupling between granules, and various aspects of disorder. The presence of a magnetic field may cause either a decrease or increase in the material’s resistivity.

The electrical properties of (Bi,Pb)-Sr-Ca-Cu-O granular superconductors obtained by the solid state crystallization method were studied in this paper. The materials may be considered as a system of granules of a high-temperature superconductor embedded in an insulating matrix. The granules were of the range from 10 nm to 40 nm. All the studied materials contained granules in the superconducting state below the transition temperature. Those which contained very small granules (10 nm) of the superconducting phase had the exponential temperature dependence of resistivity characteristic for hopping conductivity. The magnetic field’s influence on the hopping parameters was studied. In the samples containing relatively large granules of the 2212 phase (above 30 nm), a bulk superconducting state was achieved. Both groups of materials showed positive magnetoresistance.

Role of Adsorbates in Photoluminescence Emission of Si Nanocrystals

S. Gibilisco, G. Faraci, A. R. Pennisi

*Dipartimento di Fisica e Astronomia, Università di Catania
Via Santa Sofia 64, 95123 Catania, Italy
and MATIS Istituto Nazionale di Fisica della Materia
Via Santa Sofia 64, 95123 Catania, Italy*

In the last years the interest towards silicon based nanostructures has been rapidly increasing, for both fundamental and applicative reasons. In particular, many research efforts have been devoted to optical and vibrational properties of Silicon nanocrystals. In this work, Silicon nanocrystals were produced and deposited on different substrates, and characterized through photoluminescence (PL) and Raman experiments. In order to clarify the PL properties of these nanoparticles, the photoluminescence spectra of several samples were studied as a function of exposure to air, oxygen, nitrogen, and rare gases. Measurements at different pressures revealed a strong enhancement of the PL at atmospheric pressure when the sample was in air. In contrast, no significant PL was observed for clean Si quantum dots in a rare-gas atmosphere and in air at low pressure. Different behavior was detected in oxygen and in nitrogen as a function of pressure. These data point out a catalytic role of the surface adsorption adding significant information for clarifying the PL mechanism. A comparison of our results, including the decay-time spectra with the data and models from the literature, demonstrates an important role of the phonon interaction in relaxation and decay processes.

References

- [1] Faraci G, Gibilisco S, Pennisi A R, Franzò G, La Rosa S, Lozzi L 2008 *Phys. Rev. B* **78** 245425
- [2] Faraci G, Gibilisco S, Russo P, Pennisi A R, La Rosa S 2006 *Phys. Rev. B* **73** 033307

Modelling of Interface During Si Layer Growth on Partially Masked Substrate

S. Gułkowski¹, J. M. Olchowik¹, P. Moskvin²

¹*Institute of Physics, Lublin University of Technology
 Nadbystrzycka 38, 20-618 Lublin, Poland*

²*Zhitomir State Technological University
 103 Chernyakhovskogo 10005, Zhitomir, Ukraine*

High quality thin Si layers obtained from a liquid phase by the Epitaxial Lateral Overgrowth (ELO) method can play a crucial role in photovoltaic applications. Laterally overgrown parts of a layer have a lower dislocation density than the substrate. The layer's thickness and width depend on the technological conditions of the LPE process, basically the growth temperature, the cooling rate and the system geometry (mask filling factor). Therefore, it is very important to find an optimal set of growth parameters for obtaining very thin structures with a maximum width (high aspect ratio).

This paper presents a two-dimensional computational study of the epilayer interface evolution for different conditions. In order to calculate the interface motion a solute concentration in an Si-Sn solution was determined after each time step. A new interface position was obtained by calculating the growth rate in direction normal to the interface. The growth rate was computed from the concentration gradients near the growing surface. To solve the layer growth problem the mixed Eulerian – Lagrangian approach was used. According to this method the solid-liquid front was tracked explicitly while the diffusive transport was solved on a fixed Cartesian grid (Figure 1). Simulations were carried out to obtain the growth rates and the as-

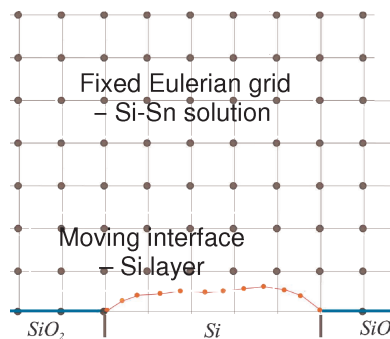


Figure 1: Configuration for the epilayer growth simulations by the front tracking method

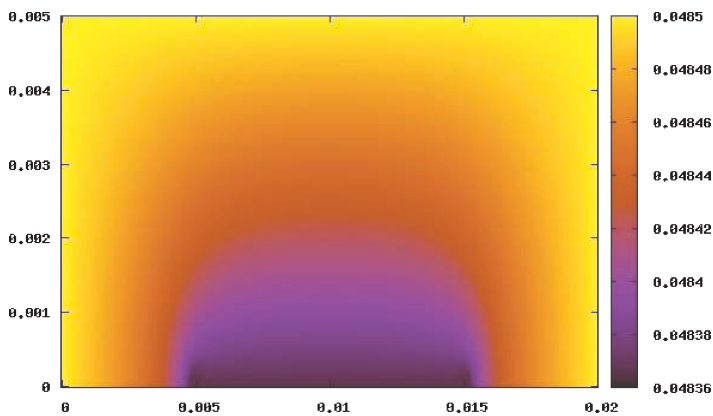


Figure 2: Concentration profile of the solute in the solution

pect ratio of the epilayer for given conditions. The calculation results were compared with the experiments.

Control of Polymers Assembling in Thin P3HT Films Grown by Electrospray

R. Gunnella^a, M. Ali, F. D’Amico, M. Abbas

*Dipartimento di Fisica, CNISM, Università di Camerino
62032 Camerino, Italy*

^a*roberto.gunnella@unicam.it*

Poly(3-hexyl)thiophene (P3HT) is one of the most used organic semiconductors in the photovoltaic field. The reasons can be found in its relatively high mobility, its ability to crystallize in a wide range of temperatures [1]. Recently a new procedure of polymer assembling control has been obtained through the fine tuning of an electric field and the speed in electrospray thin films growth [2]. In order to understand how the P3HT film characteristics were modified during the growth we performed a systematic study with ultra-violet photoemission spectroscopy (UPS), UV-Visible absorption and photocurrent measurements.

XRD and AFM measurements were used to give further support to the already well delineated picture obtained from the spectroscopies.

Summarizing, using such techniques, we have discovered, a preferential orientation of the polymer within the films and the high control obtainable on the basis of the experimental conditions. Such a control is completely absent in the most commonly employed methodology such as spin coating and casting and can be of pivotal importance in the design of future organic devices.

The study which includes a close comparison with spin coated films [3] will also cover other important properties regarding the behavior under illumination [4] and the use of rubbing of the films by both mechanical systems or by low kinetic energy ion beam irradiation [5].

References

- [1] H. Sirringhaus, N. Tessler, and R. H. Friend 1998 *Science* 280 1741
- [2] R. Gunnella M. Abbas, F. D’Amico M. Ali, to be submitted (2009)
- [3] M. Abbas, M. Ali, F. D’Amico R. Gunnella, submitted to *J. Phys.: Appl. Phys.* (2009)
- [4] F. D’Amico, M. Abbas, R. Gunnella et al., to be submitted (2009)
- [5] M. Ali, M. Abbas, R. Gunnella, to be submitted (2009)

Laser-induced Breakdown Spectroscopy Using Table-top Short-wavelength (46.9 nm) Radiation Laser

J. Kaiser¹, M. Galiová^{1,2}, R. Malina¹, K. Novotný²,
L. Ottaviano³, A. Poma³, S. Prezioso³,
L. Reale³, A. Ritucci³, P. Zuppella³

¹ *Institute of Physical Engineering, Faculty of Mechanical Engineering
Brno University of Technology
Technická 2896/2, 616 69 Brno, Czech Republic*

² *Department of Chemistry, Faculty of Science, Masaryk University
Kotlářská 2, 611 37 Brno, Czech Republic*

³ *Department of Physics, Faculty of Science, University of L’Aquila
Gc LNGS INFN, Via Vetoio, Coppito, I-67100 L’Aquila, Italy*

Laser-ablation based spectrochemical analytical methods, as e.g. Laser-Induced Breakdown Spectroscopy (LIBS) or Laser Ablation Inductively Coupled Plasma Mass Spectrometry (LA-ICP-MS) could be employed in applications in which the capability for spatially resolved, fast multi-elemental analysis in a broad variety of matrices is required. Such analysis gives a two dimensional (2D) or three dimensional (3D) map of the monitored chemical elements. Recently these methods have been utilized e.g. for large-area mapping of the elemental distribution in plant compartments [1] or for analysis of a mineral microstructure with a high spatial resolution ($\sim 200 \mu\text{m}$) [2]. The resolution of this method is basically determined by the spot size of the ablation laser.

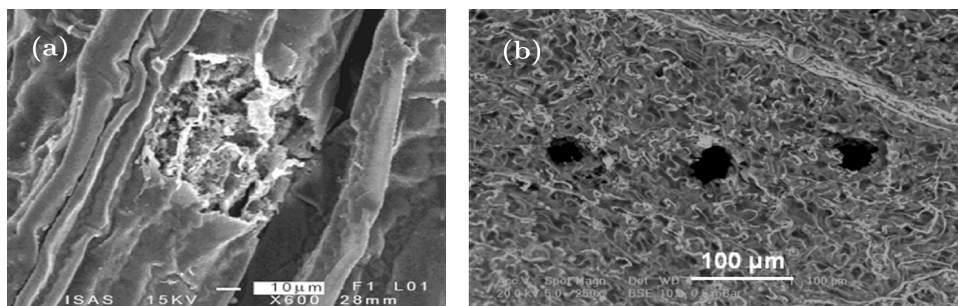


Figure 1: SEM images of the ablation pattern created by (a) fs laser and (b) capillary-discharge based soft X-ray laser on biological samples (leaves)

Here we discuss the possibilities of utilizing the table-top soft X-ray (46.9 nm) laser at the University of L’Aquila for surface ablation and subsequent chemical analysis of different materials. The capability of this laser to create small-diameter ablation holes have already been demonstrated (Figure 1). Further steps in order to characterize the ablation mechanism and to use LIBS or LA-ICP-MS for chemical analysis will be detailed.

Acknowledgements

J.K. M.G. and R.M. acknowledge the Ministry of Education, Youth and Sports of the Czech Republic for research project OC09013 and ME09015. K.N. acknowledges the Ministry of Education, Youth and Sports of the Czech Republic for research project MSM 0021622411.

References

- [1] J. Kaiser, M. Galiová, K. Novotný et al., *Spectrochim. Acta B*, **64** (2009) 67–73
- [2] K. Novotný, J. Kaiser, M. Galiová et al., *Spectrochim. Acta B*, **63** (2008) 1139–1144
- [3] L. Reale, A. Lai et al., *Microscopy Res. Tech.*, **71** (2008) 459–468

Nanostructure Modelled by δ Type Potential: Estimates for the Number of Bound States

S. Kondej

*Institute of Physics, University of Zielona Góra
Szafrańska 4a, 65-516, Zielona Góra, Poland*

A model of an electron confined by a semiconductor structure with a possibility of tunnelling is considered. In the considered problem, the nanostructure is modelled by the so called δ type potential which is supported by a line. We are interested in some spectral properties of such a system; especially, the estimates for the number of bound states.

References

- [1] Exner P and Ichinose T 2001 *Journal of Physics A: Math. Gen.* **34**, 1439–1450
- [2] Exner P and Kondej S 2005 *Journal of Physics A: Math. Gen.* **38**, 4865–4874

Atomic Oxygen Functionalization of Double-walled C Nanotubes

R. Larciprete¹, S. Gardonio², L. Petaccia², S. Lizzit²

¹*CNR-Institute for Complex Systems
Via Fosso del Cavaliere 100, 00133 Roma, Italy*

²*Sincrotrone Trieste S.C.p.A.
S.S. 14 Km 163.5, 34012 Trieste, Italy*

The technological importance of low cost routes to produce oxygen functionalized graphene sheets in the form of graphite oxide or oxygenated C nanotubes is renewing the scientific interest towards the definition and control of the chemical composition, thermal stability and chemical reactivity of oxidized sp^2 materials. Oxygen functionalization is a routinely used treatment to counteract the hydrophobic and inert character of the as-grown C nanotube surfaces and increase their chemical reactivity.

We studied the interaction of atomic oxygen with double-walled C nanotubes (DWCNTs) at room temperature (RT) by high resolution photoemission spectroscopy with synchrotron radiation. The nature of the chemical species formed on the nanotube sidewalls was followed from the initial adsorption up to advanced oxidation stages, whereas the thermal evolution of the O-related chemical species was monitored by fast photoemission. At the beginning of oxidation O atoms preferentially chemisorb forming C–O–C bonds, in ether and epoxy structures, which originate different components in the O 1s spectra and exhibit different thermal stability, with the epoxy starting to desorb below 150°C and ether at around 270°C. The onset of sp^2 lattice distortion is attested by the appearance of C–C bonds intermediate between sp^2 and sp^3 configurations. The formation of double and triple C–O bonds is favored at later oxidation stages, and is accompanied by increasing lattice amorphization and a decreasing emission in the Fermi level region. Among the highly oxidized functionalities, carbonyls seem to be the most stable thermally, whereas O–C=O bonds start to decompose below 530°C.

We also probed the DWCNT structural damage after O desorption and the interaction of the O functionalized, partially reduced and deoxygenated DWCNTs with small gas phase molecules in order to reveal possible modifications in the chemical reactivity induced by the oxygen functionalization. We found that DWCNTs, completely deoxidized after 950°C annealing, still retained lattice defects, whereas no RT interaction was observed between NO, CO and O₂ and oxidized DWCNTs, or after partial or total oxygen desorption. This result suggests that the dangling bonds are promptly healed by thermal annealing and only stable topological defects are retained in the nanotube lattice.

Gas Solubility and Mobility in Modified and Unmodified Zeolites at Low and High Pressures by P_cT Kinetic and Equilibrium Sorption

A. E. Maccallini^{1,2}, B. G. Kalantzopoulos¹, B. A. Policicchio¹,
B. M. G. Buonomenna², B. G. Golemme², C. R. G. Agostino¹

¹Department of Physics, University of Calabria
via P. Bucci, 87036, Arcavacata di Rende (Cs), Italy

²TASK Department of Chemical Engineering and Materials, University of Calabria
via P. Bucci, 87036, Arcavacata di Rende (Cs), Italy

The demand for clean and renewable energy sources in competition with the well established fossil fuels requires the development of materials which are able to convert or vehicle the energy. Several gas species (H₂, oxygenates and hydrocarbons in general) are the so-called energy vectors. However, the results obtained up to now in respect of their storage and purification are still not satisfactory, and their use in place of fossil fuels have not been economical to date. Porous materials with a high specific surface area (SSA) are studied for the gas storage [1], and, in the form of membranes, for gas separation and purification [2,3]. In specific zeolites there are porous and crystalline tectosilicates with a range of compositions, crystal structures and pore size that can be exploited to tune the interactions with gas species and modify the gas adsorption properties. When embedded in polymeric membranes, zeolites can improve to a large extent the permeability and selectivity of the sole polymer in the separation of gas mixtures [4].

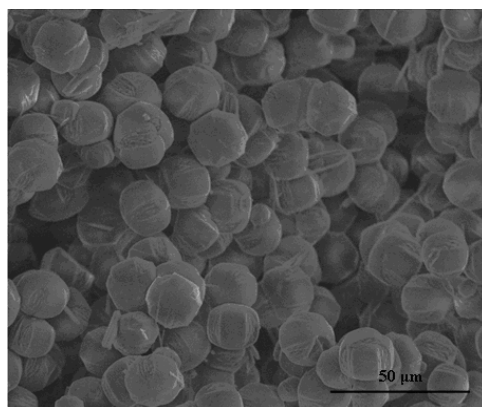


Figure 1: SEM picture of silicalite-1 (MFI)

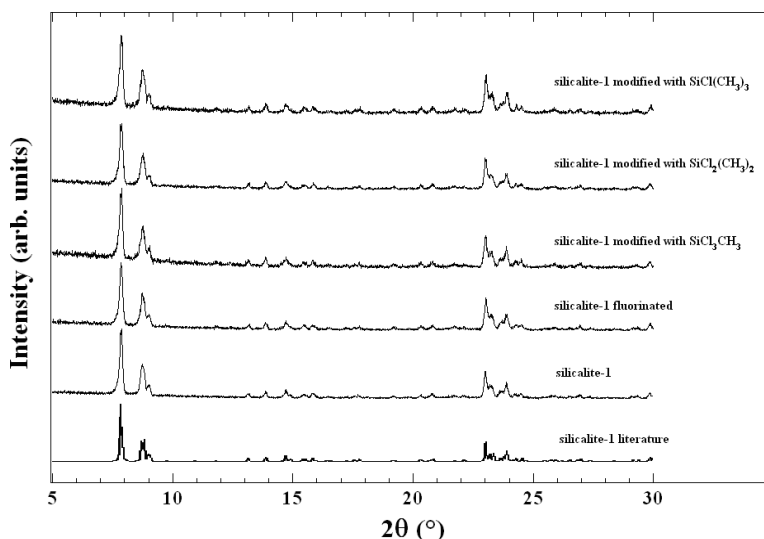


Figure 2: XRD patterns of silicalite-1 before and after modifications

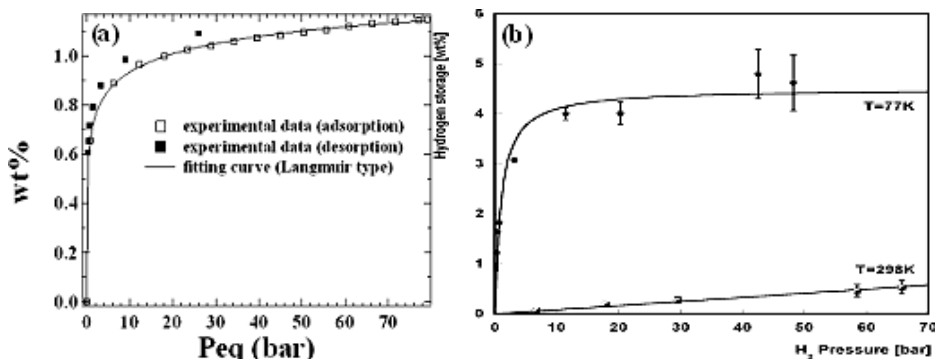


Figure 3: PcT hydrogen isotherms in a) silicalite-1 (MFI) at 77 K and b) in activated carbon at 77 K and room temperature [1]. A comparison with the literature data (Figure b) evidences a high accuracy of the measurements carried out in this work

The adsorption properties of different gases (H₂, CH₄ and CO₂) in organo-silane surface-modified silicalite-1 (MFI), and in SAPO-34 (CHA, silicoaluminophosphate) were obtained by a Sievert-type apparatus up to 80 bar at liquid nitrogen (LN₂) and room temperatures. The surface modifications which were introduced in order to tune the permeance and selectivity of the sample to different gas molecules, did not produce any change in the sample morphological and structural properties (see Figures 1 and 2). A careful analysis of Pressure-concentration-Temperature (PcT) isotherms (see Figure 3) with selected models can give information on the dynamical and equilibrium behavior of H₂ molecules. In particular, the fitting results of PcT isotherms by Toth models [5] indicate the heterogeneity/homogeneity of the adsorption properties of the samples. In the investigation of hydrogen adsorption those properties

change depending on the pressure range. However, the maximum storage capacity obtained at 8 MPa and 77 K on the different modified silicalite-1 is similar because the modification is external to the samples. On the other hand, the diffusion time of hydrogen molecules into the samples is different depending on the pressure range and the sample surface modification. In our case higher heterogeneity of the adsorption properties of the samples corresponds to a higher diffusion time. Therefore, the modification introduces variations on the dynamical properties of the samples. The same analysis was obtained on the CH₄ and CO₂ adsorption properties showing, a higher storage capacity and a slower gas diffusion in the SAPO-34 sample compared to the hydrogen adsorption which could result in significant changes in the gas permeance. The present work is also carried out with the aim to test the accuracy and reliability of the results obtained in the investigation of the adsorption properties by means of the PcT apparatus developed in collaboration with DeltaE srl [6]. A series of optimization of the mechanical, thermal and cleanness properties together with innovative software allowed us to reduce the errors in the evaluation of the adsorption properties and extract the diffusion related parameters at different temperature and pressures.

References

- [1] B. Panella, M. Hirscher and S. Roth 2005 *Carbon* **43** 2209
- [2] J. Caro, M. Noack, P. Kolsch and R. Schafer 2000 *Microporous and Mesoporous Materials* **38** 3
- [3] C. Scholes, S. Kentish and G. Stevens 2009 *Separation and Purification Reviews* **38** 1
- [4] P. Bernardo, E. Drioli and G. Golemme 2009 *Industrial & Engineering Chemistry Research* **48** 4638
- [5] J. Toth 1995 *Advances in Colloid and Interface Science* **55** 1
- [6] E. Maccallini, A. Policicchio, G. Kalantzopoulos, G. Desiderio, S. Abate and R. G. Agostino 2009, in preparation

3D Reconstruction of Graphene Waviness

L. Ortolani¹, A. Migliori¹, V. Morandi¹,
 F. Houdellier², M. Monthioux²

¹ *CNR IMM-Bologna, Via Gobetti 101, 40129 Bologna, Italy*

² *CEMES, Groupe NanoMat (CNRS UPR 8011)
 Rue Jeanne Marvig 29, 31055 Toulouse Cedex 4, France*

Graphene has increasingly attracted interest in the scientific community due to the extraordinary electronic, mechanical and optical properties. These properties are tightly bounded to the electronic structure and strongly modified in the presence of local undulations and/or bending in the structure itself. TEM investigation of freely suspended graphene membranes have shown that their surfaces are continuously undulated, over the distances of ~ 5 nm, with the height variations of less than 1 nm [1]. Moreover, theoretical studies have shown that this local curvature of the crystal lattice induces a redistribution of valence charges and modulates the electronic and transport properties of the flake [2]. For all these reasons, the methods for resolving a three-dimensional (3D) structure of graphene flakes are therefore mandatory.

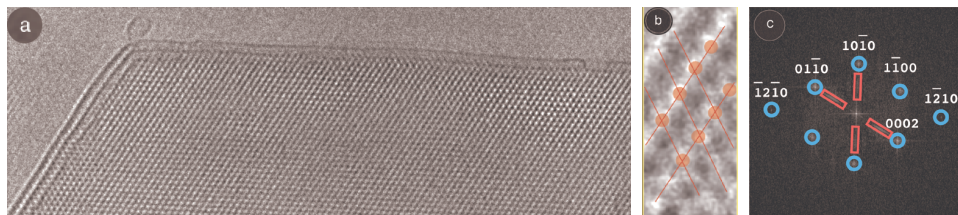


Figure 1: (a) HREM image of the border of a FGC flake. (b) Close-up of the (0002) folded zone from which it is possible to determine that the flake has an ABAB stacking sequence. (c) Fast Fourier Transform (FFT) of the HREM image, where the graphite reflections (blue circles) and the 0002 reflections of the border (red rectangles) are clearly visible

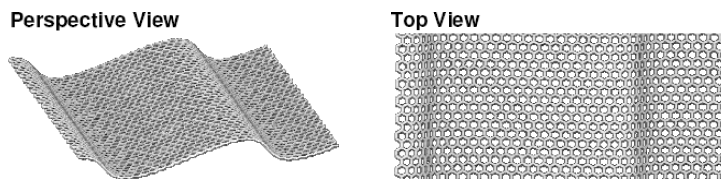


Figure 2: Scheme of a simplified graphene flake with undulations. On the left, the perspective view showing a three-dimensional structure, and on the right, the two-dimensional top view where the sloped regions appear compressed

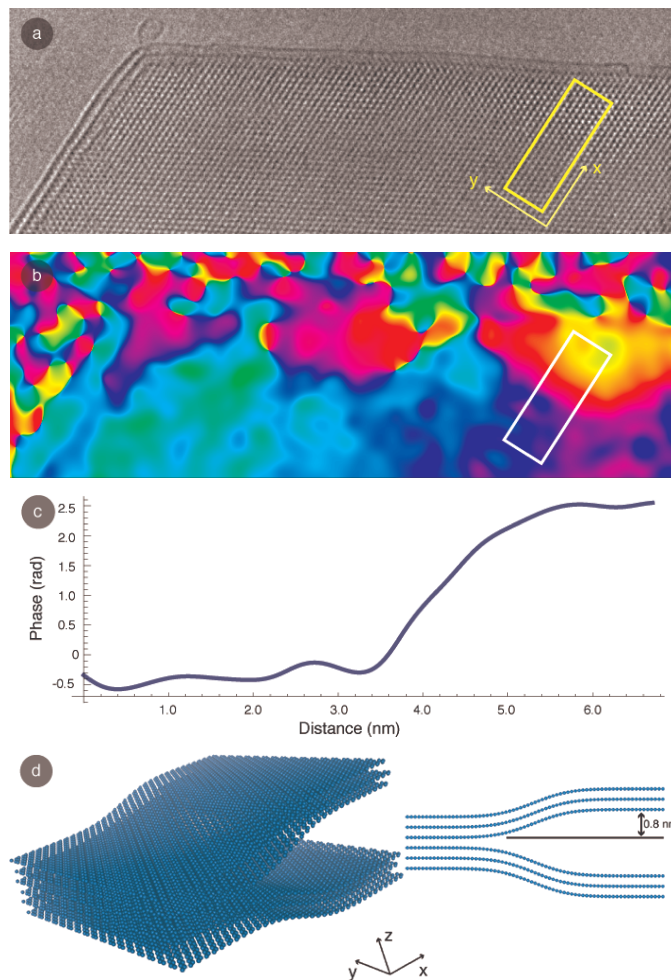


Figure 3: GPA reconstruction results. (a) HREM image of the FGC graphene flake. (b) reconstructed phase map for the [10–10] direction. (c) phase profile in the region marked by the rectangle. (d) schematics of the reconstructed structure of the flake in perspective and lateral view

To date, only few experimental results have indirectly provided information on the 3D atomic structure in graphene from the investigation of peak intensities in electron diffraction patterns [1].

Here, we present a novel method to reconstruct the 3D waviness at a nanoscale of a 2D crystal (i.e. graphene) from high-resolution transmission electron microscopy (HREM) images. Differently from other approaches, such as electron tomography, our method requires only one HREM micrograph of a crystal flake and relies on the geometrical analysis of the spatial frequencies composing the image to recover 3D information [3].

HREM images contain information on the z -projection of the crystal atomic structure, where the arrangement of crystal planes is imaged as modulated interference fringes in space according to interplanar distances. An HREM image of a Few Graphene Crystal (FGC) flake border is reported in Figure 1. The membrane is folded over itself on two sides, exposing (0002) fringes, which makes it possible to determine the number of layers in the membrane as 3. Moreover, from the disposition of the intensity peaks of the folded zone it is possible to determine that the flake has an ABAB stacking sequence. However, no information about the height variation of the folded flake is directly provided.

Nevertheless, the sample is observed using an electron beam almost perpendicular to the flake surface and the projected atomic positions will appear compressed in the regions where the flake is bended in the z -direction, as shown in Figure 2. Using the Geometric Phase Analysis (GPA) [3], a technique analyzing the geometric distortions in the HREM micrograph of a crystal lattice by means of the Fourier analysis of the image, it is possible to measure this compression. The measurement of the apparent compressions will provide a determination of the FGC flake’s slope and local height variations.

The results of the GPA deformation reconstruction for the previously shown graphene flake are reported in Figure 3. Figure 3b shows the reconstructed phase map for the [10 $\bar{1}$ 0] direction in false colors. Three regions of significant phase displacement are aligned over the border and indicated by black arrows. The one on the right, partially covered by the indicated region of interest (ROI), is larger and the most intense, and the line profile of the phase displacement over this region is reported in Figure 3c. It is possible to easily calculate the associated strain maps from this phase displacement map, and the slope of the flake from the strain profile over the same region. The final result is reported in Figure 3d where a model of the reconstructed structure of the graphene flake in the ROI is reported. The slope of the flake and the height of each stacked layer are calculated accordingly using the described experimental procedure.

References

- [1] Meyer J C, Geim A K, Katsnelson M I, Novoselov K S, Booth T J and Roth S 2007 *Nature* **446** 60
- [2] Katsnelson M I and Novoselov K S 2008 *Philos. T. R. Soc. A* **366** 195
- [3] Hytch M, Snoeck E and Kilaas R 1998 *Ultramicroscopy* **74** 131

Graphene as Nanoscale Tangential Sieve for Selecting Achiral SWCNTs

L. Ortolani¹, V. Morandi¹, M. Monthioux²

¹ *CNR IMM-Bologna, Via Gobetti 101, 40129 Bologna, Italy*

² *CEMES, Groupe NanoMat (CNRS UPR 8011)
Rue Jeanne Marvig 29, 31055 Toulouse Cedex 4, France*

Chirality dramatically affects the physical and electronic properties of single-walled carbon nanotubes (SWCNTs). The atomic level control during growth is far from being achieved, and the current growth methods result in SWCNTs of mixed chiral indices. Finding a simple and effective way to discriminate and separate chiral from achiral SWCNTs will be an important step toward their practical exploitation.

Chirality control and selection are commonly addressed in post-grown processes, and two main strategies can be identified among them: elimination (partial or total) of tubes with specific chirality [1] or selection of only one family of tubes from a solution. Within the frame of this second approach, a specific interaction between SWCNTs and the atomic structure of the poly-aromatic molecule has been investigated [2].

Following the above method we will demonstrate and discuss how graphene membranes – the largest aromatic molecule – act as effective nanoscopic tangential sieves by retaining only achiral SWCNTs. We prepared ethanol solutions of graphene flakes (obtained by mechanical exfoliation of Madagascar graphite microcrystals) – see Figure 1a – mixed with commercial SWCNTs (grown using the arc technique and exhibiting different chiralities) – see Figure 1b. SWCNTs deposited over the graphene

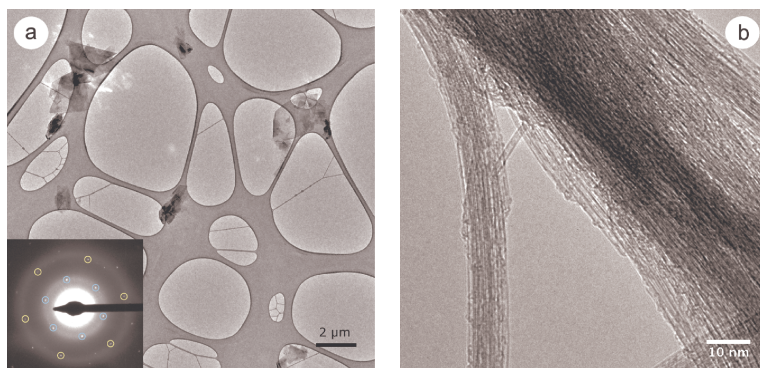


Figure 1: (a) TEM image of the produced thin graphite flakes as dispersed over a standard 3 mm TEM grid covered with a holey amorphous carbon film. (b) TEM micrograph showing the dispersion of bundles of SWCNTs before shortening sonication

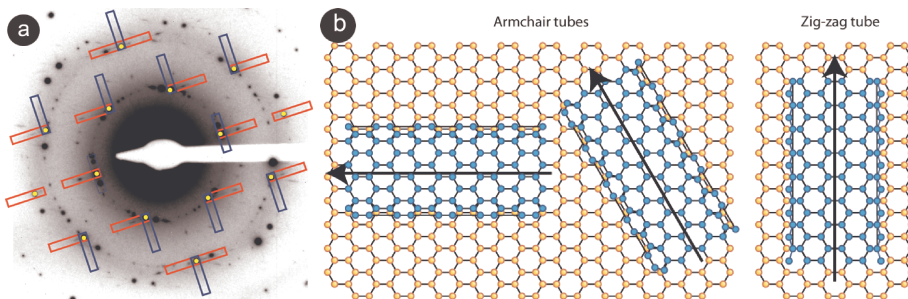


Figure 2: (a) ED pattern of aligned CNTs over graphite. There is evidence of diffraction patterns from armchair (red rectangles) and zig-zag (blue rectangles) tubes, both aligned to the same underlying pattern from graphite (yellow circles). (b) Scheme of armchair (left) and zig-zag (right) tubes matching the underlying grapheme honeycomb lattice

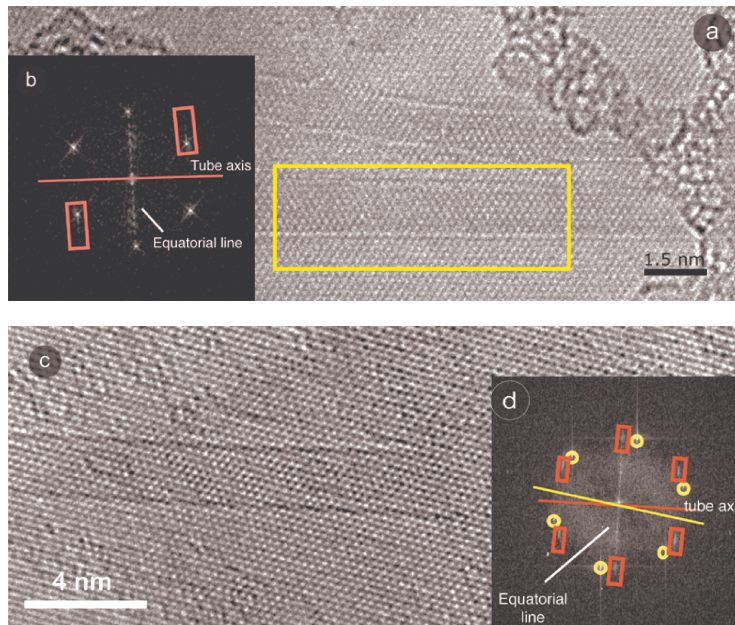


Figure 3: (a) HREM image of two armchair tubes perfectly aligned to the underlying grapheme lattice as shown by the FFT of the tube in the yellow rectangle, reported in (b). (c) HREM image of a misaligned armchair tube. Two distinct hexagonal patterns of the grapheme lattice (yellow circles) and of the tube (red rectangles), are visible as shown in the FFT in (d)

surface. Then, as a consequence of the subsequent mechanical agitation provided by ultrasonic vibrations and then centrifugation, chiral SWNCTs were found to be preferably eliminated, while achiral SWNCTs were found to continue to stick to the grapheme surface.

The samples were investigated by Transmission Electron Microscopy (TEM), first by Electron Diffraction (ED), to show the presence and the orientation of SWCNTs over graphene flakes over large areas, and then by High Resolution TEM (HREM), to investigate the interaction between SWCNTs and the graphene flake surfaces on a local scale.

Figure 2a shows an ED pattern of aligned CNTs over graphite. There is evidence of SWCNT diffraction patterns of armchair (red rectangles) and zig-zag (blue rectangles) tubes crossing at 90°. Both diffraction patterns from tubes are aligned to the same underlying honeycomb reflections marked by the yellow circles. Figure 2b reports a scheme of the relative orientation of armchair and zig-zag tubes when both lattices match the direction of the underlying graphite lattice. The relative angle between the direction of the zig-zag and the armchair tube matching the lattice is either 30° or 90°.

This perfect match between the atomic lattices of armchair tubes and that of the underlying graphene surface is demonstrated by the following HREM micrographs. Figure 3a shows two armchair tubes, both perfectly aligned to the underlying honeycomb lattice. The specific features of the non-chiral structure of the tube in the yellow rectangle, as well as the perfect orientation of the tube axis to the underlying lattice, are clearly visible in the Fast Fourier Transform (FFT) reported in the inset. Eleven SWCNTs lying on the surface of a single few graphene crystal domain were investigated, of which ten were achiral (zig-zag and armchair) and aligned with the underlying lattice, and only one, shown in Figure 3c, was armchair and not aligned with the underlying graphene network. Therefore, this latter image makes it possible to verify that the signal from the lattice of the tubes and that from the graphene lattice both contribute to the pattern of the HREM images. When a misalignment is present there is no superimposition of the diffraction patterns, as in the previous cases, and two distinct patterns are present, as shown in the FFT reported in the inset.

References

- [1] Chen Y, Wei L, Wang B, Lim S, Ciuparu D, Zheng M, Chen J, Zoican C, Yang Y, Haller G L and Pfefferle L D 2007 *ACS Nano* **1** 327
- [2] S.-Y. Ju, J. Doll, I. Sharma, F. Papadimitrakopoulos 2008 *Nature Nanotech.* **3** 356

General Strategy for Direct Synthesis of L1₀ FePt Nanoparticle Alloys from Layered Precursor

A. Capobianchi¹, D. Fiorani¹, P. Imperatori¹,
S. Laureti¹, S. Foglia², E. Palange³

¹*Istituto di Struttura della Materia-CNR
Via Salaria Km 29.300, Montelibretti, 00016 Roma, Italy*

²*Istituto di Fotonica e Nanotecnologie-CNR
Via Cineto Romano 42, Roma, Italy*

³*Dipartimento di Ingegneria Elettrica e dell’Informazione
Università degli Studi dell’Aquila
67040 Monteluco di Roio, L’Aquila, Italy*

A new chemical strategy for a direct synthesis of L1₀ FePt alloy nanoparticles starting from a polycrystalline molecular compound, iron(II)chloroplatinate hexahydrate (FePtCl₆ · 6H₂O), in which Fe and Pt atoms are arranged on alternating planes like in an fct FePt structure is reported in this work. This hypothesis is strongly supported by the structural data obtained solving the single crystal structure of FePtCl₆ · 6H₂O. A reduction of such compound, in crystalline form, by 5 % H₂ and 95% Ar at 400°C with a heating rate of 5°C/min, leads directly to a highly ordered L1₀ phase without using any metals additives. Two experiments were performed to prove this supposition: in the first experiment, reducing of amorphous FePtCl₆ · 6H₂O in SiO₂, a disordered FePt nanoparticles was obtained in the fcc phase up to 650°C. In the second experiment, reducing of the milled polycrystalline FePtCl₆ · 6H₂O in SiO₂, a complete and direct transformation in L1₀ FePt at 400°C was obtained. These results prove that the reason for the low temperature of the direct synthesis of L1₀ FePt is a peculiar crystalline and atomically layered structure of the precursor. Furthermore, our studies prove that the method is able to produce L1₀ FePt nanoparticles with an average size of 5 ± 2 nm (TEM images). The XRD pattern of nanoparticles is reported and shows the presence of peaks characterizing the L1₀ FePt phase, the lattice parameters *a* and *c* were determined from the Rietveld refinement of XRD data and are 3.8489(3) and 3.7307(5) Å, respectively. The ratio *c/a*, equal to 0.968 is comparable to the theoretical value of bulk FePt. The hysteresis loop, measured on nanoparticles at room temperature, shows a high coercivity value (*H_c* = 1.5 T), as expected for a high anisotropy L1₀ phase. The actual coercive field should be even higher, as saturation is not yet reached at the maximum applied magnetic field (5 T). Compared to other wet chemical syntheses to prepare L1₀ FePt nanoparticles, our method is employed at a lower temperature without any other metal additives, it presents a highly ordered L1₀ phase and, moreover, it does not use an organic solvent. The method could be applied to other bimetallic crystalline compounds to get ordered alloys.

Enzymatic Reactions on Surface-bound DNA Nanostructures

P. Parisse¹, A. Lucesoli², S. Radovic³, M. Castronovo⁴,
L. Casalis^{1,5}, M. Morgante^{3,6}, G. Scoles^{4,7,8,9}

¹ SISSA/ELETTRA Nano Innovation Lab, Sincrotrone Trieste
Strada Statale 14 - km 163.5, I-34149 Basovizza, Trieste, Italy

² Department of Electromagnetism and Bioengineering
Polytechnic University of Marche, 60131 Ancona, Italy

³ Department of Agricultural and Environmental Sciences
University of Udine, Via delle Scienze 208, I-33100, Udine, Italy

⁴ Department of Biology, Temple University, US

⁵ Italian Institute of Technology (IIT) – SISSA Unit, Trieste, I-34014

⁶ Istituto di Genomica Applicata, Parco Scientifico e Tecnologico di Udine “Luigi Danieli”
Via J. Linussio 51, I-33100 Udine, Italy

⁷ NanoBioMed laboratory, CBM S.c.r.l. – Cluster of Molecular Biomedicine
Trieste, I-34012, Italy

⁸ Scuola Internazionale Superiore di Studi Avanzati (SISSA)
Trieste, I-34014, Italy

⁹ International Center for Science and High Technology (ICS)
Trieste, I-34012, Italy

Addressing the efficiency of biochemical reactions over DNA nanostructures on solid surfaces is a required step for the development of a new class of highly sensitive biosensors working with extremely low amounts of genetic materials, up to a single cell limit.

Previous studies on the DpnII restriction digestion enzyme have demonstrated that it is possible to follow reactions over DNA patches of variable density, fabricated by means of nanografting, by precise Atomic Force Microscopy topographic height measurements [1].

An extension of the study to other DNA modifying enzymes (i.e. DNA polymerase and DNA ligase) will make it possible to perform several different biochemical reactions consecutively over dense/finite size molecular nanoaggregates that mimic the interactions inside living cells.

We will show here the preliminary results on DNA polymerase reactions over thiolated DNA nanostructures bound on a gold film surface. In the attached figure we report a scheme (on the left) and the atomic force microscopy images (on the right) of the various steps of the reaction:

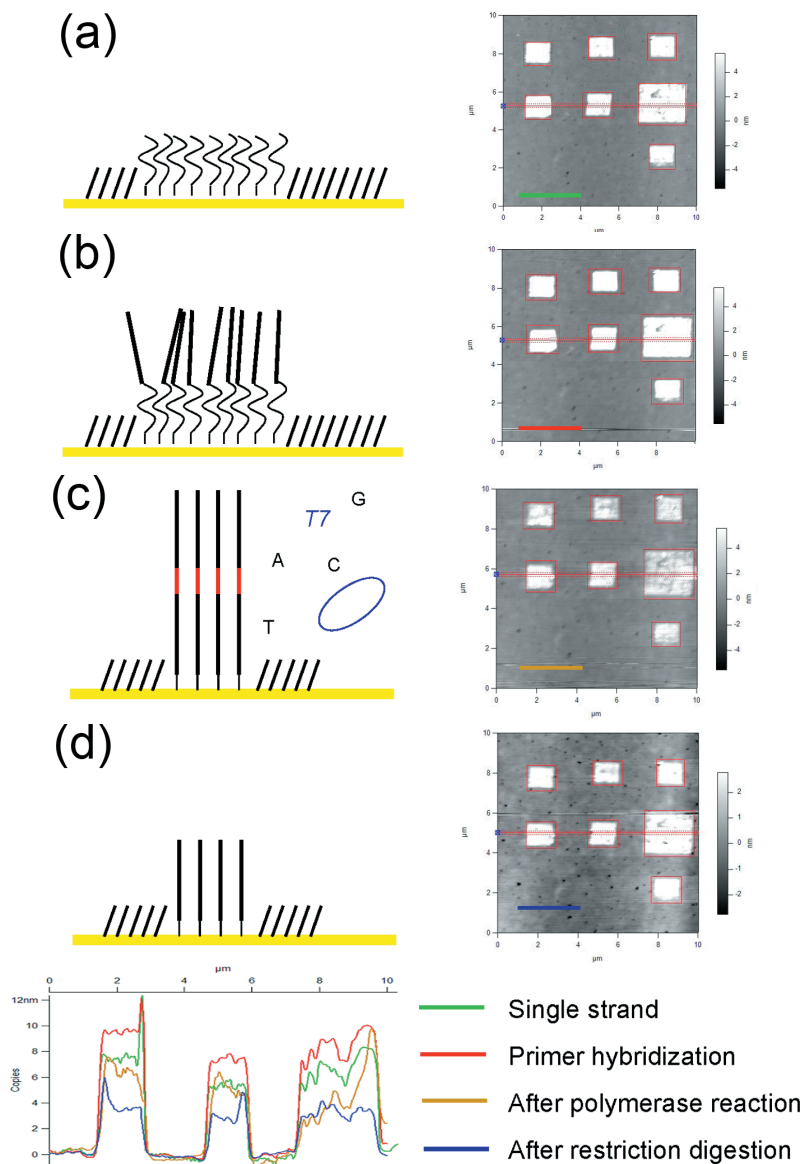


Figure 1: ??????????????????????????

- immobilization of a DNA single strand with a specific restriction site for the DpnII restriction enzymes in the middle of the molecule;
- addition of a primer oligonucleotide complementary to the terminal portion of the immobilized ssDNA strands to form a duplex region at the 3' end;
- polymerase extension of the primer to the downstream region to form a double

stranded restriction enzyme cleavage site (indicated in red);

(d) subsequent restriction digestion step cleaving the DNA duplexes to determine the polymerase extension efficiency

The bottom panel shows the differences in the height profile along the patches. Despite the unexpected lowering of the height after the polymerase reaction (**yellow line**), related to the fact that during the reaction it is possible to remove some DNA strands by the enzyme, the hybridization efficiency is demonstrated by the cleavage (reducing the height of the patches) after the DpnII restriction digestion (**blue line**).

These preliminary results highlight our ability to carry out consecutive highly efficient enzymatic reactions over the same DNA nanostructures. The use of extremely ordered DNA nanostructures would make it possible to control the crowding effect (the distance between neighboring DNA molecules) in a reproducible manner and also to extend our knowledge on the steric requirements of different DNA-modifying enzymes.

References

[1] M. Castronovo, S. Radovic, C. Grunwald, L. Casalis, M. Morgante and G. Scoles, *Nano Lett.*, 8 (2008) 4140

Photoemission of Metalloporphyrins Self-assembling Monolayer on Noble Metal {111} Substrates

M. Pedio¹, A. Resta², M. Kumar¹, R. Felici²

¹ *TASC-INFM National Laboratory, Trieste, Italy*

² *ID03, European Synchrotron Radiation Facility, Grenoble, France*

Attention on metal-metalloporphyrins interfaces is growing in relation with the development of hybrid organic-inorganic electronic and optical devices such as OLEDs [1] and thin film transistors [2]. The 3D paramagnetic porphyrin molecules, in contact with a transition metal (TM) substrate, are considered promising building blocks for the development of molecular electronic devices. Porphyrins deposited on surfaces can be used to form porous networks which can be used as a template for the growth of other molecules [3]. Moreover, magnetic properties of large molecules can be altered by deposition on metal surfaces, giving the possibility, once the chemical bond is known, of engineering magnetic nanostructures with potential use in spintronics [4].

Copper (II) and Nickel (II) octaethyl porphyrin (CuOEP, NiOEP) are molecules with an extended π -Orbital. Together with the central metal ion the π -system is responsible for interesting electrochemical and photo-physical properties. Understanding the electronic structure in the organic-metal junction is important to control the charge carrier injection between metals and organic semiconductors.

In our studies we focus on the effects that the central atom has on the molecule-substrate interaction. We use non local techniques looking at the long range order, together with the surface structure we are also aiming to determine modification in the substrate [5].

The porphyrins are deposited on Au(111) and Ag(111) by evaporation under Ultra High Vacuum (UHV) conditions. Low energy electron diffraction (LEED) shows different structures depending on the central atoms and monolayer depositions exhibit well ordered patterns.

Photoemission valence band measurements suggest a charge transfer between molecules and substrate with the molecules donating electrons to the substrate. Such charge transfer is depending on the work function of the substrate. Moreover, the separation between HOMO and HOMO-1 is measured to be bigger than the free molecule of about 0.3 eV for the monolayer case.

References

- [1] S. R. Forrest, Chemical Reviews 97, 1793 (1997)
- [2] H. E. Katz Journal of Materials Chemistry 7, 369 (1997)
- [3] for example fullerenes Spillmann et al. Adv. Mat. 18, 275 (2006); A. Kiebele et al. ChemPhysChem 7, 1462 (2006)
- [4] Zhao et al. Science 309, 1542 (2005), H. Wende et al. Nature Materials 6, 516 (2007)
- [5] R. Felici, et al., Nature Materials 4, 688–692 (2005)

Magnetocaloric Behaviour of Epitaxial MnAs Thin Films Grown on Different GaAs Substrates by MOVPE

M. Solzi¹, C. Pernechele¹, M. Ghidini¹, M. Natali², M. Bolzan²

¹*Dipartimento di Fisica and CNISM, Università di Parma
Viale G. P. Usberti 7/a, 43100 Parma, Italy*

²*Istituto ICIS-CNR
Corso Stati Uniti 4, 35127 Padova, Italy*

The room-temperature ferromagnetism and the possibility to grow high-quality epitaxial films on different semiconductor substrates has led MnAs to attract increasing attention in the field of spintronics [1]. Another interesting feature of MnAs is the large magnetocaloric effect (MCE) displayed at the Curie transition $T_c = 318$ K [2]. Bulk MnAs is characterized by a first-order magneto-structural transition between the hexagonal α -phase and the orthorhombic β -phase at T_c [3]. In this case a possible contribution from the lattice to the latent heat may give origin to an enhanced (“giant”) MCE. Furthermore, lattice deformation, as that induced by an external pressure [4] or by a proper Mn doping [5] may further enhance the MCE (“colossal”) in MnAs. However, the deduction of such enhanced MCE has been criticized [6] as due to an inappropriate application of the Maxwell’s relation in the vicinity of T_c . The presence of strain strongly influences both the temperature and the apparent nature of the transition, as is observed in epitaxial MnAs/GaAs thin films, in which the strain is due to the substrate-induced constraints. The transition observed in MBE-grown MnAs/GaAs(001) epilayers is apparently of second-order, as it results from the broad and continuous temperature dependence of magnetization. However, it has been suggested [7] that the transition proceeds by first-order, due to the coexistence of the α and β phases in a temperature interval around T_c .

The use of different GaAs templates, and thus of different strain conditions, has been recently proposed [8] to the aim of tuning the MCE behavior of MBE-grown MnAs epilayers. In particular, although the MCE intensity appears not to be markedly affected by strain, its temperature spread and peak position can be controlled by modifying the epitaxy-dependent strain. The use of MnAs thin films could in principle enable the production of innovative devices for magnetic refrigeration of micro-electromechanical systems as well as new spintronic devices. While MBE is very useful for fabrication of prototype device, the scale of future devices will require different growth techniques such as metal-organic vapor phase epitaxy (MOVPE), commonly employed by the microelectronics industry [9,10]. A magnetic characterization of epitaxial MnAs films grown by MOVPE on GaAs(001) and GaAs(111)-B substrates is presented in this paper for comparing the effect of thickness and substrate on their magneto-thermal properties.

In the case of MnAs/(001)GaAs films, SQUID magnetometry measurements show a strong in-plane anisotropy coherently with the morphology consisting of elongated grains. The thinnest films are characterized by rather smooth $M(T)$ behavior around T_c without thermal hysteresis, while the thickest films show a small thermal hysteresis which vanishes upon application of high magnetic fields. The transition temperature T_c , as deduced from the flex of initial susceptibility measurements, is found to be 317 K for the thinnest sample (18 nm), while for the thickest one (290 nm) it is 318.5 K on cooling and 327.5 K on heating. For the case of MnAs/(111)GaAs films, T_c is even larger, and ranges from 325 to 331 K on increasing the thickness from 10 to 60 nm, without thermal hysteresis. These values are appreciably larger compared to those of bulk MnAs at atmospheric pressure and a zero applied field [2], probably due to the granular nature of the films [10] together with the large surface roughness, which could lead to a compressive strain release or to an additional source of tensile strain. Moreover, T_c increases with the applied field following a linear relation with a slope of $(4 \pm 1) \cdot 10^{-4}$ K/Oe for sample MnAs(18 nm)/(001)GaAs, in agreement with that reported for bulk MnAs [2]. As the value of dH/dT_c is closely related to the maximum expected adiabatic temperature change at a first-order transition, in the case of our MnAs films one could expect, in principle, $\Delta T_{ad} \approx 4$ K for a 0–10 kOe field span. Moreover, the reduction or disappearance of thermal hysteresis in MOVPE-grown MnAs films is a favorable feature in view of possible applications of these systems for magnetic refrigeration.

We have estimated the MCE as an isothermal entropy variation, by measuring isothermal magnetization curves around the transition temperature and by applying the Maxwell’s relation. The resulting temperature dependence of the magnetic entropy change in the case of MnAs/(001)GaAs films shows a peak value of about 10 J/Kg K irrespectively of the film thickness, a value which is substantially lower with respect to that reported for bulk MnAs, 35 J/Kg K, for the same field span and at atmospheric pressure [2]. It should be noted, however, that the obtained value is affected by the uncertainty on the magnetically active volume of the films and that MCE spreads over a wide temperature range, which is a favorable feature for applications. This behavior is even more evident in the case of the MnAs/(111)GaAs thin films.

References

- [1] A. K. Das, et al., Phys. Rev. Lett. 91, 87203 (2003)
- [2] H. Wada and Y. Tanabe, Appl. Phys. Lett. 79, 3302 (2001)
- [3] C. P. Bean and D. S. Rodbell, Phys. Rev. 126, 104 (1962)
- [4] S. Gama et al., Phys. Rev. Lett. 93, 237202 (2004)
- [5] A. De Campos, et al., Nat. Mater. 5, 802 (2006)
- [6] G. J. Liu et al., Appl. Phys. Lett. 90, 032507 (2007)
- [7] A. Ney, et al., Phys. Rev. B 69, 081306(R) (2004)
- [8] D. H. Mosca, et al., Phys. Rev. Lett. 101, 125503 (2008)
- [9] G. E. Sterbinsky, et al., Physica B 388, 270 (2007)
- [10] M. Bolzan, et al., J. Magn. Magn. Mat. 316, 221–224 (2007)

Fulleride Films: Band Dispersion and Bulk *vs* Surface Contribution by Low-energy Angle-Resolved Photoemission Spectroscopy

L. Petaccia¹, P. Vilmercati¹, S. Lizzit¹, S. Gorovikov¹,
A. C. Wade^{1,2}, C. Cepek³, M. Fanetti³, E. Gayone⁴,
J. Wells⁴, Ph. Hofmann⁴, A. Goldoni¹

¹*Sincrotrone Trieste S.C.p.A.
S.S. 14 Km 163.5, 34149 Trieste, Italy*

²*Département de Physique, Université Cheikh Anta Diop
BP 5005, Dakar-Fann, Senegal*

³*Laboratorio Nazionale TASC, CNR-INFM
S.S. 14 Km 163.5, 34149 Trieste, Italy*

⁴*Institute for Storage Ring Facilities, University of Aarhus
8000 Aarhus C, Denmark*

In spite of a huge body of experimental work covering almost 25 years of research, the band structure in solid C₆₀ compounds is far from being understood due to the experimental and theoretical challenges involved [1,2]. If the fulleride monolayers on Ag surfaces [3] and the recent experiments on K₆C₆₀ thick films [4] are excluded, there is no clear evidence of the validity of the band structure calculations in bulk fullerides. This is mainly due to the lack of unambiguous angle-resolved photoemission spectroscopy (ARPES) data performed with a high momentum and energy resolution. This requirement is essential since in fullerides, the photoemission spectra can be affected by important electron-phonon, electron-electron and electron-plasmon interactions added to the effects of an orientational disorder of molecules and the small size of the Brillouin zone.

We performed new and detailed ARPES experiments of the HOMO and LUMO bands dispersion of C₆₀ and K₃C₆₀ thick films, grown *in situ* on silver single-crystals. The data were acquired at the BaD ElPh beamline [5] at Elettra. This new beamline is primarily devoted to high-resolution ARPES in the low photon energy regime. In such conditions the greatest sensitivity to *k*-vector of photoemitted electrons and high energy resolution is available.

Moreover, low photon energies provide enhanced bulk sensitivity, since the inelastic mean free path is expected to increase drastically for electrons with kinetic energies below \sim 10 eV, and are useful for tuning matrix elements, which vary rapidly at low energy.

For an undoped C₆₀ multilayer, at low photon energy the HOMO states show clear momentum dependence both at room temperature and below, where molecular rotations are frozen.

The measured dispersion is less than 500 meV and temperature independent. For K₃C₆₀, the measured dispersion of the filled LUMO-derived bands near the Fermi level is less than 100 meV, i.e. about a factor of 2 less than expected with LDA calculations. These results will be compared to the band dispersion measured for C₆₀^{3–} monolayers on Ag surfaces [3] and discussed in the light of recent models for these systems [2]. Moreover, when the bulk sensitivity is increased by reducing the photon energy, no variation in the LUMO lineshape is seen, indicating no difference in the bulk and surface electronic states.

References

- [1] Gunnarsson O 2004 *Alkali-doped Fullerides: narrow band solids with unusual properties*, World Scientific Publishing Co, Singapore
- [2] Capone M *et al.* E 2004 *Phys. Rev. Lett.* **93** 047001; Lin F *et al.* 2007 *Phys. Rev. B* **75** 075112
- [3] Brouet V *et al.* 2004 *Phys. Rev. Lett.* **93** 197601; Yang W L *et al.* 2003 *Science* **300** 303
- [4] Goldoni A, Petaccia L, Zampieri G *et al.* 2006 *Phys. Rev. B* **74** 045414
- [5] Petaccia L *et al.* 2009 *Nucl. Instr. and Meth. A*, doi:10.1016/j.nima.2009.05.001; see also <http://www.elettra.trieste.it/beamlines/BaDElPh/>